Mechanisms and Limitations for Water-Cooling of High Heat Flux Surfaces

by

Boris Lekakh

Submitted to the Department of Nuclear Engineering
in partial fulfillment of the requirements for the degree of

Doctor of Philosophy in Nuclear Engineering

at the

MASSACHUSETTS INSTITUTE OF TECHNOLOGY

May 1996

Author.....
Department of Nuclear Engineering
April 22,1996

Certified
by.....
Mujid S. Kazimi
Professor
Thesis Supervisor

Certified
by.....
John E. Meyer
Professor
Thesis Supervisor

Accepted
by.....
Jeffrey P. Freidberg
Chairman, Departmental Committee on Graduate Students

Mechanisms and Limitations for Water-Cooling of High Heat Flux Surfaces

by

Boris Lekakh

Submitted to the Department of Nuclear Engineering
on April 22, 1996, in partial fulfillment of the
requirements for the degree of
Doctor of Philosophy in Nuclear Engineering

Abstract

The divertors of planned fusion reactors such as ITER require removal of heat fluxes that are large in magnitude compared to those encountered in today's power equipment. Energy deposited on the plasma-facing surface is transferred by conduction and provides an axially and circumferentially non-uniform heat flux on the wall of the cooling channel. A promising candidate cooling systems is based on the use of highly subcooled water (subcooling more than 100 °C) flowing at very high velocities (more than 5 m/s). These conditions are quite different from those used to obtain existing correlations for single-phase convection and subcooled nucleate boiling. Through experimental assessments this work indicates that existing correlations can be applied for single-phase convection. However, for the subcooled nucleate boiling, extrapolations of existing correlations cannot be used. This study suggests that three heat transfer mechanisms must be incorporated in the correlations for heat transfer to water from high heat flux components.

First, boiling can be suppressed, resulting in high wall temperatures, sometimes far above those expected and very close to the Temperature of Homogeneous Nucleation (THN). Based on experimental data, a new correlation is proposed for the subcooled nucleate boiling region. The range of application for the new correlation is defined as follows : pressure 2-3 MPa, bulk water temperatures 19-25 ^{0}C, heat fluxes up to 25 MW/m^2, flow velocities from 3 to 15 m/s.

Second, Critical Heat Flux (CHF) can apparently occur when the wall temperature reaches the THN limit. A limit of this nature can occur only under conditions of very high mass and heat fluxes. The new proposed correlation was found to be more reliable than any of the other correlations tested for nucleate boiling for conditions encountered in the above range of thermal hydraulic parameters.

Third, THN or classical CHF limits may not be real limits with respect to the possibility of having high heat fluxes removed from the wall. In some cases, high heat fluxes can be removed by subcooled liquid, separated by a vapor film from the wall. These fluxes may be greater than the wall heat flux. This phenomena can occur only under conditions of a very high mass flux and a very high bulk subcooling. A simple analytical equation is proposed for use in calculating the value of heat flux that can be removed from a vapor film by subcooled liquid. This mechanism can be a real limit for heat removal in water-cooled plasma facing fusion reactor components.

Thesis Supervisor: Mujid S. Kazimi, Professor of Nuclear Engineering

Thesis Supervisor: John E. Meyer, Professor of Nuclear Engineering

Acknowledgments

This thesis is the culmination of 3.5 years as a graduate student at MIT. I could not begin to recount my fond memories nor mention all the people who have made this experience so full. However, the most influential persons during my tenure at MIT have been Professor Mujid S. Kazimi and Professor John E. Meyer whose incessant support and encouragement has brought my academic career to such fruition. I am speechless in my ability to convey my gratitude for their involvement in this endeavor as professors and supervisors. I am also indebted to Richard and Nancy Jacobs for their fellowship for my first year at MIT. I would like also to thank Doctor Michael Gotovskii (Russia) for the materials he sent to me. There have been too many students involved with this project to name them all but I would like to thank Anthony E. Hechanova for the interest in my research. I hope it was an experience of invaluable learning.

My intellectual and personal growth over these past years clearly resulted from the open-minded atmosphere among my peers and the bonds of friendship which I have shared with countless people. To mention names at this point would be an injustice to the memories of all experiences I have shared with so many wondrous people.

Contents

Abstract 2

Acknowledgments 3

Table of Contents 4

List of Figures 6

List of Tables 8

1 Introduction and Literature Review 9
1.1 Motivation 9
1.2 Background Information 9
1.3 ITER Divertor Plates 10
1.4 Literature Review 10
1.4.1 Single-Phase Heat Transfer 10
1.4.2 Nucleate Boiling Heat Transfer 13
1.4.3 Suppression of Nucleate Boiling 19
1.4.4 Critical Heat Flux 22
1.5 Comments 26

2 Implications of High Heat and Mass Flux on the Mechanisms for Heat Transfer 27
2.1 Suppression of Nucleate Boiling 27
2.2 Departure from Nucleate Boiling Heat Flux Limit 31
2.3 Homogeneous Nucleation Limit 33
2.4 Comments 38

3 Experiments 41
3.1 Experimental Apparatus 41
3.2 Experimental Procedure 43

4 Computational Modeling 45
4.1 Problem Definition 45
4.2 Axial Heat Conduction 46
4.3 Azimuthal Heat Conduction 48
4.4 Comments 61

5 Heat Transfer Results 62
5.1 Single-Phase Region 62
5.2 Nucleate Boiling Region 74
5.2.1 Interpretation of the Results 74
5.2.2 Discussion of Subcooled Nucleate Boiling Data 79
5.2.3 Development of Subcooled Nucleate Boiling Correlation 85
5.2.4 Subcooled Nucleate Boiling Correlation Applied to Different Velocities, Pressures and Subcooling 90
5.3 Comments 97

6 A Framework for CHF and Post-CHF Predictions 106
6.1 Interpretation of the Results 106
6.2 Discussion of CHF Data 107
6.3 Heat Flux Limit for Subcooled Liquid in Post-CHF Region 113
6.4 Development of CHF correlations 119
6.5 Comments 129

7 Concluding Remarks 140
7.1 Summary of Major Accomplishments and Findings 140
7.2 Recommendations 141

Bibliography 143

Nomenclature 145

Appendix 148

List of Figures

1-1	Cross-section of ITER vacuum vessel dimensions in mm [2]	11
1-2	Detail of divertor configuration from Figure 1-1 dimensions in mm [2]	12
1-3	Conceptual design of ITER divertor [2]	13
1-4	Single-phase heat transfer coefficient vs. heat flux	17
1-5	Heat flux as a function of wall superheat	18
1-6	Heat flux vs. the difference between the wall and saturation temperatures from [20]	20
1-7	Effect of turbulence on vapor nuclei from[20]	21
1-8	Critical heat flux vs. subcooling (T_s - T_b)	23
1-9	Critical heat flux vs. flow velocity as predicted by some look up tables	24
2-1	Relative vortex size vs. tube diameter	29
2-2	Relative vortex size vs. flow velocity	30
2-3	Heat transfer coefficients in the region of suppression of nucleate boiling	32
2-4	Temperature of Homogeneous Nucleation (THN) vs. water pressure	34
2-5	Temperature of Homogeneous Nucleation (THN) vs. water pressure	35
2-6	Heat flux limits for the low velocity region	36
2-7	Heat flux limits in the region of suppression of nucleate boiling	37
2-8	Heat flux limits due to DNB and THN at high subcooling	39
2-9	Heat flux limits due to DNB and THN at low subcooling	40
3-1	Scematic of the thermal hydraulic experimental loop	41
3-2	Test section specifications	42
4-1	Test section specifications for the axial direction	46
4-2	Test section thermocouple locations	48
4-3	Outer wall temperature profile in the axial direction	49
4-4	Peaking factors in the axial direction as a function of incident heat flux	50
4-5	Test section specifications	51
4-6	Cross section of test section model	51
4-7	Descriptive flow chart of computer modeling solution	55
4-8	Inner wall temperature profilein the azimuthal direction	56
4-9	Peaking factor in the azimuthal direction	57
4-10	Total peaking factor	58
4-11	Total peaking factor corresponding to Critical Heat Flux	59
4-12	Sensitivity analysis results	60
5-1	Outer wall temperature (TC2) vs. incident heat flux for various velocities	64
5-2	Outer wall temperature vs. incident heat flux for various velocities	65
5-3	Single-phase heat transfer coefficient vs. maximum local heat flux	67
5-4	Single-phase heat transfer coefficient vs. maximum local heat flux	68
5-5	Single-phase heat transfer coefficient vs. maximum local heat flux	69
5-6	Heat transfer coefficient as a function of maximum local heat flux	70
5-7	Heat transfer coefficient as a function of maximum local heat flux	71
5-8	Heat transfer coefficient ratio vs. flow velocity	72
5-9	Heat transfer coefficient vs. flow velocity	73
5-10	Outer wall temperature (TC2) vs. incident heat flux for nucleate boiling region	76
5-11	Outer wall temperature (TC4) vs. incident heat flux for nucleate boiling region	77
5-12	Local heat transfer coefficient vs. local heat flux	78
5-13	Local heat transfer coefficient vs. local heat flux; comparison with Jens-Lottes correlation	80
5-14	Local heat transfer coefficient vs. local heat flux; comparison with Yin's correlation	81
5-15	Local heat transfer coefficient vs. local heat flux; comparison with Shah correlation	82
5-16	Local heat transfer coefficient vs. local heat flux; comparison with Chen correlation	83

5-17 Heat transfer coefficient based on wall superheat temperature difference vs. local heat flux 84
5-18 Suppression factor due to velocity as a function of the Reynolds number 87
5-19 Suppression factor due to heat flux as a function of relative local wall heat flux 88
5-20 Single-phase correction multiplier (F) as a function of suppression factor due to velocity.. 89
5-21 Local heat flux as a function of wall superheat 91
5-22 Local heat flux as a function of wall superheat 92
5-23 Local heat flux as a function of wall superheat 93
5-24 Local heat flux as a function of wall superheat 94
5-25 Comparison between experimental and calculated results 95
5-26 Heat transfer coefficient as a function of flow velocity 98
5-27 Heat transfer coefficient as a function of flow velocity 99
5-28 Heat transfer coefficient as a function of bulk temperature 100
5-29 Nucleate boiling suppression ratio as a function of pressure 101
5-30 Pressure correction factor as a function of pressure 102
5-31 Local heat flux as a function of wall superheat 103
5-32 Local heat flux as a function of wall superheat 104
5-33 Local heat flux as a function of wall superheat 105
6-1 Critical heat flux as a function of flow velocity 108
6-2 Stanton CHF number as a function of Peclet number 110
6-3 Maximum inner wall temperature as a function of flow velocity 111
6-4 CHF in overheating at nucleate site 112
6-5 CHF due to Temperature of Homogeneous Nucleation (THN) limit 114
6-6 Critical heat flux as a function of flow velocity 115
6-7 Heat flux limit for Subcooled Liquid in post-CHF region 117
6-8 Film boiling regions 118
6-9 Critical heat flux as a function of velocity 120
6-10 Enhancement ratio in post-CHF region as a function of flow velocity 121
6-11 Heat flux limit (Equation (6.13))as a function of flow velocity 123
6-12 CHF as a function of flow velocity 124
6-13 CHF as a function of flow velocity 125
6-14 CHF as a function of flow velocity 126
6-15 CHF as a function of flow velocity 127
6-16 CHF as a function of flow velocity 130
6-17 CHF as a function of flow velocity 131
6-18 CHF as a function of flow velocity 132
6-19 CHF as a function of flow velocity 133
6-20 CHF as a function of flow velocity 134
6-21 Heat flux limit as a function of flow velocity 135
6-22 CHF as a function of flow velocity and pressure 136
6-23 CHF as a function of flow velocity and subcooling 137
6-24 Heat flux ratio as a function of flow velocity 138
6-25 Heat flux ratio as a function of flow velocity 139

List of Tables

1.1	Main Operating Requirements and Thermal Hydraulic Parameters for ITER Divertors [2,3]	12
1.2	Range of Data in Tong-75 Critical Heat Flux Correlation	25
3.1	Test Range of Present Study	42
5.1	Measured Variables for Single-Phase Region	62
5.2	Synopsis of Reduced Data for Single-Phase Region: Major Thermal Hydraulic Variables.	63
5.3	Measured Variables for Nucleate Boiling Region	74
5.4	Synopsis of Reduced Data for Nucleate Boiling Region: Major Thermal Hydraulic Variables	75
6.1	Bench Mark Case for Critical Heat Flux Data	107
6.2	Bench Mark Case for Critical Heat Flux Data [23]	107

Chapter 1

Introduction and Literature Review

1.1 Motivation

It is important to continue to develop fusion energy technology for use by future generations, particularly in regards to its economic and environmental aspects. Fusion programs around the world are steadily making progress in understanding plasma phenomena. Now fusion technology requires in-depth engineering studies. These studies are needed for future energy generated in fusion power reactors. The International Thermonuclear Experimental Reactor (ITER) concept uses toroidal magnetic field lines to confine a plasma. However, the highly energetic ions in the plasma diffuse out of their toroidal confinement and impact upon a material structure. In order to minimize the damage of such particles and to vent them out of the reactor chamber, the particles are diverted along a well characterized magnetic surface onto a component known as a divertor plate.

The present thermal hydraulic investigation is focused on the mechanisms for heat transfer in divertor plates water-cooling, where high subcooling, and high heat and mass fluxes may be required . This study should help fusion reactor designers to establish cooling requirements for the divertor plates and for other plasma facing components. A failure in the divertor plate could result in an irreparable and/or destructive accident resulting from coolant leaking into the vacuum chamber. Thus, reliability for high heat flux components is very important to fusion reactor technology. Today, very few investigators are producing data relevant to fusion reactor conditions, i.e., at very high heat and mass fluxes.

Knowledge of heat transfer mechanisms in high velocity flow of subcooled water with extremely high wall heat flux is also very important for fusion reactor accident analyses including Loss of Flow Accident (LOFA) and Loss of Coolant Accident (LOCA).

Results of the present study would also be useful for particle accelerator target and high neutron flux fission reactor designers. Should the energy received by these components increase beyond the cooling capability of the component, failure may result due to excessive stresses, melting and/or vaporization.

The purpose of this study is to investigate and characterize mechanisms for extreme heat transfer conditions in highly subcooled high velocity water flow in order to have appropriate design goals with adequate safety margins to prevent failure of plasma facing components.

1.2 Background Information

Experiments in the large fusion research reactors are not specifically designed to study the physical structure surrounding the plasma. Therefore, the thermal-hydraulic design has relied heavily on extrapolation and/or theoretical modeling.

This situation is not unreasonable since definitive validation only comes from actual testing in a fusion reactor. Unfortunately right now no real fusion power reactor exists in the whole world. That is why large uncertainties exist in the reactor conditions that define the task as well as the calculated performance of the component under those conditions.

The ITER is a joint design, research and development effort involving European Community, Russia, Japan, the United States and other countries. The overall objective of the ITER project is to "demonstrate

the scientific and technological feasibility of fusion power" [1]. The ITER team has finished the conceptual design and is presently working on the engineering design of ITER.

1.3 ITER Divertor Plates

The divertor plates in ITER are the focus of the present study because they must endure the harshest physical environment under normal and sometimes abnormal operation conditions.

The ITER divertor reactor specifications are shown in Table 1.1 [2, 3]. These conditions define the physical environment that the divertor must withstand. As one can see, thermal hydraulic conditions are quite different from those most used to obtain existing correlations for single-phase convection, subcooled nucleate boiling and CHF. The layout of the divertor plates for which these conditions are relevant is shown in Figures 1-1 and 1-2. This ITER conceptual design for a divertor plate consists of a copper coolant tube and graphite protective tiles brazed together via a soft interlayer as shown in Figure 1-3.

Divertor design is a demanding task because of the large uncertainties that exist both on the plasma side and the coolant side of the channel. The plasma side uncertainties cannot be validated until a real fusion machine will be built. But the coolant side conditions can be evaluated using both experimental and theoretical methods. Thus, the divertor performance depends to a large extent on the ability to calculate the heat transfer conditions for the coolant. These conditions can be evaluated only when most of the mechanisms for heat transfer at high heat and mass fluxes are known.

1.4 Literature Review

1.4.1 Single-Phase Heat Transfer

Three single-phase heat transfer correlations were assessed under the divertor operating conditions. The Dittus-Boelter [4] correlation, Equation (1.1), can be computed in two different ways.

$$Nu = 0.023\, Re^{0.8}\, Pr^{0.4} \tag{1.1}$$

First, it can be computed as it was originally proposed by it's authors using bulk temperature for property evaluation. However, for high heat fluxes one can think about using film temperature, which is defined as $T_f = (T_w + T_b) / 2$, for evaluating the properties, μ, ρ, k and Pr. The original application range for the above equation is as follows: $Re > 10^4$, $0.7 < Pr < 160$ and $L/D > 60$.

The Petukhov [4] correlation, Equations (1.2) and (1.3), takes into account the wall roughness and the wall viscosity changes. The properties μ_b, ρ, k and Pr are to be evaluated at bulk temperature, and μ_w at wall temperature. The friction factor, f, is obtained from Moody diagram. This correlation was developed based on a much wider data base.

$$Nu = \frac{f\, Re\, Pr}{8Z}\left(\frac{\mu_b}{\mu_w}\right)^{0.11} \tag{1.2}$$

$$Z = 1.07 + 12.7(Pr^{2/3} - 1)\left(\frac{f}{8}\right)^{0.5} \tag{1.3}$$

The range of application for Equation (1.2) is: $10^4 < Re < 5\ 10^6$, $0.5 < Pr < 2000$ and $0.08 < \mu_w / \mu_b < 40$.

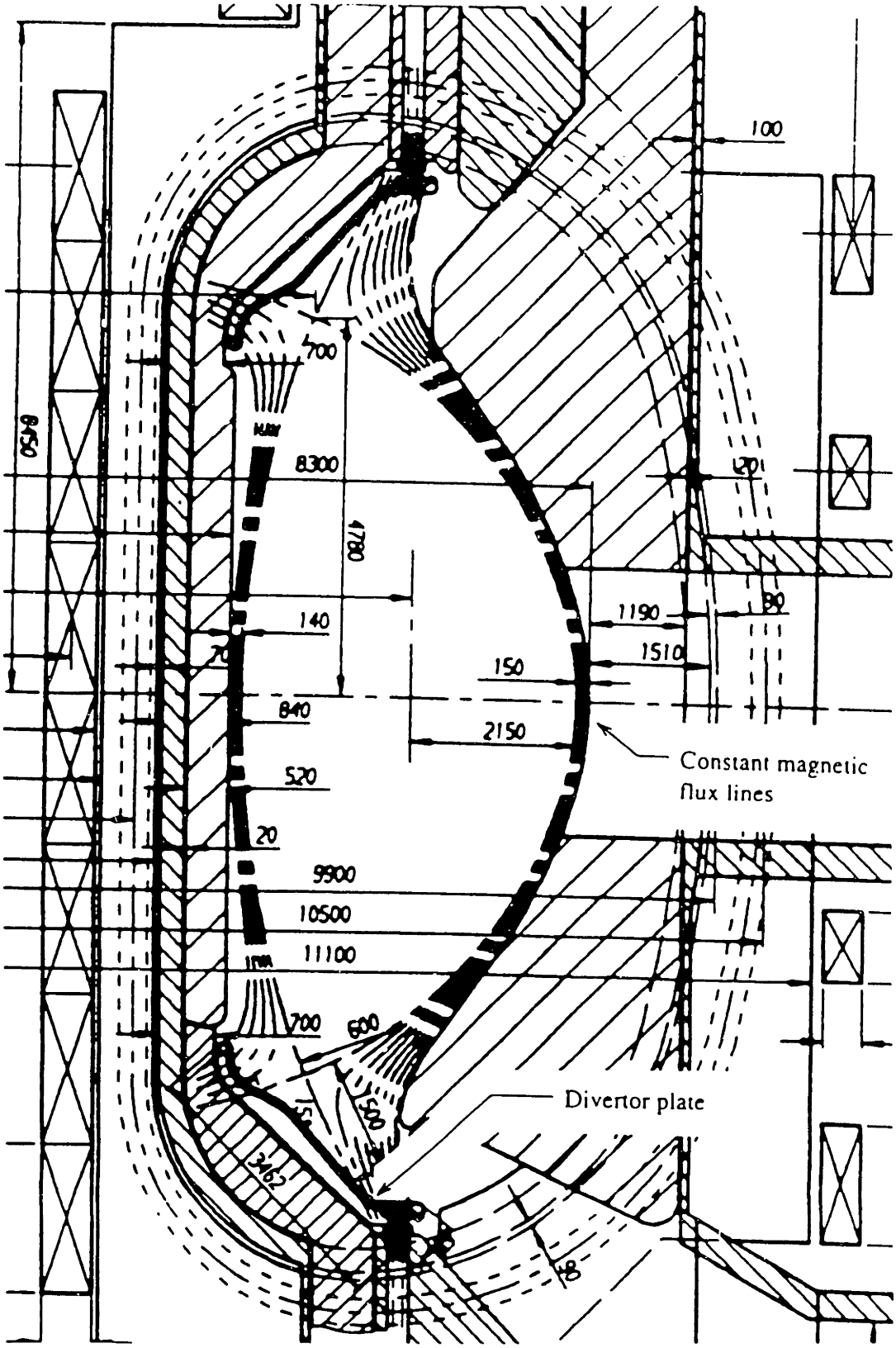

Figure 1-1: Cross-section of ITER vacuum vessel, dimensions in mm [2]

Table 1.1: Main Operating Requirements and Thermal Hydraulic Parameters for ITER Divertors [2,3]

Parameter (Nominal Operation)	Physics Phase	Technology Phase
Fusion Power (MW)	1000	850
Divertor Power (MW)	160	210
Divertor Neutron Load (MW/m^2)	0.7	0.5
Nominal Peak Steady-State Heat Flux, (MW/m^2)	15 (5)*	
Inlet Water Temperature (°C)	50 (150)*	
Inlet Water Pressure (MPa)	3.5 (4)*	
Inlet Velocity (m/s)	10	
Tube Inner Diameter (mm)	15 (10)*	
Tube Cross-Section	circular	
Desired burnout safety margin	4	

* Thermal hydraulic parameters for dynamic gas target divertor [3]

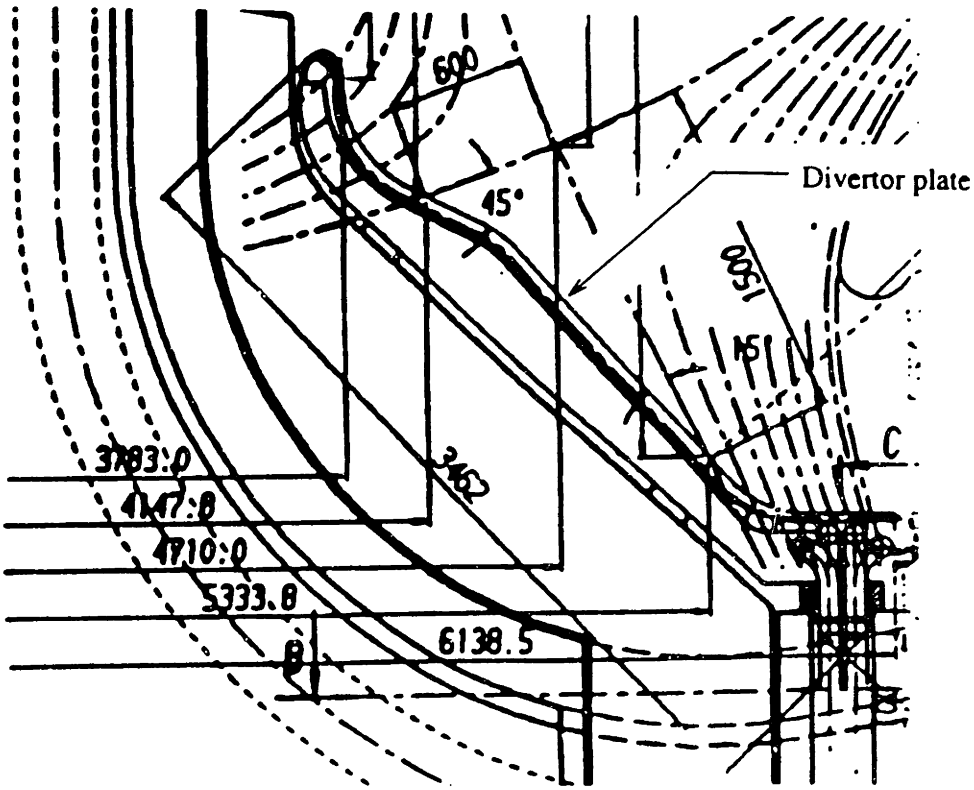

Figure 1-2: Detail of divertor configuration from Figure 1-1, dimensions in mm [2]

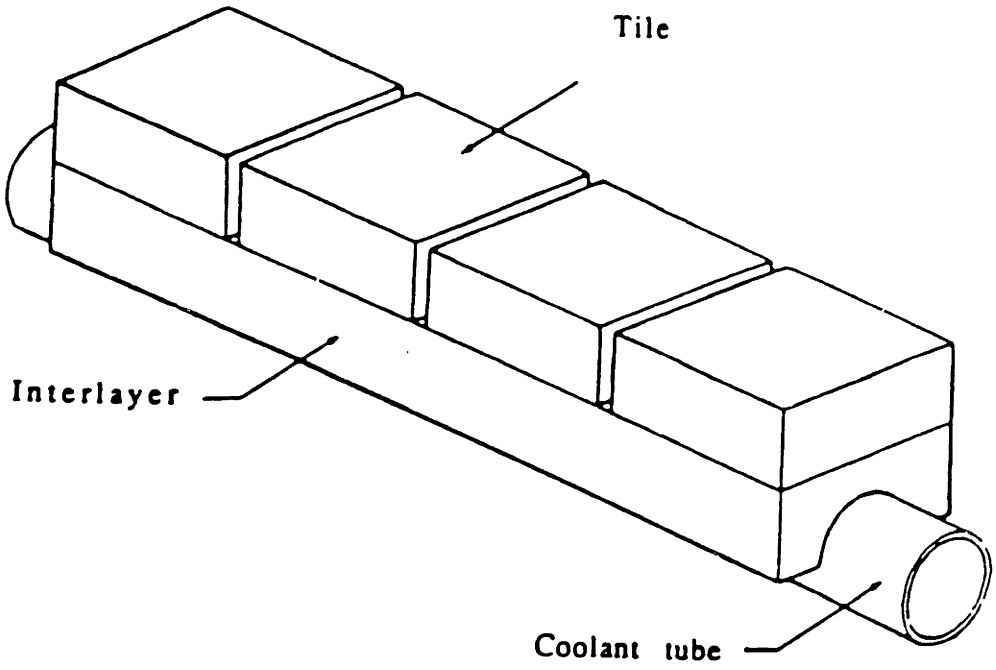

Figure 1-3: Conceptual design of ITER divertor [2]

The Sieder-Tate [1] correlation , Equation (1.4), is a modification of the Dittus-Boelter correlation and it, as the Petukhov correlation, takes into account the effect of wall viscosity variation.

$$Nu = 0.027\,Re^{0.8}\,Pr^{1/3}\left(\frac{\mu_b}{\mu_w}\right)^{0.14} \tag{1.4}$$

The application range for equation (1.4) is: $Re > 10^4$, $0.7 < Pr < 16700$ and $L/D > 60$.

The correlations presented above yield quite different values of heat transfer coefficient in the range of interest (see Figure 1-4). Hence, validation of the above three correlations (Equations (1.1), (1.3) and (1.4)) with a new data base in the appropriate parameter range is required.

1.4.2 Nucleate Boiling Heat Transfer

For subcooled liquid, if the wall temperature exceeds a minimum temperature required for nucleation, subcooled nucleate boiling can occur. Correlations exist for calculating the incipience of boiling (Bergles' correlation [14], for example). However, use of such equations is felt to add undue complication. Subcooled nucleate boiling can be considered to occur whenever the subcooled nucleate boiling heat transfer coefficient equals or exceeds that for single phase convective heat transfer (h_c). A Nucleate boiling region exists in many types of power equipment. Predicting the rate of heat removal during nucleate boiling is an important and sometimes difficult problem. With the local conditions given, prediction of the heat flux amounts to no more than answering two very basic questions. The first is "What

is the appropriate heat transfer correlation to use?" The second question is then simply "what heat flu.. and/or wall temperature does this correlation predict?" This requires evaluating correlations for nucleate boiling region. In addition to describing correlations comments and discussion of a review nature are supplied. Subcooled boiling heat transfer is also of crucial importance as it is closely related to the divertor's performance.

Nucleate boiling is a very complicated phenomenon, hence most of the correlations are empirical. At least five boiling correlations based on relatively low heat flux data have been used by the process, thermal and nuclear power industries.
The Jens-Lottes [5] correlation, Equation (1.5), was derived in the early days of the U.S. aerospace and nuclear programs.

$$\Delta T_{sat} = 25.0 q^{0.25} e^{(-P/62)} \qquad (1.5)$$

Where P is in bars, wall superheat $\Delta T_{sat} = T_w - T_s$ is in $^{\circ}C$, and q is the heat flux in MW/m^2.

The correlation was developed from data bases generated by three different groups. The test ranges covered: tubular channel geometries with ID from 3.63 to 5.74 mm (L/D from 50 to 108), system pressures from 0.7 to 17.2 MPa, water inlet subcooling from 19 to 130 $^{\circ}C$, mass fluxes from 11 to 1040 $kg/(m^2 s)$ and heat fluxes up to 6.62 MW/m^2.

The ΔT_{sat} was found empirically to be proportional to the $q^{0.25}$. Significant scatter is noted in the data bases used by Jens-Lottes. As pointed out by these authors, the maximum equation-fitting errors with two or three data groups that were used reached 23% and 60% respectively. The Jens-Lottes equation is known to give low predictions of wall superheat for subcooled nucleate boiling

Thom et al. [6] modified the Jens-Lottes correlation based on subcooled boiling water equipment with a channel ID of 12.7 mm (L/D = 120), pressures at 5.2, 7.0 and 13.8 MPa, heat fluxes up to 1.6 MW/m^2 They adopted the form of the Jens-Lottes equation, but modified the coefficient and the exponential to arrive at the following expression:

$$\Delta T_{sat} = 22.65 q^{0.5} e^{(-P/87)} \qquad (1.6)$$

The units to be used for the variables in Equation (1.6) are the same as those for Equation (1.5). Due to the relatively low heat fluxes involved in their measurements, application of the Thom correlation for fusion reactor analysis would require extrapolations of Equation (1.6) almost 10 times beyond the heat flux of its original data base. Such extrapolated results, as demonstrated subsequently, are not satisfactory.

The inadequate performance of the existing correlations at fusion flux levels necessitates the development of a more suitable correlation for application under the high subcooling and high heat flux fusion reactor conditions. Yin [7] derived the empirical Equation (1.7) to serve that purpose.

$$\Delta T_{sat} = 7.195 q\, \gamma^{1.82} P^{-0.072} \qquad (1.7)$$

Where γ = subcooled boiling location, measured from the inlet as a fraction of total heated length.
The range of application for Equation (1.7) is defined as follows: P = 1.0 to 12.0 MPa; T_{in}= 30 to 150 $^{\circ}C$; q = 0 to 16.0 MW/m^2 ; γ = 0.7 to 1.0.

For boiling heat transfer to a saturated two-phase mixture, the Chen correlation [8] is unquestionably one of the best choices, since it is physically based (albeit semi-empirical), it works well for a wide variety of

fluids (including water) [9], it covers both the low and high quality regions, and it automatically transforms into the well-known Forster-Zuber relation for pool-boiling [10] at low flows. It has the additional desirable property that it accurately predicts the down flow data of Sani [11], having an average deviation of only 8.5% [9].

The Chen correlation is relatively complicated, but requires no iteration when the wall superheat is known. The Chen correlation is:

$$h = 0.023F\frac{k_f^{0.6}}{\mu_f^{0.4}}G^{0.8}(1-x)^{0.8}c_{pf}^{0.4}D^{-0.2} +$$

$$0.00122Sk_f^{0.79}c_{pf}^{0.45}\rho_f^{0.49}(T_w - T_{sat})^{0.24}(P(T_w) - P(T_{sat}))^{0.75} / (\sigma^{0.5}\mu_f^{0.29}H_{fg}^{0.24}\rho_g^{0.24}) \quad (1.8)$$

Where $P(T_w)$ is that saturation pressure corresponding to T_w. The functions F and S, given graphically by Chen, can be computed using the following scheme. The inverse of the Lockhart-Martineli parameter is :

$$X_{tt}^{-1} = \left(\frac{X}{1-X}\right)^{0.9}\left(\frac{\rho_f}{\rho_g}\right)^{0.5}\left(\frac{\mu_g}{\mu_f}\right)^{0.1} \quad (1.9)$$

The Reynolds number factor, F, can be computed as

$$\begin{aligned} &F = 1.0 && \text{if} && X_{tt}^{-1} < 0.10 \\ &\text{or } F = 2.35(X_{tt}^{-1} + 0.213)^{0.736} && \text{if} && X_{tt}^{-1} > 0.10 \end{aligned} \quad (1.10)$$

S is the nucleate boiling suppression factor, and can be represented by functions

$$S = \begin{cases} [1+0.12(Re_{TP}^{'})^{1.14}]^{-1}, & \text{if } Re_{TP}^{'} < 32.5 \\ [1+0.42(Re_{TP}^{'})^{0.78}]^{-1}, & \text{if } 32.5 < Re_{TP}^{'} < 70.0 \\ 0.1 & \text{if } Re_{TP}^{'} > 70.0 \end{cases} \quad (1.11)$$

Where

$$Re_{TP}^{'} = \frac{G(1-X)D}{\mu_f}F^{1.25}(10^{-4}) \quad (1.12)$$

The curve fits for F and S were developed by Butterworth [12]. The original data bases covered pressures from 0.17 MPa to only 3.5 MPa, velocity from 0.06 m/s to 4.5 m/s, heat flux up to 2.4 MW/m^2. Because it is physically based and tested for a variety of fluids, however, the extension of the Chen correlation to higher pressures seems to be a reasonable proposition. For further convenience, the two additive portions of the Chen correlation (Equation (1.8)) can be rewritten as:

$$h = h_c + h_{nb} \quad (1.13)$$

Using many experimental data points Russian scientists proposed a correlation, Equation (1.14) for developed nucleate boiling [13].

$$h = [h_c^2 + (0.7h_{pb})^2(1 + 7*10^{-9}(H_{fg}(V_g + V_l)\rho_l / q)^{1.5}]^{0.5} \quad (1.14)$$

Where h_{pb} = heat transfer coefficient for pool boiling case, W/(m^2 s)

V_g = vapor superficial velocity, m/s

V_l = liquid superficial velocity, m/s

$$h_{pb} = 4.34 q^{0.7} (P^{0.14} + 1.37 * 10^{-2} P^2) \quad (1.15)$$

Where P is in MPa, q in W/m^2. Equation (1.15) is based on mass fluxes up to 4-5 Mg/m^2s over a pressure range of 0.1 - 22 MPa; it can be also rewritten as :

$$h = [h_c^2 + h_{nb}^2]^{0.5} \quad (1.16)$$

Subcooled nucleate boiling heat transfer can be computed using the extension to the Chen correlation originally suggested by Butterworth [12], which was compared to varied data by Moles and Shaw [15] within it's original range of parameters (pressure from 0.17 MPa to 3.5 MPa, inlet velocity from 0.06 m/s to 4.5 m/s, heat flux up to 2.4 MW/m^2)

$$q = h_c (T_w - T_b) + h_{nb} (T_w - T_{sat}) \quad (1.17)$$

The single-phase convective heat transfer coefficient (h_c) in Equation (1.17) is calculated using the first part of Equation (1.8) with steam quality equals to zero, which leads to F = 1. Equations (1.11) and (1.12) are used to determine a new suppression factor, S. This extension of the Chen correlation has been reported to compare satisfactorily for subcooled boiling data from water, butyl alcohol, and ammonia [16]. It was found to underpredict the highly subcooled data analyzed by Moles and Shaw [15], but it is not a serious underprediction.

Russian correlations (Equations (1.14)-(1.16)) can be also used for subcooled nucleate boiling region [13] in the form :

$$q = h_c (T_w - T_b) + (0.7 h_{pb}) [1 + 7 * 10^{-9} (H_{fg} (V_g + V_l) \rho_l / q)]^{0.75} (T_w - T_{sat}) \quad (1.18)$$

Shah [17] proposed the following correlation for a high subcooling region

$$q_w = \psi \Delta T_{sat} h_c \quad (1.19)$$

where:

$\psi = 1 + 46\ Bo^{0.5}$ if $Bo < 0.3\ 10^{-4}$

or $\psi = 230\ Bo^{0.5}$ if $Bo > 0.3\ 10^{-4}$

where:

$Bo = q_w / (G\ H_{fg})$ = Boiling number,

G = mass flux, (kg/(m^2 s))

The Chen and Shah equations take into account both two physical processes which occur in the nucleate boiling region: single phase heat transfer and heat transfer by vapor bubbles.

Figure 1-5 shows a comparison between different correlations described above. It is quite clear that the correlations presented above yield quite different values of heat transfer coefficient in the range of interest.

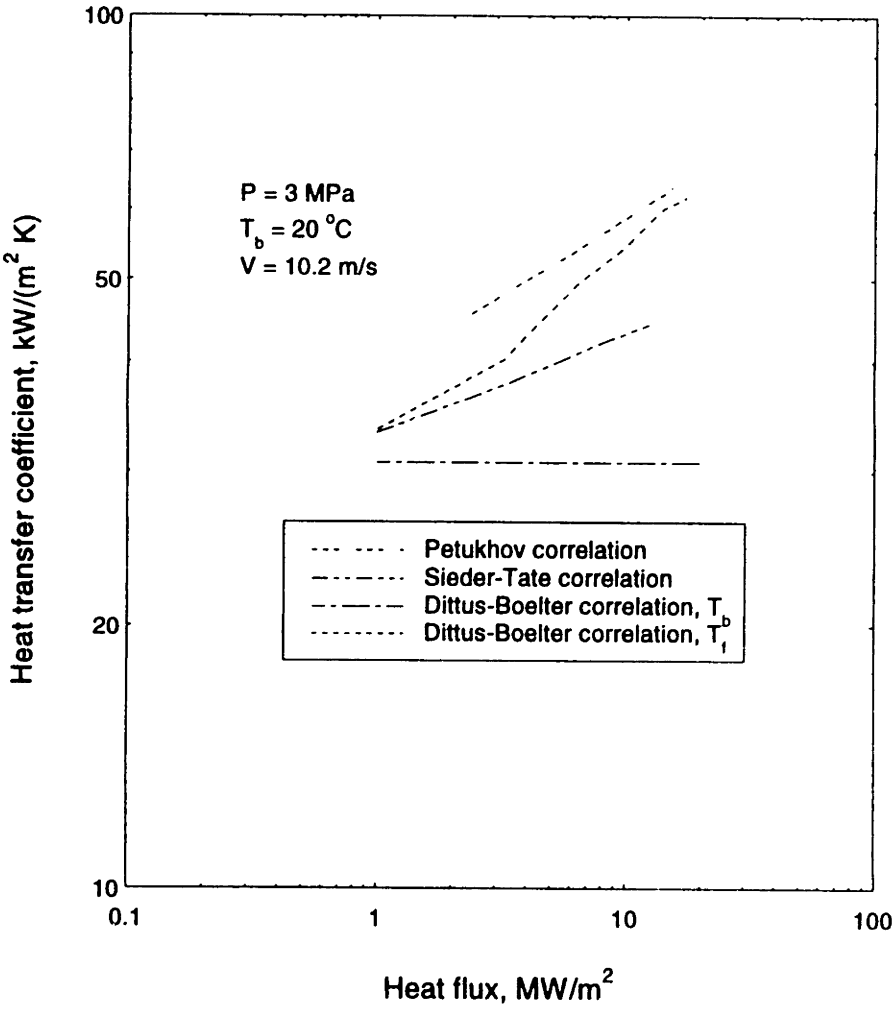

Figure 1-4: Single-phase heat transfer coefficient vs. heat flux

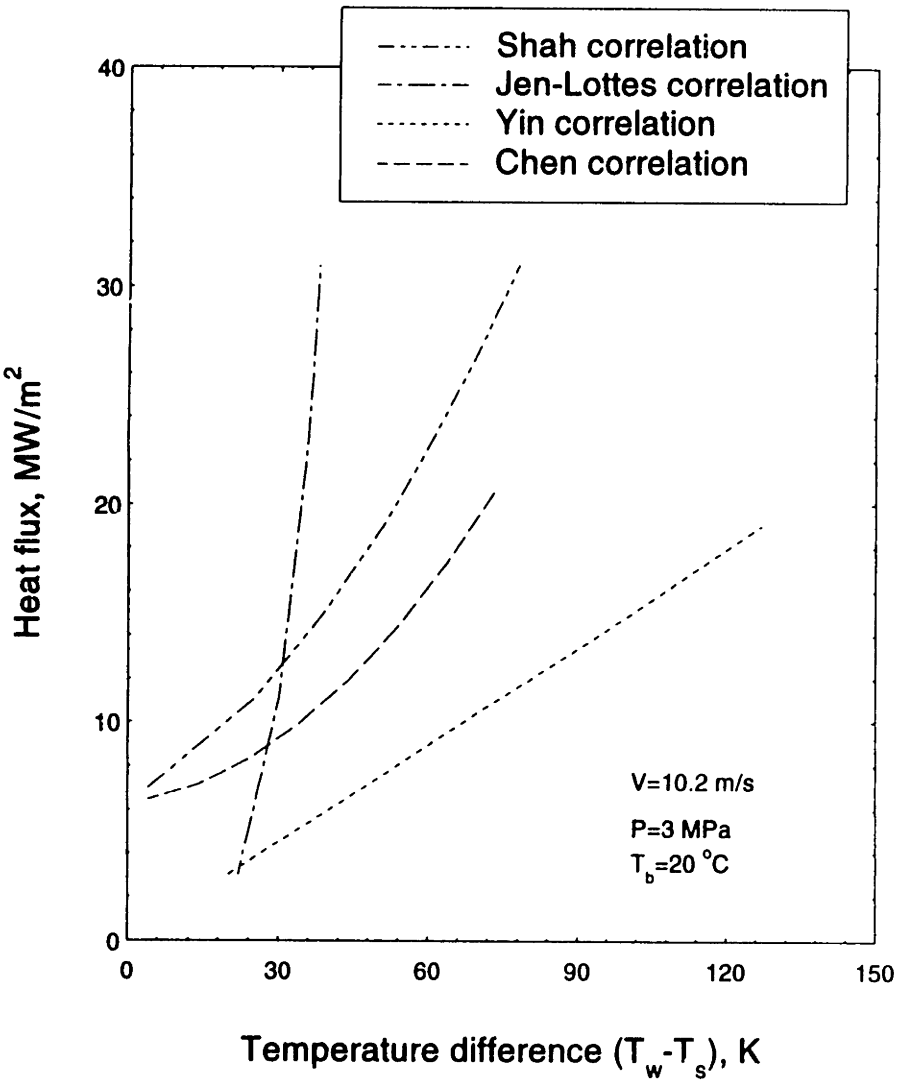

Figure 1-5: Heat flux as a function of wall superheat

1.4.3 Suppression of Nucleate Boiling

Most of the correlations listed above, except Yin's (1.7), predict a very low value of wall temperature difference (wall temperature minus saturation temperature = ΔT_{sat}). However in some specific cases (swirl flow in tubes with internal twisted tapes) [18-20] the values of this temperature difference were found to be very high. Kudryavtsev and Lekakh [20] proposed and proved analytically that steam bubbles at a heated wall can be destroyed by turbulent vortices. Turbulent vortices in swirl flow can be formed due to the centrifugal force and water density gradient. These vectors have opposite directions in the case of a heated tube with internal twisted tape. Their experimental results are shown on Fig.1-6. Interaction between turbulent vortices and a steam bubble is shown on Fig.1-7. Kudryavtsev and Lekakh results [20] show that for low water pressure, nucleate boiling curves of both smooth- and swirl flows merge together, and for high values of pressure (>5 MPa) there is a suppression of nucleate boiling for a swirl flow. But in any case no heat transfer enhancement is proposed for nucleate boiling in swirl flow.

Turbulent influence on steam bubble growth was reported by Vasil'yev and Kirillov [21] for high velocity flows in smooth tubes. For this case the values of transverse velocity oscillations can be very high and the probability of the turbulent vortex destroying vapor bubbles on the wall gets larger as the flow velocity increases.

There are two physical processes which occur in the nucleate boiling region : single phase heat transfer and heat transfer by vapor bubbles. The single phase heat transfer mechanism can be divided into two parts: heat transfer by convection and heat transfer by conduction. These mechanisms cannot exist independently. Thus, in some cases due to water density gradient near the heated wall region, single phase heat removal is enhanced (the physical mechanism of these phenomena is very similar to natural convection) and is higher than typical forced single-phase heat transfer rate.

Equations (1.5) and (1.6) can predict heat transfer removal by vapor bubbles, because $\Delta T_{sat} \sim q^{.25...0.5}$.

Yin's correlation (Equation (1.7)) shows that $\Delta T_{sat} \sim q^{1}$, but it empirically incorporates not only single phase heat removal, but also some heat removal by vapor bubbles. Unfortunately, there is no flow velocity in Equation (1.7) and, hence, it is impossible to determine when nucleate boiling begin to be suppressed. It is quite clear that for these conditions (high flow velocities) nucleate boiling is suppressed, because for some high values of heat fluxes, wall temperature is very close to the value of Homogeneous Nucleation Temperature. Because water cannot exist as a liquid phase at temperatures greater than Temperature of Homogeneous Nucleation (THN), it is quite obvious that this can be a limit for the case of suppressed nucleate boiling.

The homogeneous nucleation limit (THN limit) is the limit that has not been discussed widely in the literature concerning fusion reactor thermal hydraulics. However, the heat fluxes are so high that this mechanism may be present, especially in a region of suppressed nucleate boiling due to high velocity as will be discussed later on.

Chen's correlation can take into account both single phase and nucleate bubble heat removal. It also shows that for high velocities (high values of Re'_{TP}) there is suppression of nucleate boiling. Also the correlation has single-phase enhancement factor F, which increases with the two-phase mixture velocity. There is no influence of wall heat flux (q) on this enhancement factor (F), but it is obvious that there must be such influence. For high values of wall heat flux, there will be many bubbles near the wall and it will be impossible to enhance single-phase heat removal.

The Russian code correlation shows that there is some suppression of nucleate flow boiling and this suppression factor is equal to 0.7 (see Equation (1.18)). But this suppression factor is a constant number

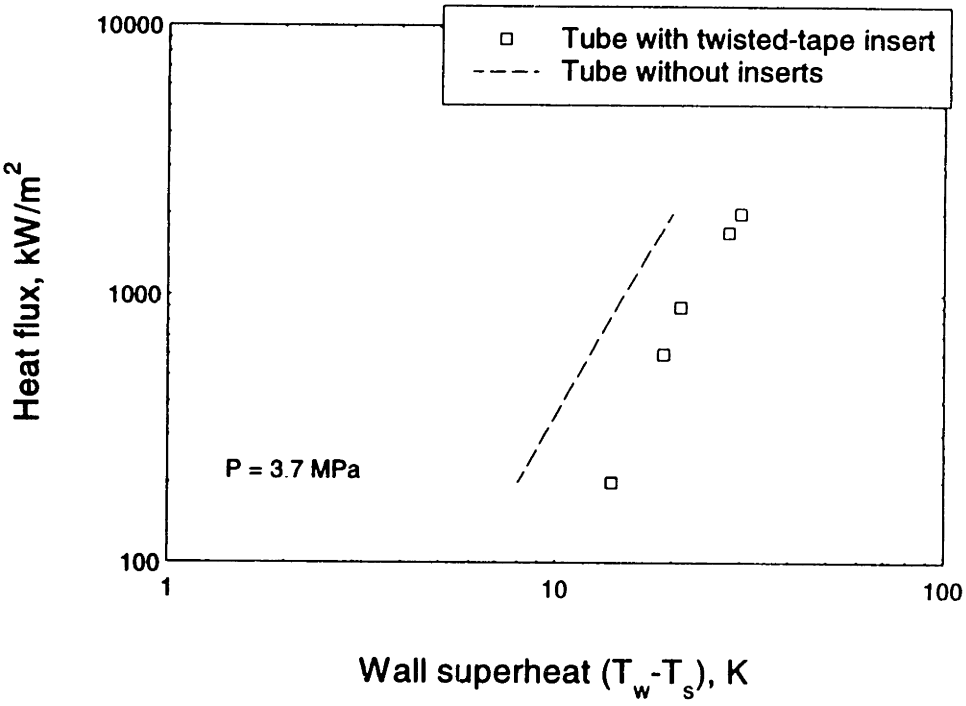

Figure 1-6: Heat flux vs. wall superheat, from [20].

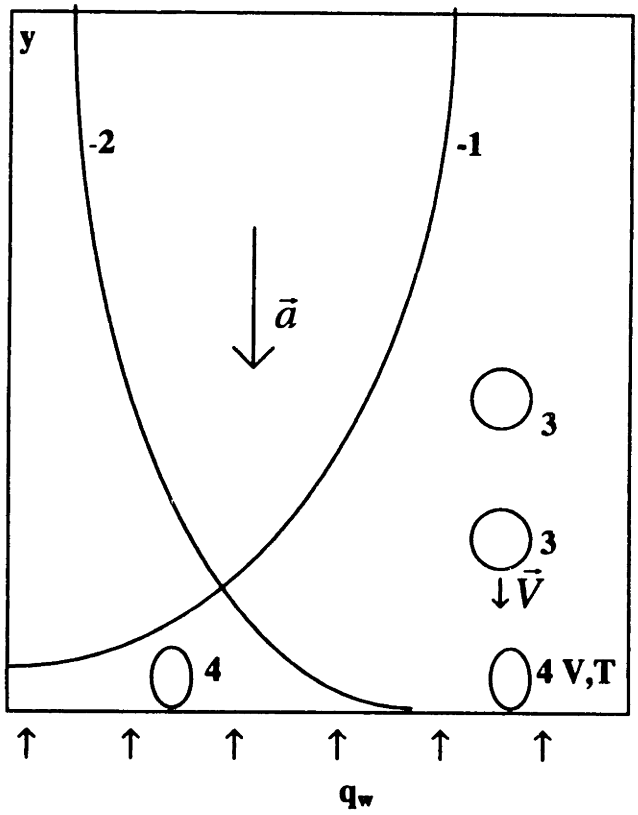

Figure 1-7: Effect of turbulence on vapor nuclei, from [20].
1 - Fluid velocity profile (V = V(y));
2 - Fluid temperature profile (T =T(y));
3 - Turbulent lump;
4 - Bubble nucleus on the heated wall.
$\vec{a}$ - Centrifugal acceleration

and does not change with flow velocity, which is physically unrealistic. In comparison with Chen's correlation, the enhancement factor is a function of wall heat flux (again see Equation (1.18)).

It seems that both the Chen and Russian code correlations (both are semi-empirical) account for heat removal by conduction through a water film in annular flows. For high flow velocities the liquid film on the wall is very thin and heat removal through conduction can be very high. For this case the enhancement factor F in Equation (1.8) and number $\frac{H_{fg}(V_g + V_l)\rho_l}{q}$ in Equation (1.18) have very high values. Although it is unrealistic to have a thin liquid film on the wall in the presence of very high heat fluxes, but Chen's correlation would predict high heat removal for this case due to the thin water film presence on the heated wall.

Continuing validation and improvement of nucleate flow boiling correlations are necessary. So are the development of new correlations and the collection of new relevant data, especially for the region where the suppression of nucleate boiling can occur. There is an influence on the steam bubble growth for a high velocity flows. For high velocity flows in the subcooled region a Homogeneous Nucleation Temperature limit can be reached, which will produce an unwanted CHF.

1.4.4 Critical Heat Flux

The literature contains many CHF data and correlations, and several theories exist for the physical mechanisms [22]. Hechanova [23] provided a good review of CHF data as related to fusion reactor divertor conditions. He found that, except for a few investigators, the data are usually outside the operating parameter space of divertors both in flow conditions and in heat flux profiles. Nevertheless, many studies have shown that very high heat fluxes can be accommodated by using highly subcooled water at very high velocities.

Since most empirical correlations and analytical models have a limited range of application, the need for a more general technique is obvious. Attempts have been made in the former USSR to construct a table of CHF values for a given standard geometry - a circular tube with D = 8 mm (Doroshchuk et al. [25]). The CHF Table development has been continued at Chalk River Nuclear Laboratories and completed at the University of Ottawa by Groenveld et al. [24]. A comparisons between data from [24] and [25] are shown on Figures 1-8 and 1-9. It is very clear from these figures that extrapolations for higher velocity can be done, subcooling extrapolations can be done only for very rough estimation of CHF.

Hechanova [23] derived a CHF correlation based upon experiments having low to high mass fluxes (1 to 10 Mg/m^2s), very high subcooling (an exit equilibrium quality typically less than -0.45), moderate pressures (about 3 MPa), and single-sided heating. Fifteen bench mark CHF points were used to determine the parameters of a phenomenological equation partly based upon the method of Tong (1975) [26]. The correlation was tested against a database containing 202 points having comparable thermal hydraulic parameters. The correlation, below, was found to predict the trend of the data and even appears to be a low bound. It may thus be an appropriate conservative limit for design applications for extremely high flow subcooling.

$$St_{CHF} = 50\frac{\rho_l}{\rho_v}\left(\frac{1}{Ja} + 0.0021 p_r^{1.8}\, Re^{0.5}\right)\left(1 + \frac{10}{20 + L_h / D}\right) Pr^{0.6}\, Pe^{-0.9} \qquad (1.20)$$

The main parameter-space constraints are Pe greater than 70,000, St_{CHF} less than 0.0065 for hydraulically fully-developed, smooth tube flows in large (greater than 5 mm) diameter tubes. The recommended range of main parameters are Pe (70,000 to 1,000,000), pressure (1 to 7 MPa), coolant channel diameter (5 to 25 mm), and heated length to diameter ratio (5 to 80).

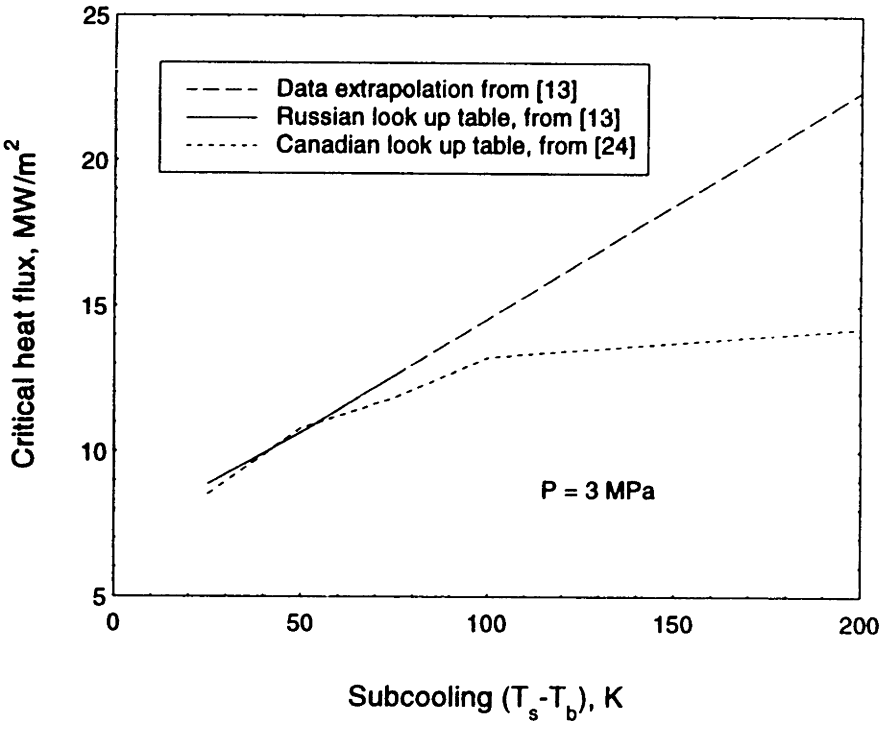

Figure 1-8: Critical heat flux vs. subcooling (T_s - T_b).

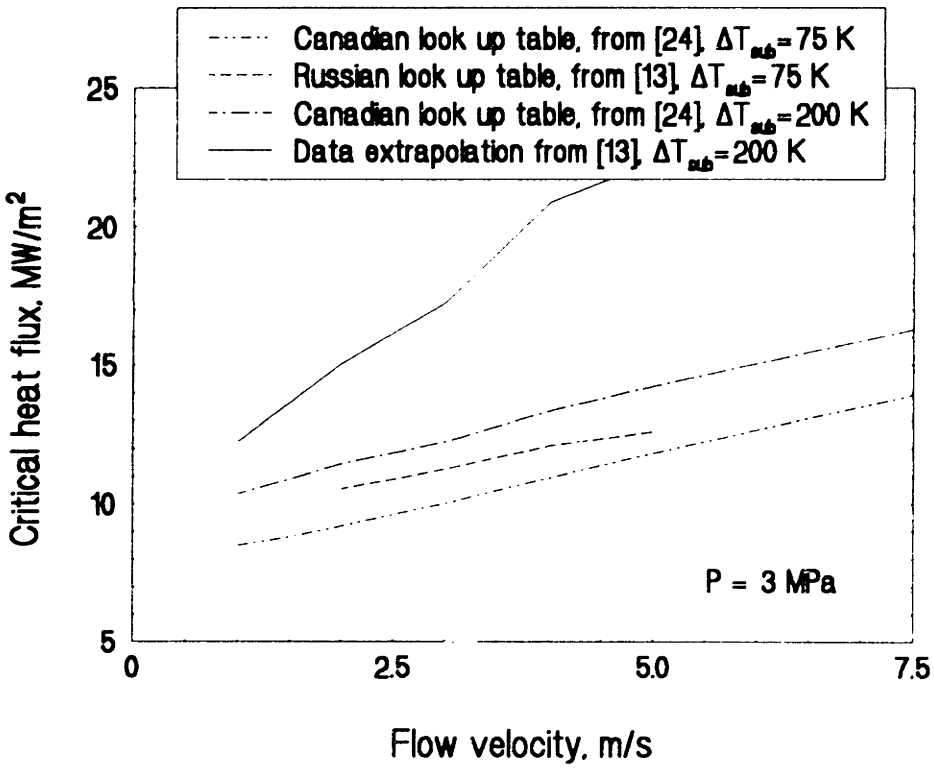

Figure 1-9: Critical heat flux vs. flow velocity as predicted by some look up tables.

It is quite clear that because St_{CHF}=CHF/(G C_{pl} (T_s-T_b)) Equation (1.20) will predict CHF = 0 for saturated flow and/or very small values of CHF for relatively small values of subcooling. Hence, it can be used only for CHF predictions in a very highly subcooled flows.

Traditional design practices suggest that tube destruction by melting will proceed rapidly when local wall CHF limit is reached. However, theoretical and experimental research by Tanchuk [27] suggest that it is possible for a divertor plate's incident heat flux to exceed its local CHF by as much as 80% before causing global distruction of the plate.

Experiments using the Sandia National Laboratory Electron Beam [33] have started to address critical heat flux questions for fusion applications. These experiments use an electron beam focused onto a coolant tube to emulate divertor thermal boundary conditions. Using water at the inlet temperature of 30 °C and pressurized to 1.14 MPa, incident critical heat flux values of 40 MW/m^2 were achieved in unobstructed flow. The addition of internal twisted tapes to increase CHF lead to an incident critical heat flux of 60 MW/m^2. Koski et al. [34] found good agreement between their nine experimental data points and the 1975 Tong critical heat flux correlation (Tong-75 correlation) [35]:

$$\dot{q}_{CHF} = 8C_0C_1GH_{fg}(1+0.0021p_r^{1.8}\,Re^{0.5}\,Ja)\left(\frac{GD_h}{\mu_l}\right)^{-0.6}\left(\frac{D_h}{D_o}\right)^{0.32} \qquad (1.21)$$

Where:
$\dot{q}_{CHF}$ = Critical Heat Flux, W/m^2
C_0C_1 = 0.23
p_r = Reduced pressure (absolute pressure/critical pressure)
D_h = Heated perimeter, m
D_o = 0.0127 m (reference diameter).
Mass flux (G) and Reynolds number (Re) are calculated for the total flow for subcooled flow case.

This correlation was based on data at very different conditions having much lower subcooling and higher pressure (relevant mostly to fission reactors). The original data used by Tong [35] for the above correlation are shown in Table 1.2.

Table 1.2: Range of Data in Tong-75 Critical heat Flux Correlation

Channel Geometry	Heat Flux Distribution	P MPa	Void Fraction	G Mg/(m^{2}s)	Data Points
Circular Tube	Uniform	7-14	< 0.35	0.5-4.4	469
Annulus	Uniform	10.5-14	< 0.30	1.0-3.0	317
Rod Bundle	Non-Uniform	7-18	< 0.61	0.5-4.3	201

The use of this correlation for fusion reactor components goes beyond the range listed in Table 1.2. Therefore, Koski et al. [34] indicate that the choice of the Tong-75 correlation is somewhat arbitrary and the close comparison to their data may be fortuitous.

A contemporary correlation suggested by Inasaka and Nariai (1993) [36] intended to extrapolate the Tong (1968) critical heat flux correlation (Tong-68 correlation) [37] from a recommended pressure range of 7-14 MPa to 0.1-7 MPa. TheTong-68 correlation is as follows:

$$\dot{q}_{CHF} = \frac{C_{Tong}H_{fg}G^{0.4}\mu^{0.6}}{D^{0.6}} \qquad (1.22)$$

Where:

$C_{Tong} = 1.76\text{-}7.433\ X_{ex} + 12.222\ X_{ex}^2$
X_{ex} = Thermal equilibrium steam quality at tube exit

Inasaka and Nariai modified C_{tong} for the pressure range 0.1-7 MPa as follows:

$$C_{Tong}(\text{modified}) = C_{Tong}(1 - 52.3 + 80X_{ex} - 50X_{ex}^2 / 60.5 + (P * 10^{-5})^{1.4}) \quad (1.23)$$

Where:
P = Pressure, MPa
Yin et al [38] found out that the predictions by this modified correlation are somewhat conservative, compared with the Tong-75 correlation.

Celata et al. (1994) [39] recently developed a mechanistic model to predict CHF based on dryout of a thin liquid layer beneath an intermittent vapor blanket formed by the coalescence of small bubbles. The model was tested on an extensive data base. Agreement with 1888 data points (from various sources) was typically within 30%, however, the minimum exit quality of the data base was above -0.35. Hechanova [23] found out that Celata's model greatly overpredicts CHF at high mass fluxes. Furthermore, for high subcooled flow with little thermal boundary layer development, the ability of a bubble layer to exist away from the wall is doubtful since any vapor that forms should condense very close to the wall. On the other hand, the bubble departure criterion is surpassed in the low flow data. For low flow data, the thermal boundary layer has a much better opportunity to develop and agreement with the Celata et al. [39] prediction suggests that the mechanism assumed is plausible, provided a different temperature profile is assumed.

1.5 Comments

Analysis of the existing data has indicated that very little data exist to validate characterization of the thermal hydraulic phenomena expected in a divertor. This characterization is integral to design procedure and the main motivation of the present study.

Chapter 2 will expand on the current phenomenological understanding of limiting heat fluxes and detail heat transfer mechanisms in water cooling at high heat flux that will be used in subsequent chapters to aid in deciphering experimental data.

Chapter 2

Implications of High Heat and Mass Flux on the Mechanisms for Heat Transfer

2.1 Suppression of Nucleate Boiling Phenomena

In order to explain the results of high values of wall superheat for swirl flow, which were discussed briefly in Chapter 1, it was postulated [20] that steam bubbles at the heated wall are destroyed by turbulent vortices. For swirl flow, turbulent vortices can form due to the centrifugal acceleration force and density gradient (see Figure 1-5). These vectors have opposite directions in the case of a heated tube with internal twisted tape. If the steam bubble is growing near the turbulent vortex the kinetic head associated with a transverse velocity gives rise to a net force per unit area

$$\tau = \rho_f V^2 / 2 \tag{2.1}$$

The forces associated with this kinetic head can destroy the bubble. To find the condition for the bubble's growth Kudryavtsev and Lekakh [20] considered the dimensionless number

$$A = \tau r / (2 \sigma) \tag{2.2}$$

where r = vapor bubble radius
If $\tau >> 2 \sigma / r$ or $A >> 1$ the bubble will be destroyed, if $\tau << 2 \sigma / r$ or $A << 1$ the bubble has an opportunity to grow. It was found [23] that for low pressure (0.1 to 1.5 MPa) the nucleate boiling curves of both smooth- and swirl flows merge and for high values of pressure (P>2 MPa) there is suppression of nucleate boiling for the swirl case. In any case, no enhancement factor is proposed for subcooled boiling in swirl flow.

The only realistic explanation for Yin's observations [7] (see also Equation 1.7) of high values of wall superheat is that suppression of nucleate boiling occurs due to interaction between turbulent vortices and vapor bubbles on the heated wall. For smooth flow, the movement of a turbulent vortex is chaotic, in comparison with the swirl flow case where it can be called semi-chaotic. However, for extremely high values of axial velocity the values of transverse velocity oscillations can become very high and the probability of the turbulent vortices destroying vapor bubble on the wall can be relatively large.

It is usual to consider that a vapor bubble in thermal equilibrium with the surrounding liquid has a radius given by [30]

$$r > r^* = \frac{2\sigma T_s}{\rho_g H_{fg} \Delta T_s} \tag{2.3}$$

The size of the smallest turbulent vortex (η) can be evaluated using [28]

$$\eta = (\nu_l^3 / \varepsilon)^{0.25} \tag{2.4}$$

where: ν_l = liquid kinematic viscosity

The average energy dissipation rate per unit mass in a tube of diameter D

$$\varepsilon = f V^3 / (2 D) \tag{2.5}$$

The value of friction factor can be evaluated as

$$f = \frac{0.316}{Re^{0.25}} \tag{2.6}$$

The value of superheat (ΔT_s) can be obtained from

$$\Delta T_s = \left(\frac{dT}{dy}\right) l \tag{2.7}$$

where: $\left(\frac{dT}{dy}\right) = \frac{q}{k_f}$, and

l = thermal boundary layer thickness, m.

It is logical to make an assumption that the distance l is proportional to ν_f / V^*, where V^* is the characteristic velocity. It is assumed that for the value of l the characteristic velocity may be set equal to the axial flow velocity. Hence,

$$\Delta T_s = \frac{q\nu_f}{k_f V^*} \tag{2.8}$$

It follows from (2.4) - (2.8) that

$$\frac{\eta}{r^*} = \left(\frac{\nu_f^3 D}{0.5 f V^3}\right)^{0.25} \left(\frac{H_{fg} q \rho_g \nu_f}{2\sigma T_s k_f V}\right) \tag{2.9}$$

For P = 3.5 MPa, q = 10 MW/m^2, V = 7 m/s the value of η / r^* obtained from Equation (2.9) is equal to 0.53. Hence $\eta < r^*$ and the vapor bubble can be destroyed if it is located near a turbulent vortex, because if $\eta > r^*$ the vapor bubble can penetrate inside the vortex. On Figures 2-1 and 2-2, η / r^* ratio is plotted for different heat fluxes as a function of diameter and flow velocity. From these figures it is very clear that the probability of nucleate boiling suppression increases as the flow velocity increases and/or channel diameter decreases. That is one can expect. As the velocity goes up the turbulence transverse velocity oscillations become larger and the probability that turbulent vortex will touch the wall and destroy a vapor bubble also is larger for smaller diameter channels than for larger channels. This simplified analysis argues that there are interactions between turbulent vortices and steam bubbles.

Now let us assume that transverse velocity can be expressed as

$$v = (b)^{0.5} V \tag{2.10}$$

where b is a coefficient that can be obtained from the experimental data. It follows from Equations (2.10) and (2.2) that for smooth flow

$$A = \frac{b\rho_f V^2}{4\sigma} r \tag{2.11}$$

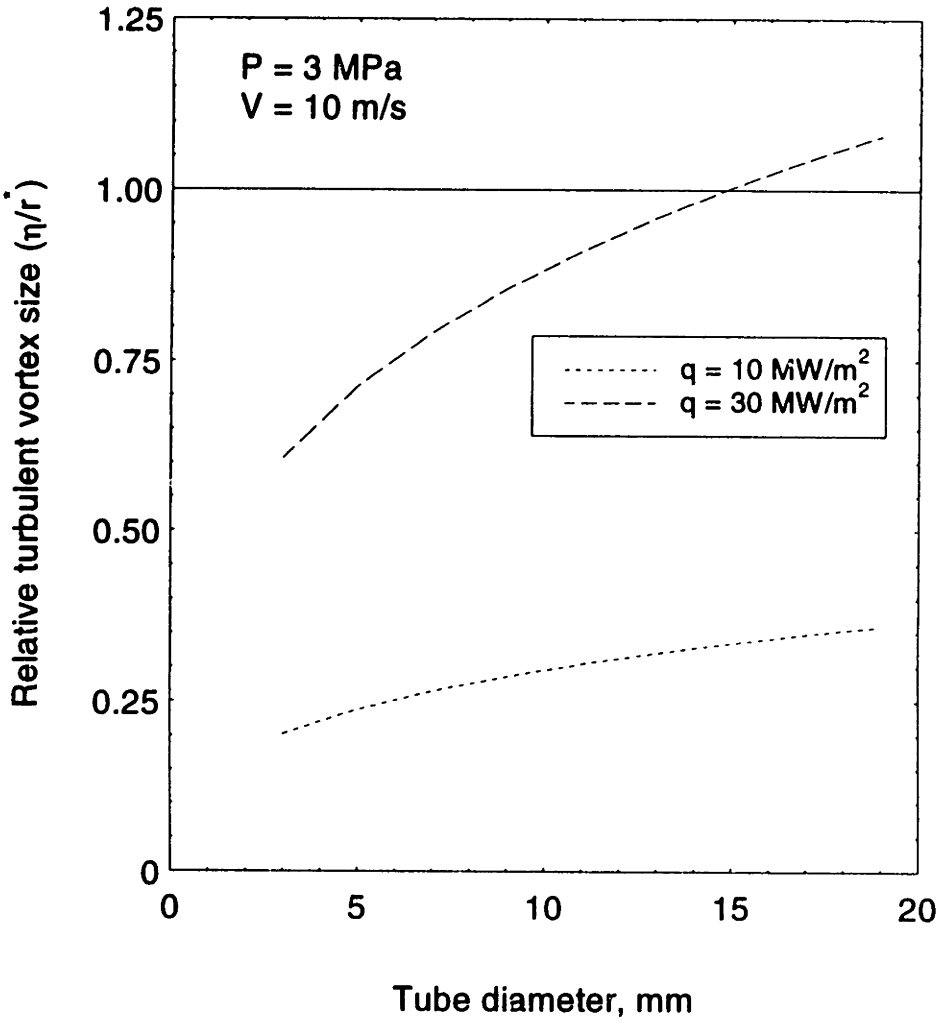

Figure 2-1: Relative vortex size vs. tube diameter

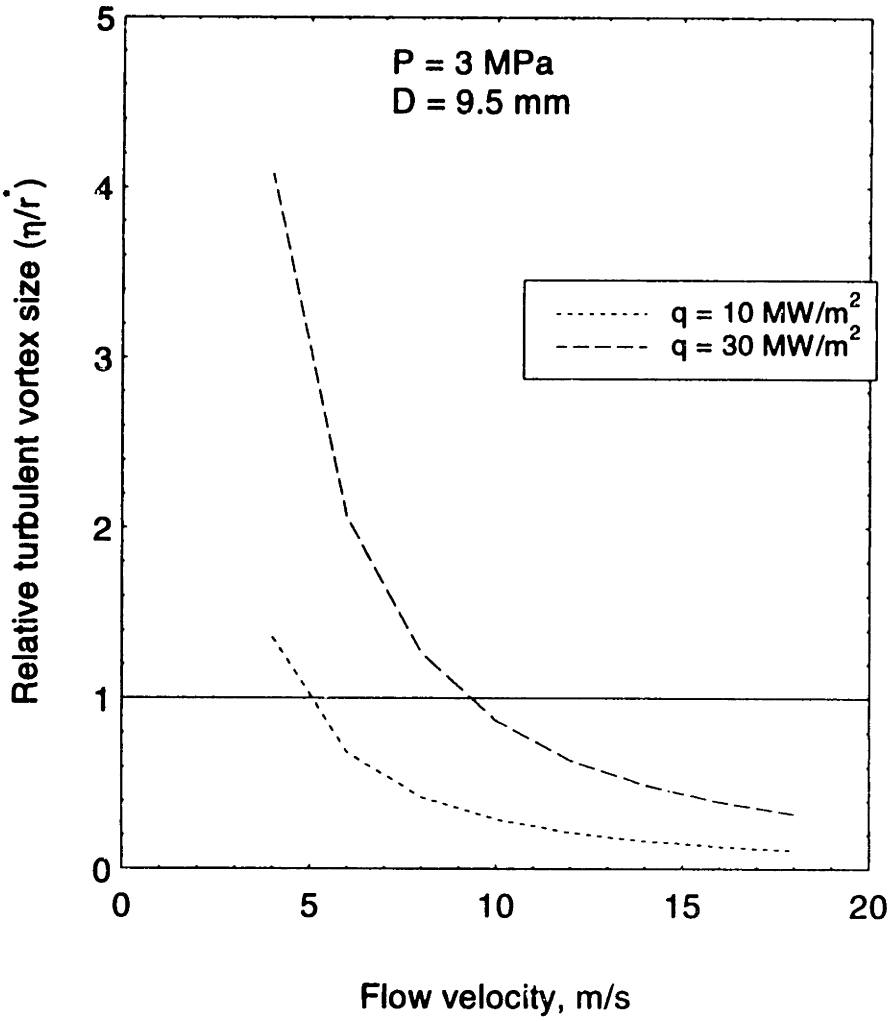

Figure 2-2: Relative vortex size vs. flow velocity

As previously we did for the value of l, it is reasonable to assume that r is also proportional to v / v^*. For this particular case v^* must be equal to the vapor velocity which is proportional to the value of $q / (H_{fg} \rho_g)$. Hence,

$$A = \frac{b \rho_f V^2 H_{fg} \nu_f \rho_g}{4 \sigma q} \tag{2.12}$$

Yin's results [7] may be used to find the value of b

$$b = 333150 ((T_w - T_s) / T_s)^{3.85} (7.6 / V)^2 (\rho_g / \rho_l) \tag{2.13}$$

where values of temperatures are in °C. Yin's data points are shown on Figure 2-3 as are the data points obtained in [20] for swirl flow. Using these data a correlation to find the heat transfer coefficient for both swirl and smooth high velocity flows is obtained as:

$$h / h_{nb} = 0.7 A^{-0.23} \tag{2.14}$$

Where the value of h_{nb} is calculated using Equation (1.18) for fully developed (non-suppressed) nucleate boiling and the value of h corresponds to the heat transfer coefficient for the flow where nucleate boiling can be suppressed. It should be noted also that while general expressions for the dimensionless number A are the same for both swirl and smooth high velocity flows (see Equation (2.2)), the particular Equation for A for swirl flow according tc [20] is calculated as

$$A = (8.5\ 10^8)\ \rho_f\ a\ \beta\ (\nu_f / V)^2 (H_{fg}\ \nu_f \rho_g / (2\ \sigma\ k_f)) \tag{2.15}$$

Equation (2.12) should be used only for smooth high velocity (V > 7 m/s) flows in a water pressure range of 2 to 11 MPa.

Because the same curve (Equation (2.14)) was obtained for both cases the conclusions can be made that there is an influence of turbulent vortices on steam bubble growth and the nature of this phenomena for both swirl and smooth high velocity flows is the same.

2.2 Departure from Nucleate Boiling Heat Flux Limit

The existence of a CHF caused by departure from Nucleate Boiling (DNB) could limit the utilization of water as a coolant for the ITER divertor plates. The DNB phenomenon is now generally accepted as being mainly of hydrodynamic origin. The mechanism is one where sufficient liquid is unable to reach the heating surface due to the rate at which vapor is leaving the surface. Critical heat flux corresponding to DNB can be characterized as a limiting vapor volumetric flux from the heated surface. In other words CHF occurs when vapor generation at the hot wall prevents effective heat removal from the surface and the temperature of the surface material increases. This temperature increase can occur rapidly especially in cases with very high wall heat fluxes and the wall material strength can be degraded or melted.

Many investigations have been made of DNB and its characteristics; the physical nature of this phenomenon is clear now. But even now the CHF characteristics caused by DNB conditions for extremely high mass flux and high subcooling are not well known. However, even for highly subcooled and high flow applications, CHF caused by DNB can in principle be a limiting factor.

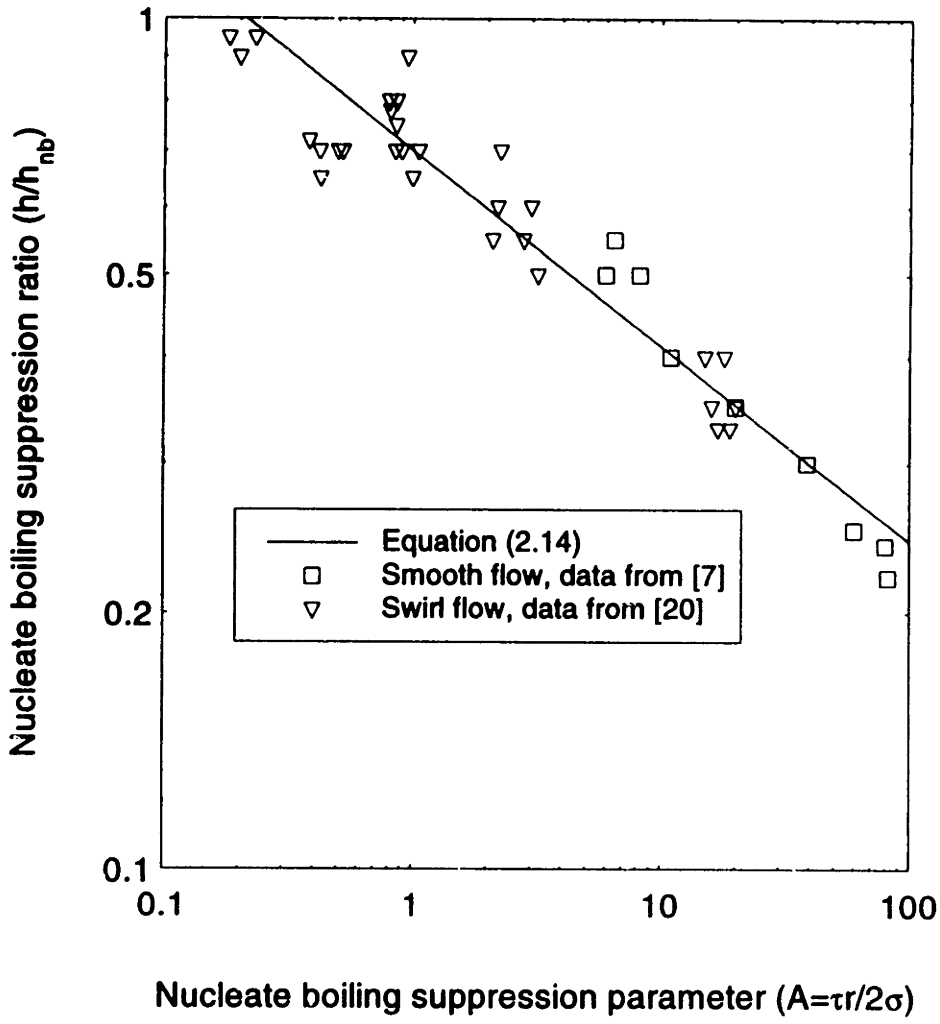

Figure 2-3: Heat transfer coefficients in the region of suppression of nucleate boiling

2.3 Homogeneous Nucleation Limit

Under ordinary conditions the heat flux limit depends on the DNB phenomenon. But for high water temperatures it is important to consider another thermo-fluid limitation for single-phase liquid water, called the Temperature of Homogeneous Nucleation (THN) or the temperature limit of water superheat. The attainable values of water superheat, obtained by Skripov et al. [29] are shown on Figures 2-4, 2-5. THN is usually a function of log(J), where J is spontaneous nucleation rate per unit volume. On Figures 2-4 and 2-5 the curve which corresponds to the Lienhard [30] THN correlation (Equation (2.16)) is also shown.

$$THN_r - T_{s,r} = 0.905 - T_{s,r} + 0.095 \left(T_{s,r} \right)^8 \qquad (2.16)$$

where subscript r means reduced temperature value (absolute temperature (K) / the critical temperature (K)). The meaning of the curves presented on Figures 2-4 and 2-5, is that for nucleate boiling heat transfer regimes the wall temperature should likely be between the saturation temperature and THN.

For convective flow at relatively low velocity, this limit is usually disregarded because at the value of CHF due to DNB, the wall temperature is less than the value of THN (see Figure 2-6). This will take place if the region of developed nucleate boiling exists at values of heat flux smaller than CHF based on DNB.

If nucleate boiling is suppressed, the THN limit can be reached before the heat flux corresponding to DNB can be reached. CHF corresponding to DNB usually increases steadily with increasing mass flux (see Figure 1-7) and subcooling (see Figure 1-6) due to the increase of the available liquid. Thus, for relatively low velocity the THN limit is typically disregarded.

But if nucleate boiling is suppressed the homogeneous temperature limit can be reached earlier than the CHF limit, which is growing steadily with the increase of the mass flux and subcooling. The THN limit can occur in smooth tube high velocity flows and at heat flux less than the expected CHF value. In particular, a THN limit can occur if the flow has low bulk temperature and high velocity. The limit is reached when there are no steam bubbles on the heated wall. When the value of flow velocity is not high and/or the bulk temperature is high, the CHF is reached at the point when there are steam bubbles on the heated wall.

When the wall temperature reaches THN, nucleation occurs spontaneously in the liquid even with a complete absence of preferred nucleation sites on the wall. Various cases are shown on Figure 2-7 for CHF limits. Equation (1.7) was obtained for flow velocities greater than about 6 m/s, for this case the THN limit may prevail. This limit can be evaluated, if $q''_{CHF} < q_{onb}$, by:

$$q''_{CHF} = h_c (T_{HN} - T_b) \qquad (2.17)$$

and, if $q''_{CHF} > q_{onb}$, by:

$$q''_{CHF} = h_{nb} (T_{HN} - T_s) + h_c (T_{HN} - T_b) \qquad (2.18)$$

where: T_{HN} = Homogeneous Nucleation Temperature, K;
T_b = Bulk coolant temperature, K;
T_s = Saturation temperature, K;
h_{nb}, h_c, = heat transfer coefficients (see Equation (1.17)).

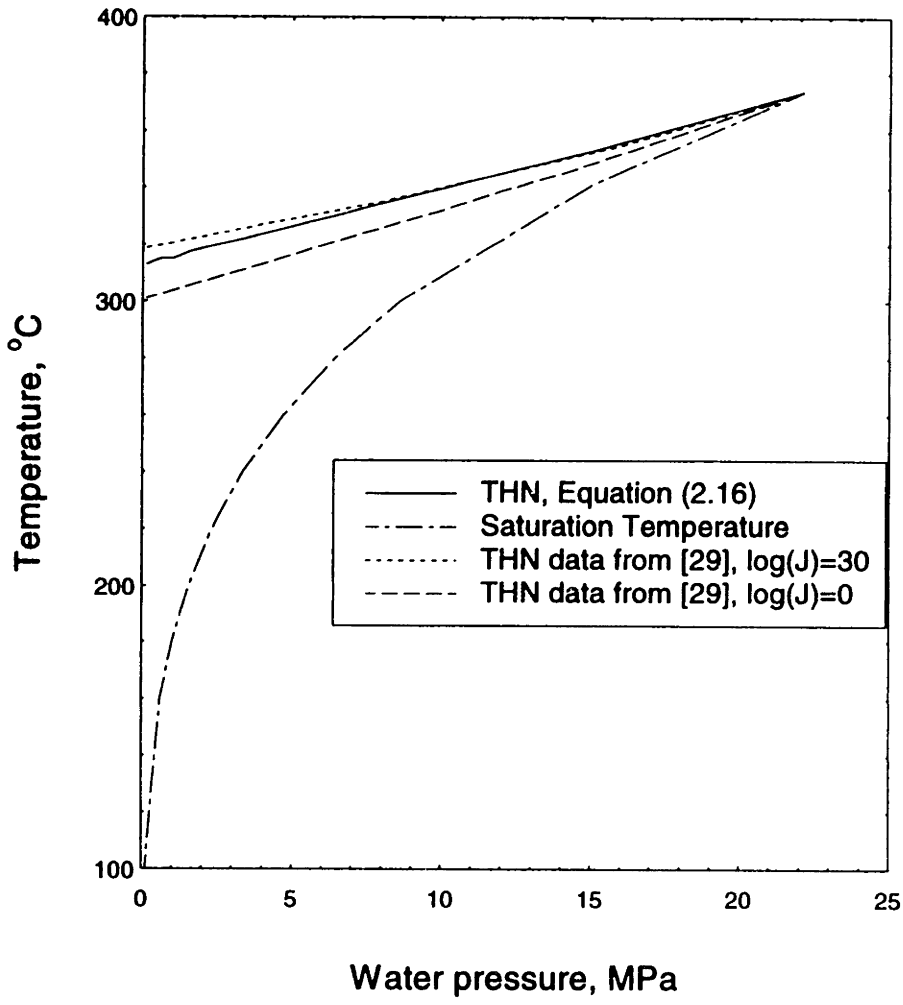

Figure 2-4: Temperature of Homogeneous Nucleation (THN) vs. water pressure

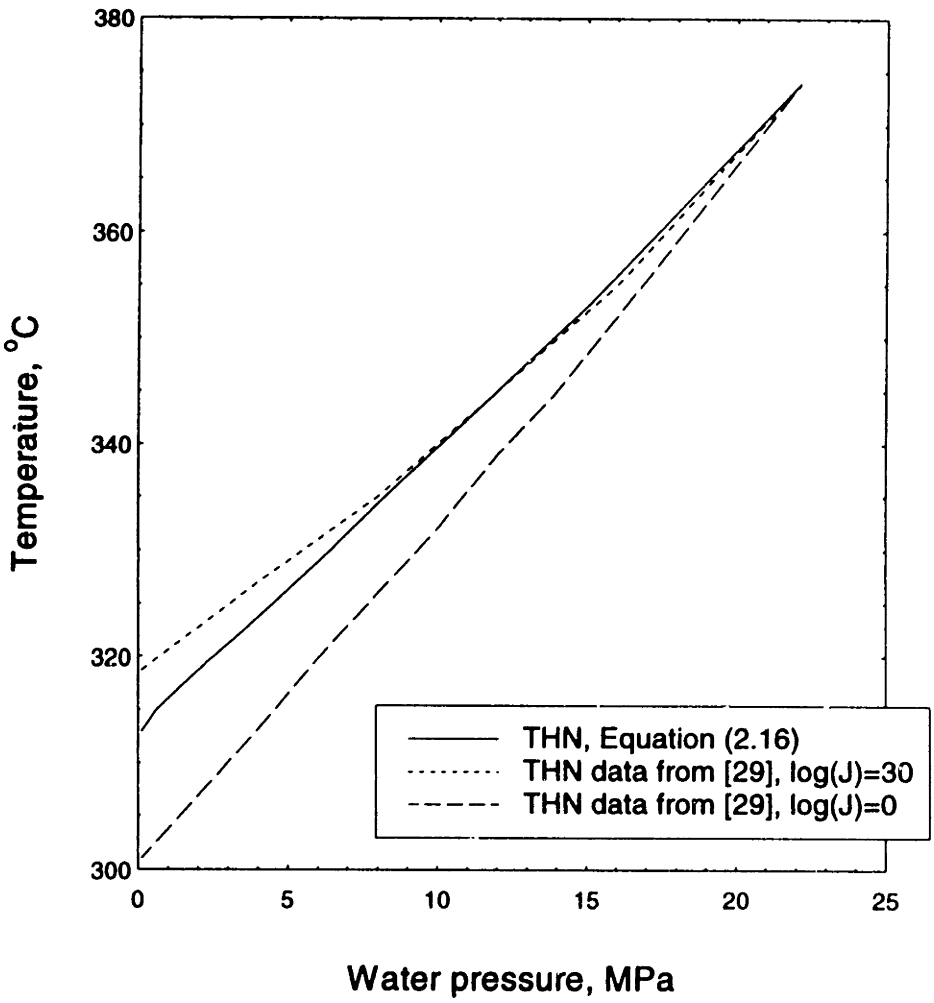

Figure 2-5 : Temperature of Homogeneous Nucleation (THN) vs. water pressure

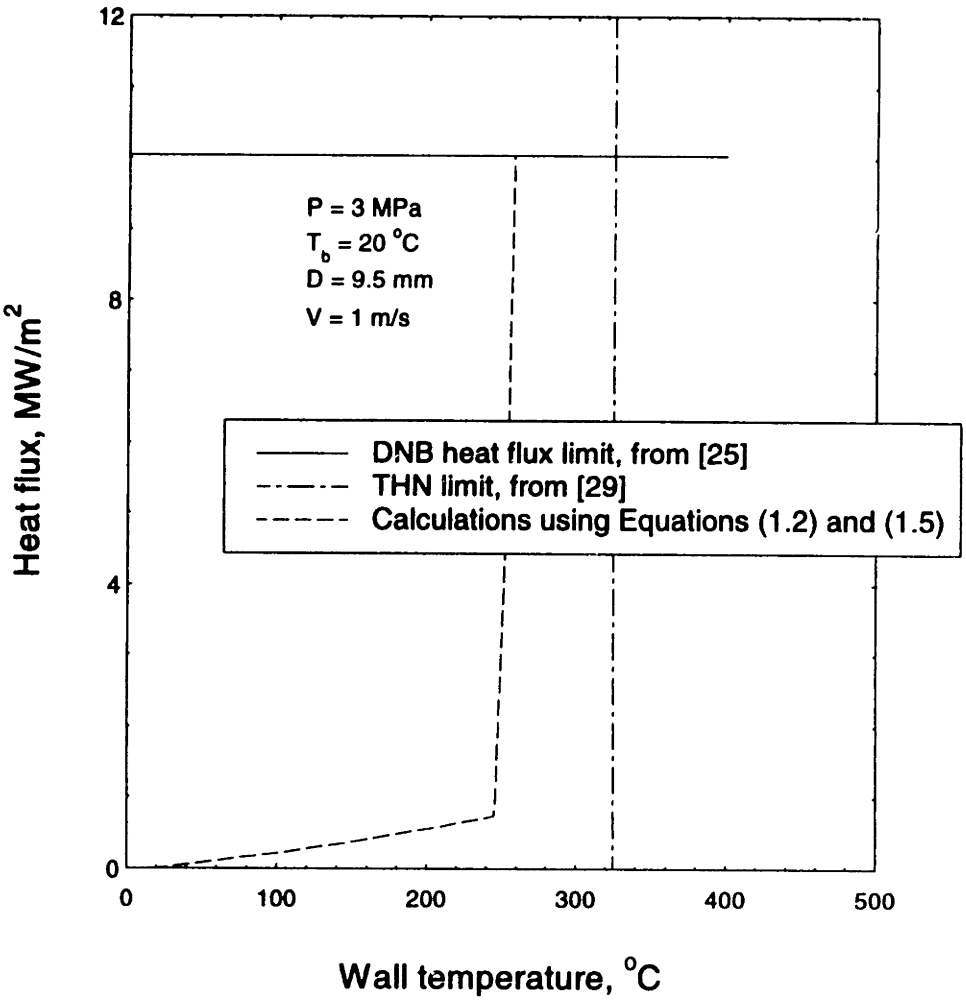

Figure 2-6: Heat flux limits for the low velocity region

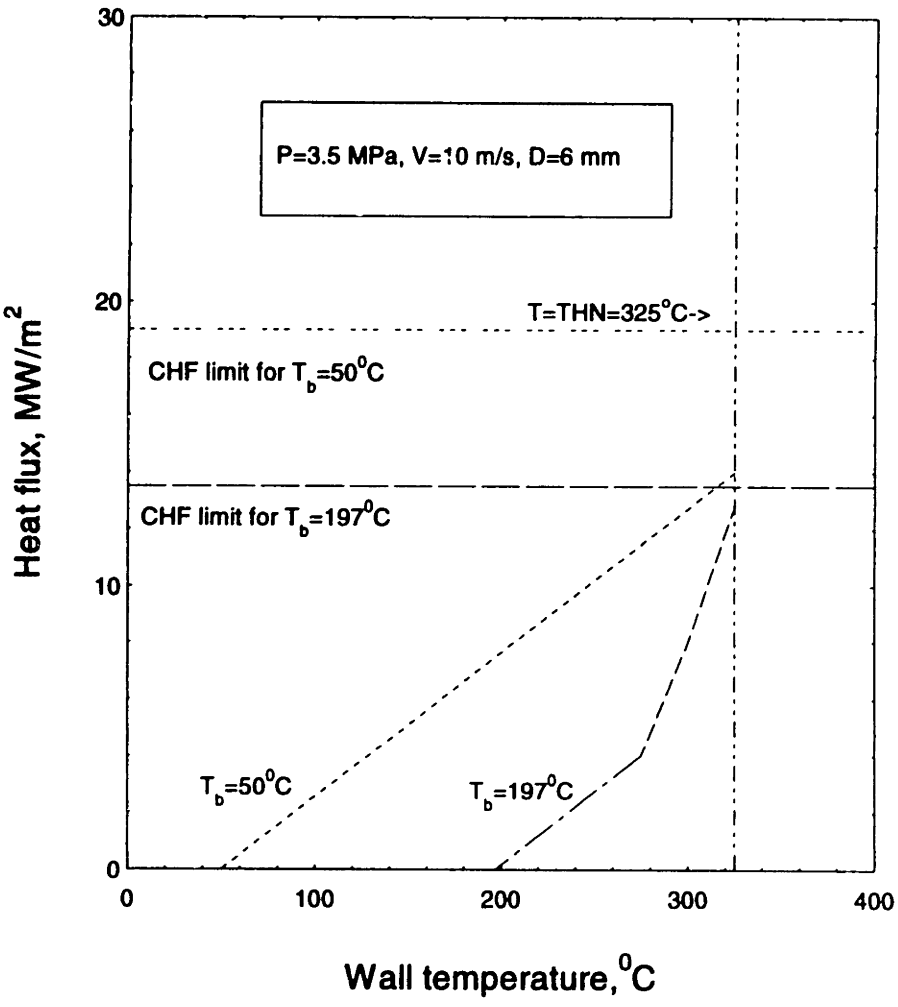

Figure 2-7: Heat flux limits in the region of suppression of nucleate boiling

The values of the single-phase convective heat transfer coefficient (h_c) can be obtained using any of the well established correlations for this region (see Chapter 1). The value of the nucleate boiling heat transfer coefficient (h_{nb}) for the conditions of interest can be obtained from Equation (1.7).

The results obtained with the help of Equations (1.7), (2.17) and (2.18) with $\gamma = 1$ are shown on Figure 2.8 for a high degree of subcooling. The heat flux limit due to DNB is also shown on Figure 2.8. This curve was obtained by extrapolation of the data from tables given in [25].

Similar results can be obtained if Chen's correlation - Equation (1.8) is used for calculations in Equation (2.18). Results for this approach are shown on Figure 2.9 for low subcooling. For this case when nucleate boiling is not suppressed, THN heat flux limit is only slightly below the CHF limit due to DNB phenomena.

The fact that THN limit in the last example lies below the CHF limit due to DNB phenomena suggests that homogeneous nucleation can be the mechanism leading to CHF for the suppressed boiling conditions of high velocity flows.

2.4 Comments

Turbulent vortices have significant influence on the vapor bubble growth for high velocity flows.

Two causes exist for CHF. One is the (DNB) flux limit and the other is the temperature (THN) limit. For flow velocities less than 5 m/s and for flow in a finned tube sheet, the flux limit is always lower than the temperature limit. For other cases, special attention is required to consider this temperature limit, often neglected in flow boiling research. The THN importance is that it may produce an unwanted CHF at unexpectedly low heat flux.

Continuing validation and improvement of CHF correlations are necessary. So are the development of new physically based correlations and the collection of new relevant data.

This chapter has indicated that there is still much to be determined about high heat flux fusion reactor components. This is evident that the mechanisms mentioned above must be used in order to develop correlations for single-phase and nucleate boiling regions.

This chapter has also illustrated analytical tools to help identify and define different heat transfer mechanisms. Equation (2.9) and Figure 2-7 best illustrate the importance of considering suppression of nucleate boiling mechanism in heat transfer analysis for high velocity high heat flux flows.

Equations developed in this chapter should be considered as preliminary. The purpose of their derivation was just to show from very simple models that the suppression of nucleate boiling phenomenon and a temperature limit (THN) for high heat flux, high velocity flows exist.

The following two chapters outline the experimental apparatus and computational procedure used to investigate possible heat transfer mechanisms in water cooling at high heat flux. Subsequently, raw results and interpretation will be presented; and a new correlations will be proposed for fusion divertor applications.

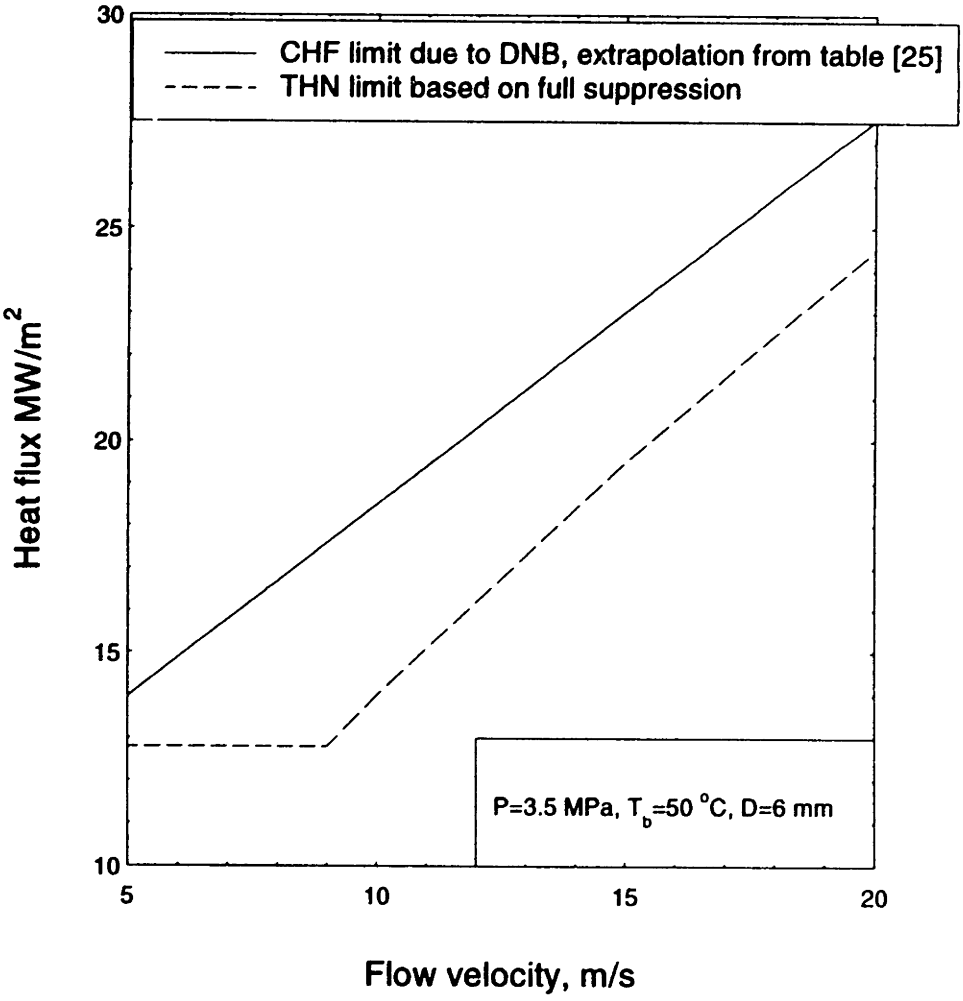

Figure 2-8: Heat flux limits due to DNB and THN at high subcooling

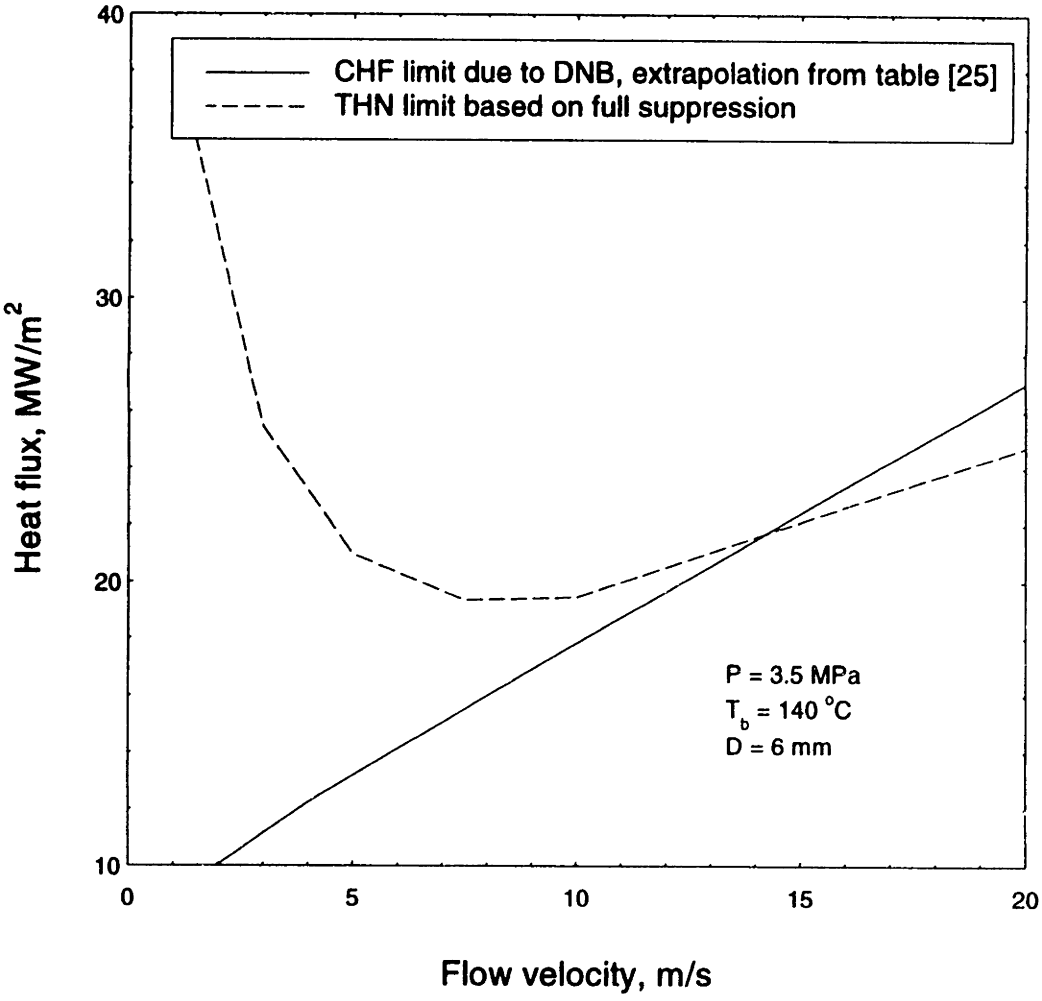

Figure 2.9: Heat flux limits due to DNB and THN at low subcooling

Chapter 3

Experiments

3.1 Experimental apparatus

Heat transfer experiments under representative azimuthally non-uniform conditions have been performed by Hechanova [23] and subsequently by the present author using the same heat transfer apparatus. Hechanova was interested in the CHF limit, while in the present work we are interested in the entire range of pre and post CHF regimes as well. The purpose of this study is to obtain heat transfer rates for single-phase and nucleate boiling regimes in order to verify the ideas presented in Chapter 2.

Figure 3-1 shows a schematic of the open loop in which water was pumped from Tank 1 to Tank 2 during an experimental run and then recirculated back to Tank 1 between runs using a bypass loop. The pump is a 16-stage centrifugal pump with stainless steel wetted components to minimize corrosion. A stainless ball valve upstream and needle valve downstream were used to adjust the coolant pressure and velocity. The pressure was measured downstream of the test section, but before the needle valve, using a Bourdon gauge. A current-controlled 45 kW Power Supply provided up to 2200 Amps to the test section heater.

The test section was resistively heated by passing current through a thin tungsten layer (76 mm long x 0.25 mm thick) which was plasma sprayed over an alumina coating (about 0.1 mm) as indicated in Figure 3-2. The alumina coating electrically isolates the copper coolant channel walls from the tungsten. The copper is too conductive to have any significant volumetric heating should current find a path through the alumina. If electric current does flow into the copper, however, the current limitation of the power supply causes a noticeable drop of the test section power.

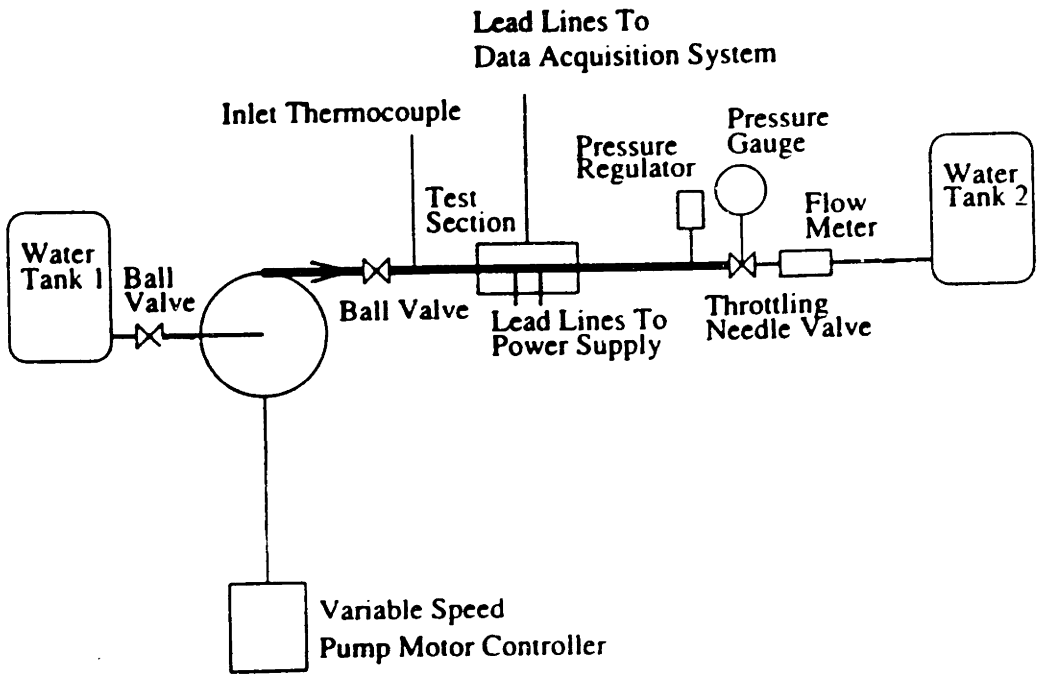

Figure 3-1: Schematic of the thermal hydraulic experimental loop [23].

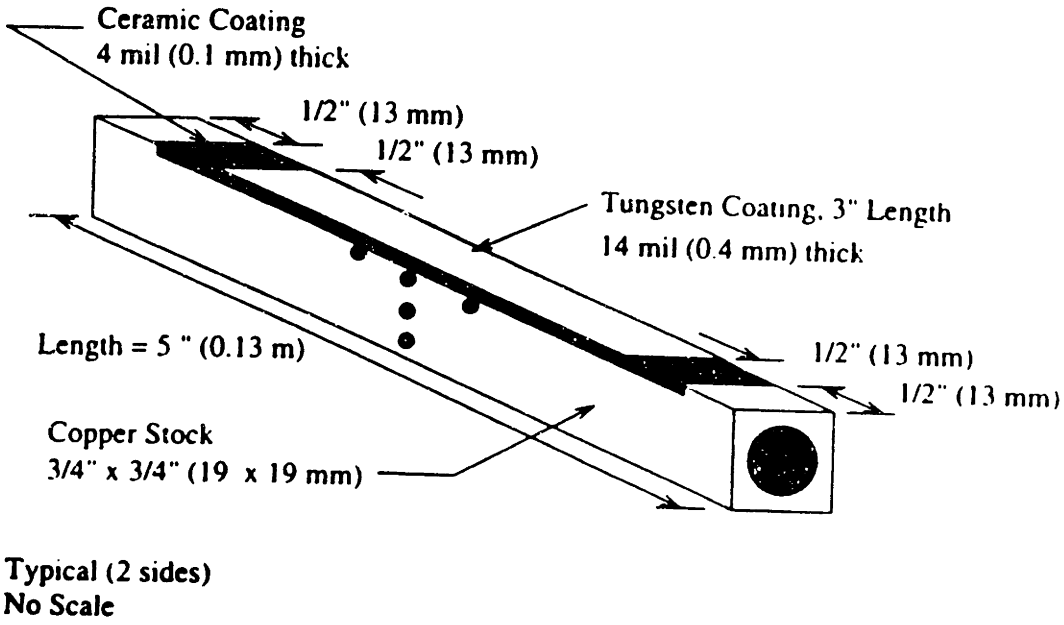

Figure 3-2: Test section sketch

The coolant flowed through a 9.5 mm diameter channel in the center of the 19x19x130 mm copper block.

A computerized data acquisition system capable of reading and storing thermocouple voltages, the flowmeter signal and the electrical power was set up. Full description of this system is given in [23].

Five thermocouples were placed at the non-coated side of the test section such that three thermocouples measured the wall temperature close to the heater and two thermocouples measured the wall temperature at other positions on the midsection wall. A thermocouple was also placed on the entrance-length pipe far enough from the heater to measure the inlet bulk temperature. All thermocouples used in this study are K-type.

The experimental facility was operated within the test ranges given in Table 3.1.

Table 3-1: Test range of present study

Parameter and/or Variable	Tested Range	Units
Pressure	1.79 - 3.01	MPa
Inlet temperature	19 - 23	°C
Velocity	3 - 20	m/s
Tube inner diameter	9.5	mm
Heated length	50	mm

3.2 Experimental Procedure

This section details the experimental procedure for gathering, and the method of calculating the thermal hydraulic variables such as the coolant velocity and incident heat flux. The next chapter will indicate a computer modeling procedure for heat transfer coefficient, local heat flux and nucleate boiling interpretations. Table 3.1 contains the test matrix used in the present study. The coolant velocity was the main parameter which was varied and high velocities (about 20 m/s) were achieved. The experiment data were logged using the data acquisition scanner which eventually creates text files of the data for the thermocouples, flow meter, resistor (heater and shunt), voltages measurements. The operator controlled the power supply, pump speed and manually logged the current and voltage reading from the power supply, the shunt resistor voltage from the voltmeter, and the pressure from the test gauge. The precise procedures are delineated below.

The following step-by-step procedure was performed by the operators. It typically took just 10 to 15 minutes to perform and resulted in a steady flow established with known pressure, velocity and inlet bulk coolant temperature. The current to the test section was stepped up slowly by small increments of about 100 A. At a given power level (e.g., at each 100 A current increment), the test section heating was allowed to stabilize (which took on the order of a ten - twenty seconds). At this time, the power supply current and shunt resistor voltage were logged. Then the power supply voltage was logged. If legible, the tank water levels were noted with time of day. measurements were taken until component failure (usually accompanied by flashing and/or arcing on the test section heater). The resulting data were manual readings of power supply voltage and current, shunt resistance voltage and tank water levels versus time, flow meter readings at the beginning and at the end of test run; and, a computer file containing the heater, shunt resistor and five thermocouple voltage measurements versus time.

All thermocouples are standard 20 or 28 gauge chromel-alumel (K-type) thermocouples. Thermocouple voltages were measured via a data acquisition (Daqware) conditioning module which outputs a voltage between 0 and 5 V. These voltages were linearly calibrated with temperature according to the following equation

$$T = 290\,U - 100 \tag{3.1}$$

where: T = Temperature (°C),
U = Daqware thermocouple voltage measurement (V).
The Daqware flow measurements (e.g., recorded at the beginning and end of a test run) were converted into frequency using a Fortran code written by Hechanova [23].

The incident heat flux (defined in the present study as the power input to the tungsten per unit area) is simply determined using the following expression

$$q_o'' = I\,V / A_h \tag{3.2}$$

where: q_o'' = Incident heat flux (W/m^2),
I = Power supply current (A),
V = Electrode voltage potential (V),
A_h = Heater area (m^2).

Other hydraulic variables such as pressure, inlet and outlet temperatures were measured directly with no further manipulation.

Heat transfer coefficients and the coolant side heat fluxes were obtained using the measurements described above for steady state regions of the power curves versus time and wall temperatures versus time using computational modeling technique. This technique is discussed in the next chapter.

It is clear that the presence of particles in the flow near homogeneous nucleation may cause nucleation at lower heat fluxes. Conductivity measurements of water samples were done by Hechanova [23]. A Cole-Parmer conductivity meter [31] was used to measure the water conductivity. The electrical conductivity of coolant water for present study was about 75 μΩ/cm. Thus, although filtering system does not produce freshly distilled water, the water used in the present study is on the lower end of the potable water range.

Chapter 4

Computational Modeling

This chapter details the computational modeling aspect of the method of solution used for single phase heat transfer region analyses and nucleate boiling heat transfer region analyses in the present study. First, the problem is described and outlined. Subsequently, the details of analyses are delineated and the solution methods are defined. Finally, the results of interest to the present study are discussed.

4.1 Problem definition

Heat transfer phenomena and representative quantities, such as the heat transfer coefficients, applicable to the coolant side of the test section cannot be calculated directly from the measurements described in the previous chapter. However, the measured heat deposition and outer wall temperatures profiles can be used to determine inner wall heat transfer coefficients by solving the heat conduction problem.

In his study Hechanova [23] used a multi-dimensional heat conduction computer code entitled HEATING7.2 [32] with temperature dependent thermal properties in order to calculate temperature profiles the test section. This was done with the assumption that heat transfer coefficients for single phase and nucleate boiling regions are known, because HEATING7.2 requires a single heat transfer coefficient as the boundary condition on a region of the coolant side. However, practically no one has checked before the acceptability of well known correlations for fusion reactor divertor thermal-hydraulic conditions (see Chapter 1). There are no reports in the literature so far that Petukhov single-phase correlation (Equations (1.2) and (1.3)) cannot be used for single-phase high velocity flow, but there are many contradictions about using heat transfer correlations for nucleate boiling in high velocity flows. So, even though HEATING7.2 computer code can give very precise results, because of very high probability of errors in the input file (heat transfer coefficients as a boundary conditions) there is a high chance that the output results (local heat fluxes at the test section inner surface) could be incorrect. The only way to validate the final results of these calculations is to compare a measured outer wall temperature profile to a calculated one. This was done in [23]. It was found that only ~50% (17 out of 30) test runs temperature profiles were consistent with the temperature profiles calculated by the help of the HEATING7.2 computer code.

But even for those seventeen data points which fall into the category of consistent temperature analyses, it is impossible to say that the heat transfer coefficients for inner wall were correct. This is mainly due to non-uniform heating. With this type of heating involved there are at least two regions inside the test section with possibly different heat transfer mechanisms. One is single phase convection region and the other is nucleate boiling region. The heat transfer coefficient will vary axially and azimuthally around the coolant channel. Thus, for example, if a correlation predicts a higher value of heat transfer coefficient for single phase region and a lower value for nucleate boiling region, the net result of the calculations can be consistent with an experimental measurement. The last statement also makes it impossible to use HEATING7.2 or some analogous computer codes for heat transfer coefficient predictions. All these codes require an iterative solution since heat transfer coefficients for highly subcooled flows for single phase and nucleate boiling regions are functions of the inner wall temperatures. Even though it is possible by change heat transfer coefficient values by trial and error methods to get the solution, the likelihood of getting a good answer is pretty small.

It was decided for the present study to create a computational modeling technique that will allow more accurate estimate the values of heat transfer coefficients. Because the test section has unheated ends, it is necessary to solve this problem for both azimuthal and axial directions. New model predictions should be close enough to the HEATING7.2 calculations if both codes use the same values of heat transfer coefficients. With an assumption that the Petukhov correlation (Equations (1.2) and (1.3)) is valid for

divertor conditions, another acceptance criterion can be established. The results for a pure single phase region should be consistent with the Petukhov correlation.

Heat conduction analyses should result in the conversion of experimental thermal power input and wall temperature measurements to wall heat flux distributions in azimuthal and axial directions and heat transfer coefficients (without the use of correlations). This was achieved by creating a multi-dimensional heat conduction code described in the next section. The heat conduction was divided into two problems (axial and azimuthal) which were solved independently.

4.2 Axial Heat Conduction

The final goal of solving this problem is to obtain an axial heat flux distribution. This can be achieved by treating the test section as a finite fin with no heat transfer at the two unheated edges of the test section (13 mm each). The test section specifications for this case are shown in Figure 4-1.

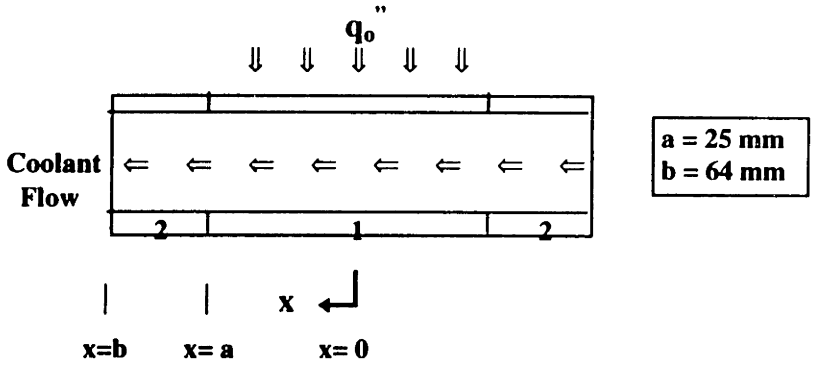

Figure 4-1: Test section geometry for the axial direction

For zone#1 we have heat input in the form of incident heat flux (q_o''). Heat is removed by water flowing through channel. It was assumed that because of the high velocity flow we have, there is no bulk coolant temperature increase inside the test section due to heating. This assumption can be made because the difference between exit and inlet temperatures for V = 3.67 m/s (minimum value of velocity for the present experiments), N = 12 kW (maximum power for this velocity) is equal to 10 °C. Because of the large incident heat fluxes during all experiments (on the order of several MW/m^2 , wall temperatures on the order of hundreds degrees), the difference of even ten degrees in bulk temperature does not lead to significant errors in the heat transfer coefficient values defined in this study as

$$h = q_{local} / (T_{w,local} - T_b) \qquad (4.1)$$

The incoming heat is removed from zone#1 by water going through the test section and by axial conduction into zone#2. Treating this problem as one-dimensional we can write the following heat balance equation

$$\frac{q_o''\delta}{kA} = -\frac{d^2T_w}{dx^2} + \frac{\Pi h(T_w - T_b)}{kA} \qquad (4.2)$$

where δ = width of the test section (m),
Π = inner wall perimeter (m),
h = heat transfer coefficient ($W/(m^2 K)$),
A = test section cross-section normal to x-axis (m^2).

Equation (4.2) can be simplified as following

$$\frac{d^2\theta}{dx^2} - \beta^2\theta = -\frac{q_o''\delta}{kA} \tag{4.3}$$

where: $\beta = \sqrt{\frac{\Pi h}{Ak}}$,

$\theta = T_w - T_b$

For zone#2 there is no incident heat flux ($q_o'' = 0$) and for this case Equation (4.3) becomes

$$\frac{d^2\theta_w}{dx^2} - \beta^2\theta = 0 \tag{4.4}$$

Due to symmetry, the problem was solved only for half of the test section; axial conduction beyond the test section is neglected; boundary conditions are as following

$$\frac{d\theta_1}{dx}(x=0) = \frac{d\theta_2}{dx}(x=b) = 0 \tag{4.5}$$

Continuity of axial heat flow and temperatures at the zones# 1 and 2 interface implies:

$$\frac{d\theta_1}{dx}(a) = \frac{d\theta_2}{dx}(a); \quad \theta_1(a) = \theta_2(a) \tag{4.6}$$

Because in reality heat is also transported azimuthaly the test section perimeter is defined as

$$\Pi = \pi D s \tag{4.7}$$

where s = some unknown coefficient, which will be defined later in this chapter.

The solutions of differential Equations (4.3) and (4.4) are

$$\theta_1(x) = C_1 \sinh(\beta x) + C_2 \cosh(\beta x) + \frac{q_o'' b}{\Pi h} \tag{4.8}$$

$$\theta_2(x) = C_3 \sinh(\beta x) + C_4 \cosh(\beta x) \tag{4.9}$$

Constants C_1 to C_4 are found numerically using boundary conditions (Equations (4.5) and (4.6)). The input parameters for these calculations are: test section geometry, copper thermal properties, incident heat flux, the heat transfer coefficient and the s parameter (see Equation (4.7)) originally set equal to one. The heat transfer coefficient for this part of the problem (not for the azimuthal one of the next subsection) was obtained from the Petukhov correlation (Equations (1.2) and (1.3)). Then the s parameter was changed until an experimental thermocouple reading of wall temperature close to the heater at the midsection position (thermocouple TC2; see Figure 4-2) was obtained from calculations.

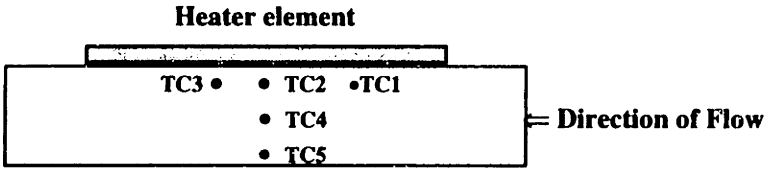

Figure 4-2: Test section thermocouple locations

Then for this condition the value of axial peaking factor was calculated as following

$$pf_x = \frac{h\theta(0)}{q_o''} \tag{4.10}$$

In order to justify the use of the computational modeling described above, a comparison is made with HEATING7.2 computer code calculations with same values of heat transfer coefficients in the input file. This comparison is presented in Figure 4-3. As one can see, there is good agreement between the two methods of calculations. This is mainly due to two reasons. The first reason is that copper is a very good conductor (k = 380 W/(m K)), thus 1D approximation is not too bad for this type of calculations. Second, there is a parameter s (see Equation (4.7) with the help of which it is possible to take into consideration the conduction in azimuthal direction. In all calculations the value of s is less than one, and the physical meaning of it is that some part of the inner wall perimeter does not transfer heat via convection.

In Figure 4-4 the value of axial peaking factor is shown as a function of heat flux. As the velocity goes up more heat will transfer via convection, which means that more heat will go directly to the coolant using the shortest way. That means increasing of the local heat flux or the peaking factor coefficient. Results shown in Figure 4-4 also prove the importance of performing multi-dimensional analyses for this test section rather than considering only a heat conduction problem in azimuthal direction.

4.3 Azimuthal Heat Conduction

The purpose of solving this problem is to obtain the circumferential heat flux distribution for the midsection position (maximum heat flux position). Like the previous section, the test section is treated as a finite fin, but now in the azimuthal direction. The test section is divided into three zones (see Figures 4-5, 4-6).

For zone#1 the incoming heat flux (q_{inc}) is calculated as

$$q_{inc} = q_o'' \, pf_x \tag{4.11}$$

where the peaking factor value for the azimuthal direction was obtained using Equation (4.10).

It was assumed that the values of heat transfer coefficients for zones#2 and 3 are equal to each other ($h_2 = h_3$). Calculations showed that no boiling occurs in zones#2 and 3 because wall temperatures there are less than saturation temperature. For low values of the incident heat flux and for $T_w < T_s$ for zone#1 it was assumed that the value of heat transfer coefficient for this zone (h_1) is equal to the values for zones#2 and 3, or in other words $h_1 = h_2 = h_3$. An assumption was made that when $T_w > T_s$ for zone#1 (nucleate boiling in zone#1) $h_{2,3}$ have the same values as they had for $T_w = T_s$ for the same specified value of coolant velocity.

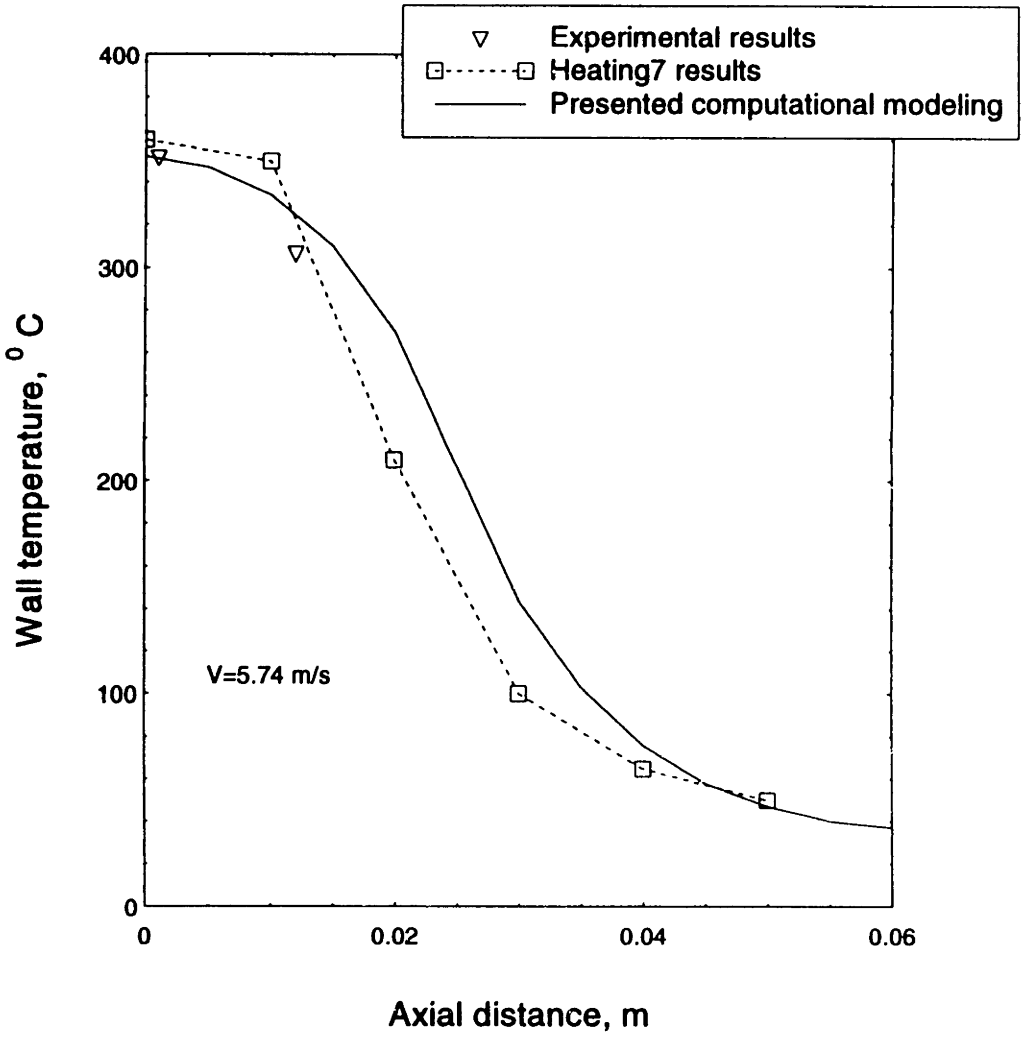

Figure 4-3: Outer wall temperature profile in the axial direction

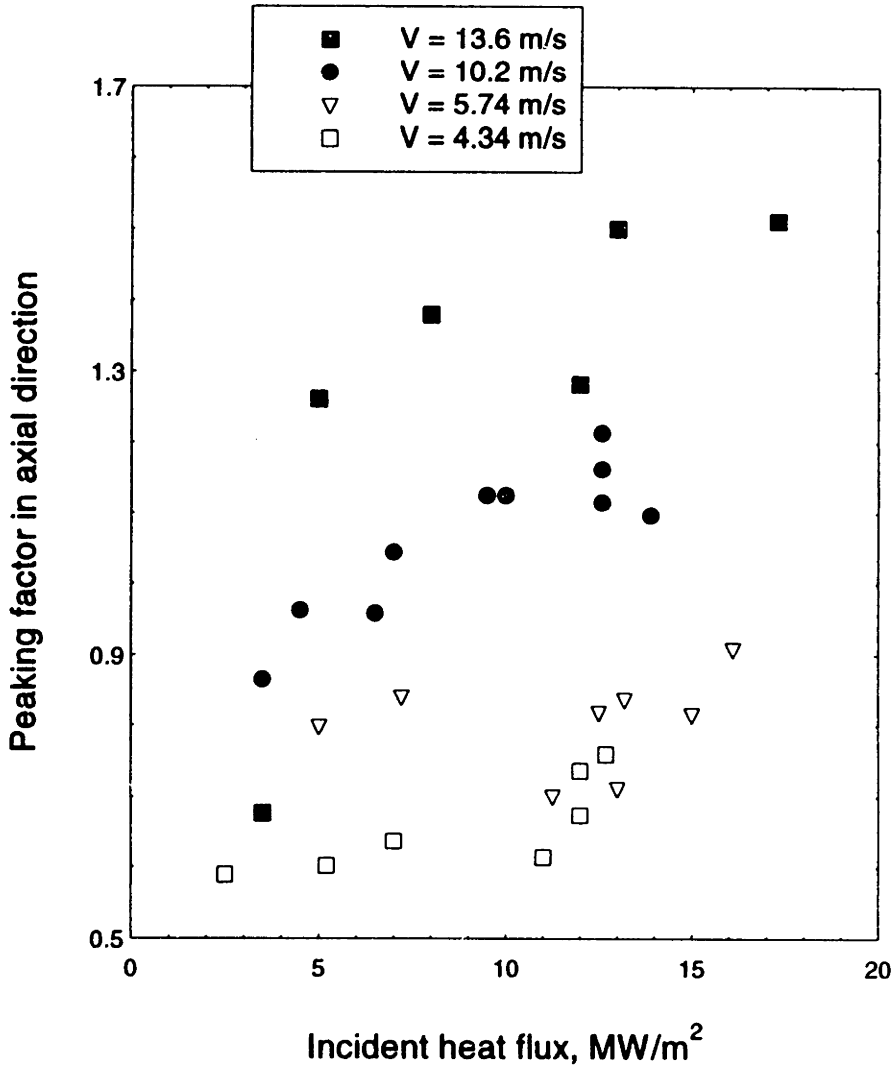

Figure 4-4: Peaking factor in the axial direction as a function of incident heat flux

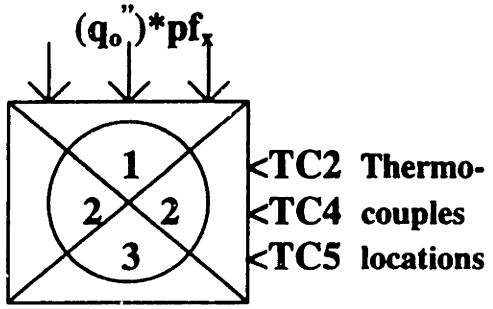

Figure 4-5: Test section specifications

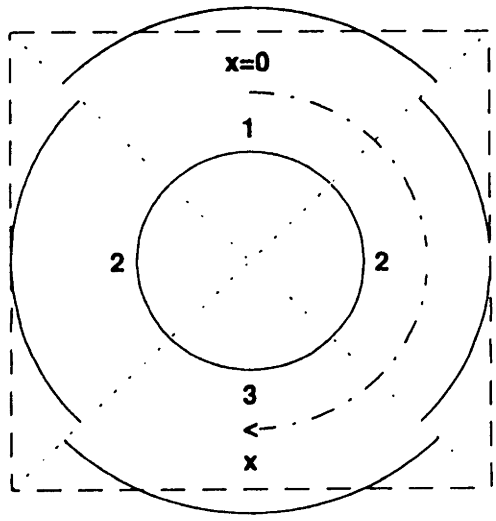

Figure 4-6: Axial cross section of test section model

The outer radius of zone#1 ($r_{1,out}$)was obtained from a condition that the outer perimeter of zone#1 should be equal to the test section width (19 mm). With this condition the heat input per unit length to the modeled test section will be exactly equal to the real one.

For zone#1 we have heat added as an incident heat flux, defined by Equation (4.11). heat is removed by water flowing through channel. Treating this problem as one-dimensional the following heat balance equation can be written

$$q_{inc}\frac{r_{1,out}}{r_{mid}} = h_1\theta\frac{r_{in}}{r_{mid}} - kt_1\frac{d^2\theta}{dx^2} \tag{4.12}$$

where: $r_{1,out}$ = radius of the outer surface of the zone#1 of test section model (see Figure 4-6);
r_{mid} = 7.125 mm = middle radius of test section model;
r_{in} = radius of the test section coolant passage, also the radius of x coordinate axis (r_{in} = D/2);
t_1 = thickness of the zone#1 of test section model.

Equation (4.12) can be simplified as following

$$\frac{d^2\theta}{dx^2} - B_1^2\theta = -q_{inc}\frac{r_{1,out}}{r_{mid}kt_1} \tag{4.13}$$

where: $B_1 = \sqrt{h_1\frac{r_{in}}{r_{mid}kt_1}}$

For zones#2 and 3 there is no incident heat flux and for this case Equation (4.13) becomes

$$\frac{d^2\theta}{dx^2} - B_2^2\theta = 0 \tag{4.14}$$

where: $B_2 = \sqrt{h_2\frac{r_{in}}{r_{mid}kt_2}}$

$$\frac{d^2\theta}{dx^2} - B_3^2\theta = 0 \tag{4.15}$$

where: $B_3 = \sqrt{h_3\frac{r_{in}}{r_{mid}kt_3}}$

Note that for all calculations heat transfer coefficients for zone#2 and zone#3 will be taken equal to each other (h_2=h_3).

The boundary conditions were analogous to those used for the axial calculations (see Equations (4.5) and (4.6)).

The solutions of differential Equations (4.13) - (4.15) are

$$\theta_1(x) = c_1\sinh(B_1x) + c_2\cosh(B_1x) + \frac{q_{inc}r_{1,out}}{hr_{in}} \tag{4.16}$$

$$\theta_2(x) = c_3 \sinh(B_2 x) + c_4 \cosh(B_2 x) \tag{4.17}$$

$$\theta_3(x) = c_5 \sinh(B_3 x) + c_6 \cosh(B_3 x) \tag{4.18}$$

Constants c_1 - c_4 were found numerically using the boundary conditions. The input parameters of these calculations were: test section geometry, copper thermal properties, incident heat flux, peaking factor coefficient from the solution of axial conduction problem (see previous subsection) and w - the top/bottom heat transfer coefficient ratio ($w = h_1 / h_2 = h_1 / h_3$).

For low values of heat flux, that means that $T_w < T_s$, it was assumed that there is no difference in heat transfer coefficients values ($h_1 = h_2 = h_3 = h_{s.p.}$ or $w = 1$). For these conditions the values of single-phase heat transfer coefficients ($h_{s.p.}$) were obtained using Equations (4.16) - (4.18) with which the reading of the thermocouple TC4 (see Figure 4-5) was matched.

Because we are neglecting heat conduction in the radial direction, it was necessary to develop a correlation between the wall temperature value corresponding to TC4 obtained from calculations (θ) which is a sort of mean temperature and the outer wall temperature which should be compared with the TC4 reading. It was assumed that the radial temperature profile can be described by the following equation

$$T(r) = (a + b\,r + c\,r^2)\,\theta + \theta \tag{4.19}$$

where; r = relative radial coordinate (r = 0 at the outer wall, r = 1 at the inner wall)
a, b, c = some coefficients that should be determined.
Because the outer surface is isolated

$$\frac{dT(0)}{dr} = 0 \tag{4.20}$$

The heat flux at the inner surface can be obtained from Equation (4.17), thus

$$\frac{k}{t_2}\frac{dT(1)}{dr} = \theta_2 h_2 \tag{4.21}$$

And because θ is an average temperature

$$\int_0^1 T(r)dr = \theta \tag{4.22}$$

where: t_2 = thickness of the zone#2 of test section model.
From Equations (4.22) and (4.19) it is clear that

$$\int_0^1 (a + br + cr^2)dr = 0 \tag{4.23}$$

With the help of equations (4.20), (4.21) and (4.23) the needed correlation was found

$$T_{TC4} = T_b + \theta\,(1 + \frac{t_2 h_2}{6k}) \tag{4.24}$$

The procedure of the calculations was the following. First, an initial value is assigned to the heat transfer coefficient. Then with the help of Equations (4.17) and (4.24) the value of temperature that should be compared with TC4 reading (T_{TC4}) is obtained. If they are found about equal, the value of heat transfer coefficient is assumed to be correct, in case of a difference between experimental and calculated temperatures, the calculations are continued until the two numbers are found about the same (within 1%).

An assumption was made that that when in zone#1 $T_w > T_s$ (nucleate boiling in zone#1), $h_{2,3}$ have the same value as they had for $T_w = T_s$ for the same specified value of coolant velocity. For this condition (nucleate boiling in zone#1, single-phase convection in zones#2 and 3) with the help of Equations (4.17) and (4.24) the value of nucleate boiling heat transfer coefficient (h_1) was obtained using the procedure described above.

After that, the value of azimuthal peaking factor was calculated as follows:

$$pf_{az} = \frac{h_1 \theta_1}{q_0'' pf_x} \tag{4.25}$$

The total peaking factor coefficient was defined as follows

$$pf = pf_x \, pf_{az} \tag{4.26}$$

The descriptive flow chart of the computer modeling solution is shown in Figure 4-7.

In order to justify the proposed methodology, a comparison was made with the HEATING7.2 computer code calculations. This comparison is presented in Figure 4-8. Value of the peaking factor for this particular test run obtained with the HEATING7.2 code is equal to the value obtained by proposed modeling. As one can see there is good agreement between the two methods of calculations. The difference between them is due to two reasons. The first one is that there are some assumptions and simplifications involved in the proposed method. The second one is that HEATING7.2 results are based on heat transfer coefficients from Petukhov's correlation with film properties for the single phase region and Shah's correlation for nucleate boiling region. It will be shown in the next chapter that these correlations do not work well for present thermal-hydraulic conditions.

In Figure 4-9 values of the azimuthal peaking factor are shown versus heat flux for the midsection position. For low heat flux values (less than 10 MW/m^2) the low velocity peaking factor is lower than for a high velocity. For heat fluxes greater than 10 MW/m^2 boiling occurs in zone#1. It is known that heat for the boiling region there is a strong dependence of heat transfer coefficients on heat flux, not on velocity. Thus, as one can see from Figure 4-9 there are no large differences between data points corresponding to different velocities. As heat flux increases, more heat will transfer via nucleate boiling and consequently more heat will go directly to the coolant. That results in increasing the value of peaking factor coefficient in azimuthal direction.

In Figure 4-10 values of the total peaking factor coefficient are shown for midsection position versus heat flux.

Again as the values of velocity and heat flux increase, more heat is transferred by convection using the shortest way through the test section. This results in the increasing the peaking factor values.

In Figure 4-11 a comparison between HEATING7.2 calculations and the present modeling calculation is shown for the data points corresponding to Critical Heat Flux. There is quite good agreement between these different methods. Again the difference is due to the same reasons described above.

Program 1: Heat Conduction in Axial Direction

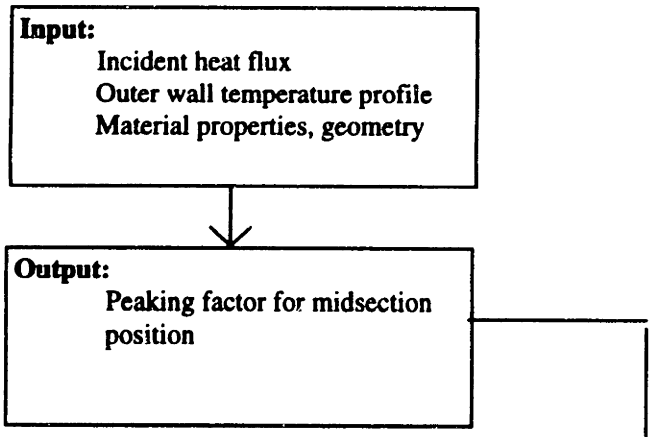

Program 2: Heat Conduction in Azimuthal Direction

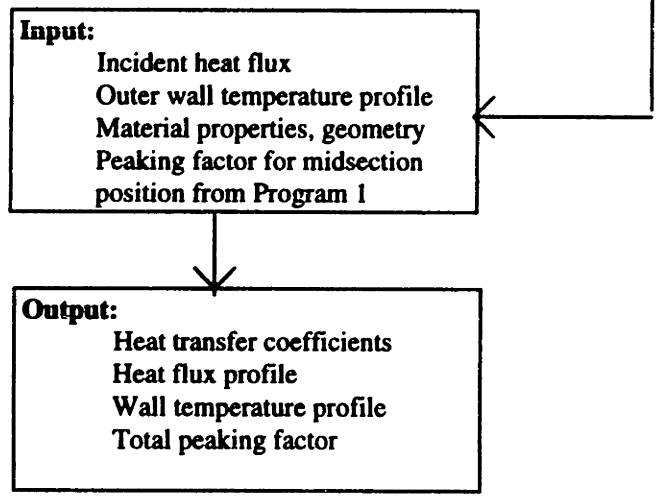

Figure 4-7: Descriptive flow chart of computer modeling solution

In order to see how possible errors in thermocouple reading influence on heat transfer coefficients obtained from calculations sensitivity analysis has been done. Results of this analyses are presented in Figure 4-12. From this figure one can see that the error in thermocouple reading of outer wall temperature produces about the same error in the value of heat transfer coefficient. The maximum possible error in thermocouple reading cannot be greater than $\pm 1\%$.

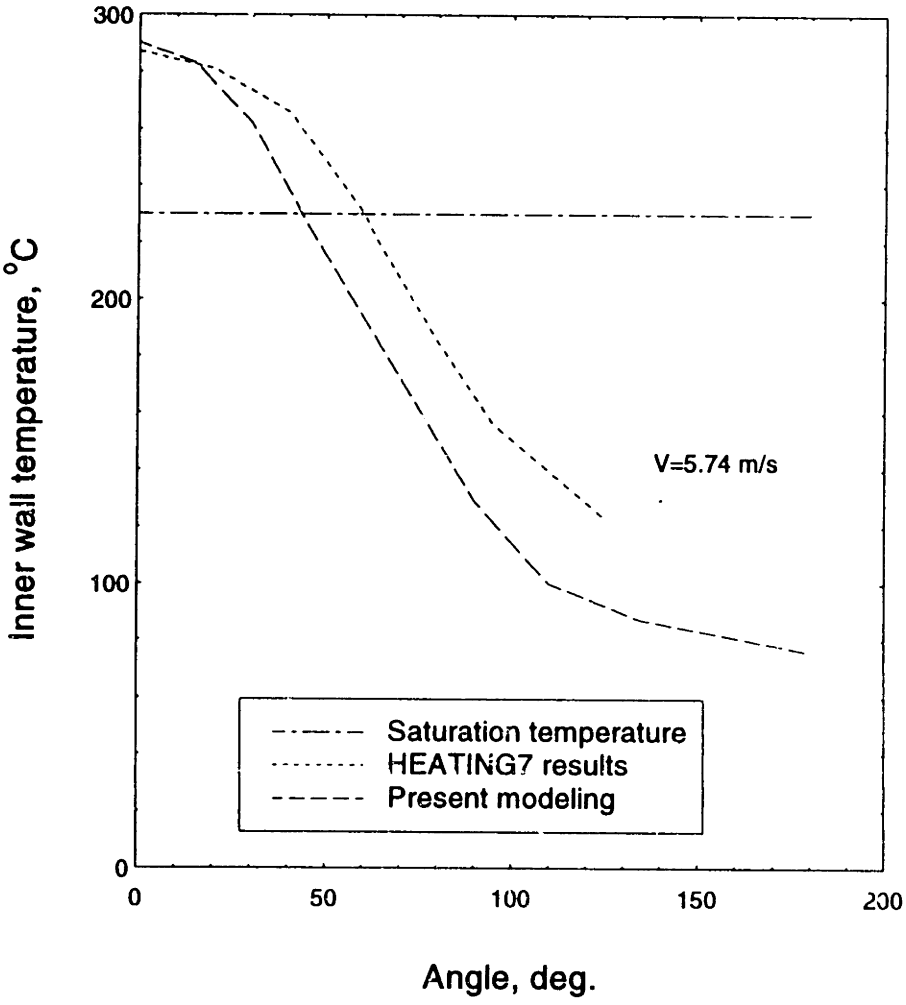

Figure 4-8: Inner wall temperature profile in the azimuthal direction

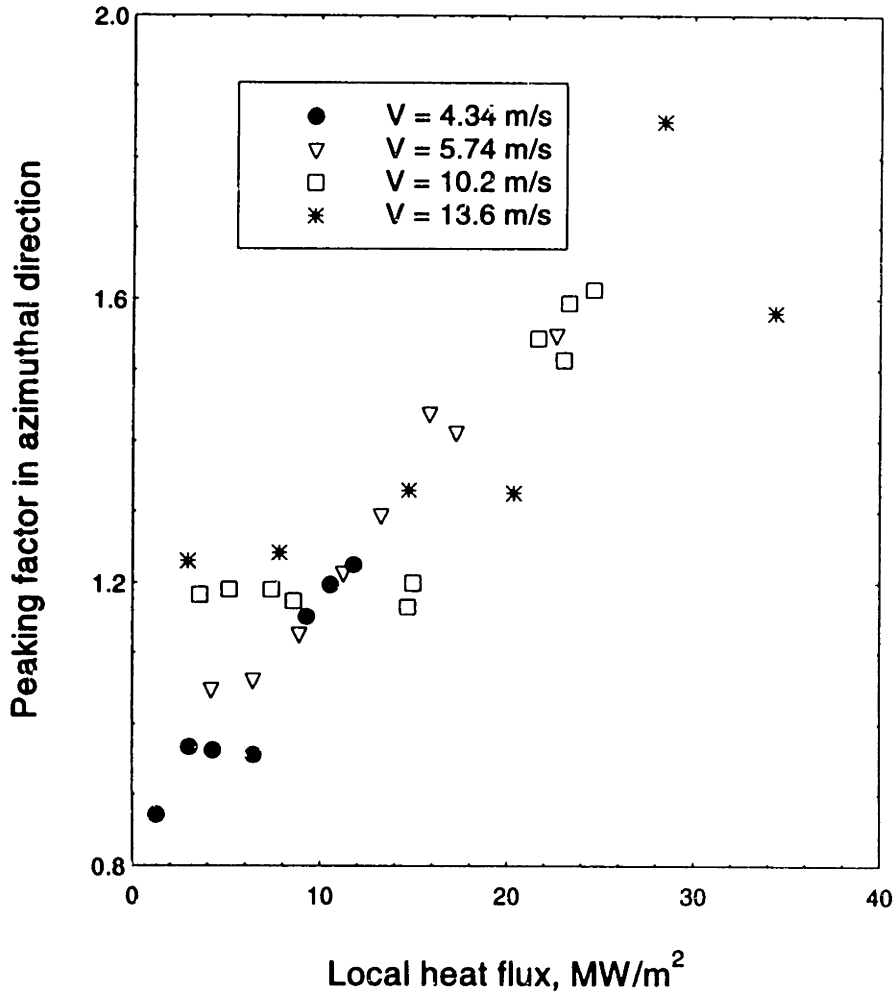

Figure 4-9: Peaking factor in the azimuthal direction

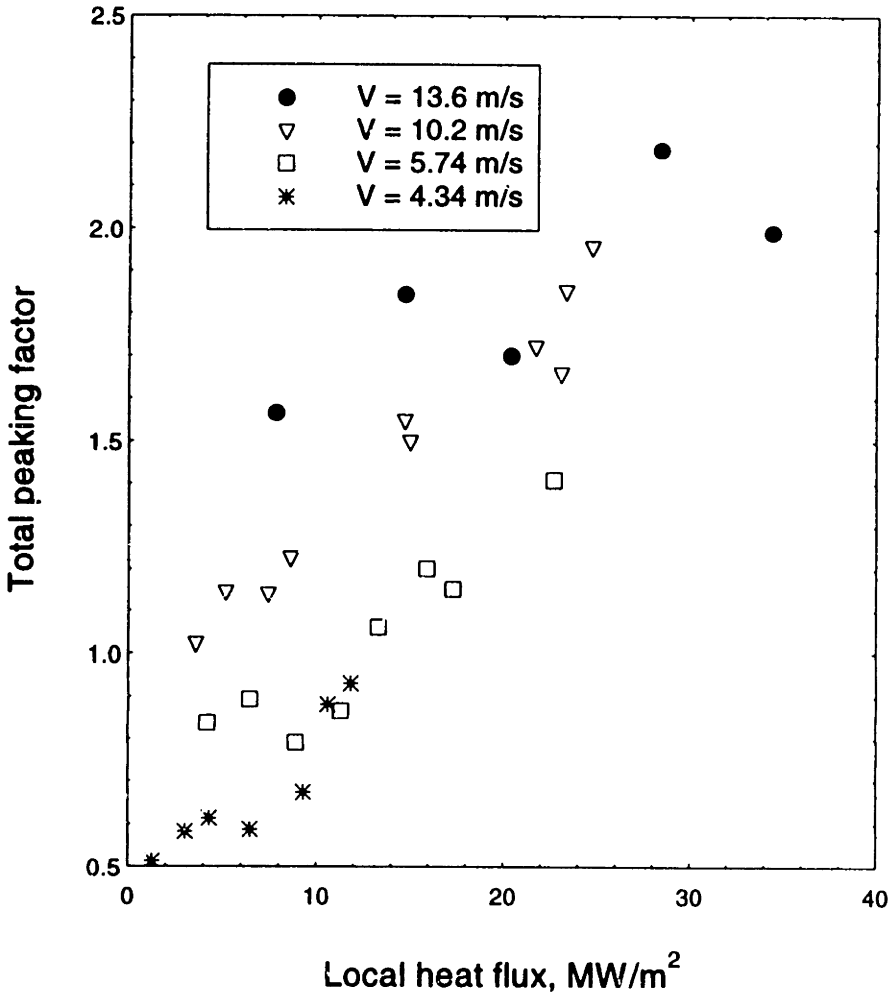

Figure 4-10: Total peaking factor

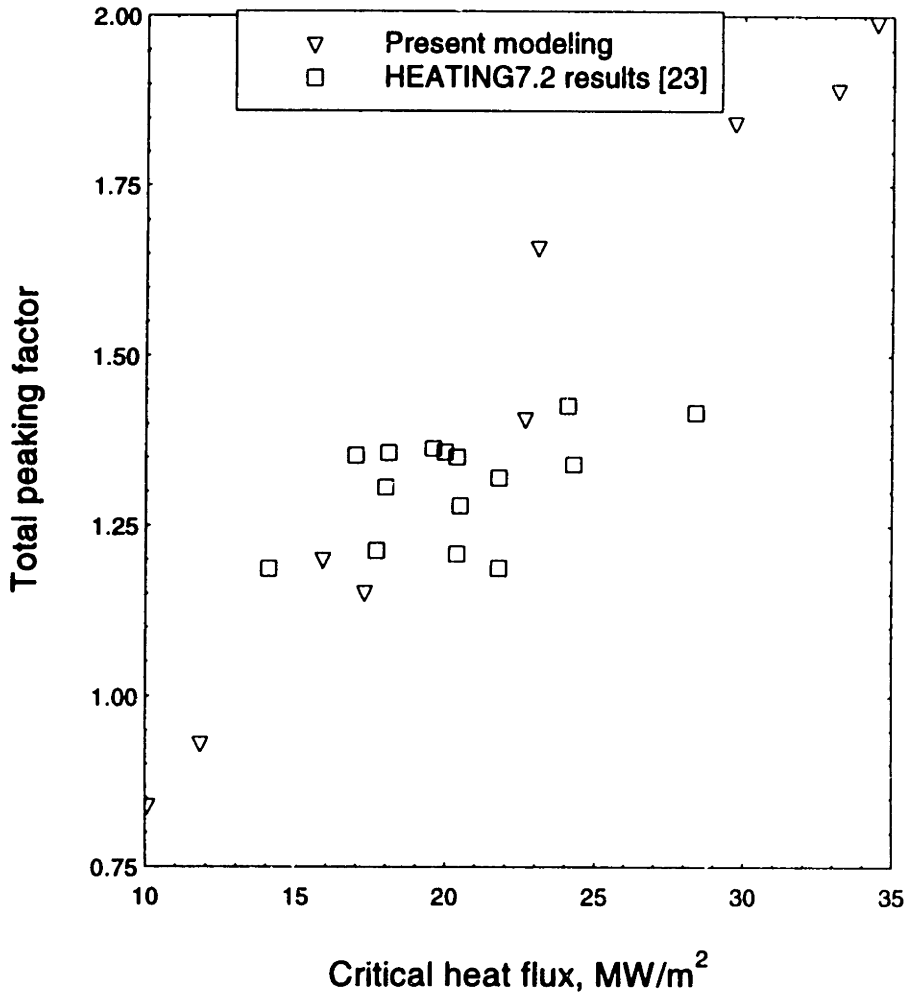

Figure 4-11: Total peaking factor corresponding to Critical Heat Flux

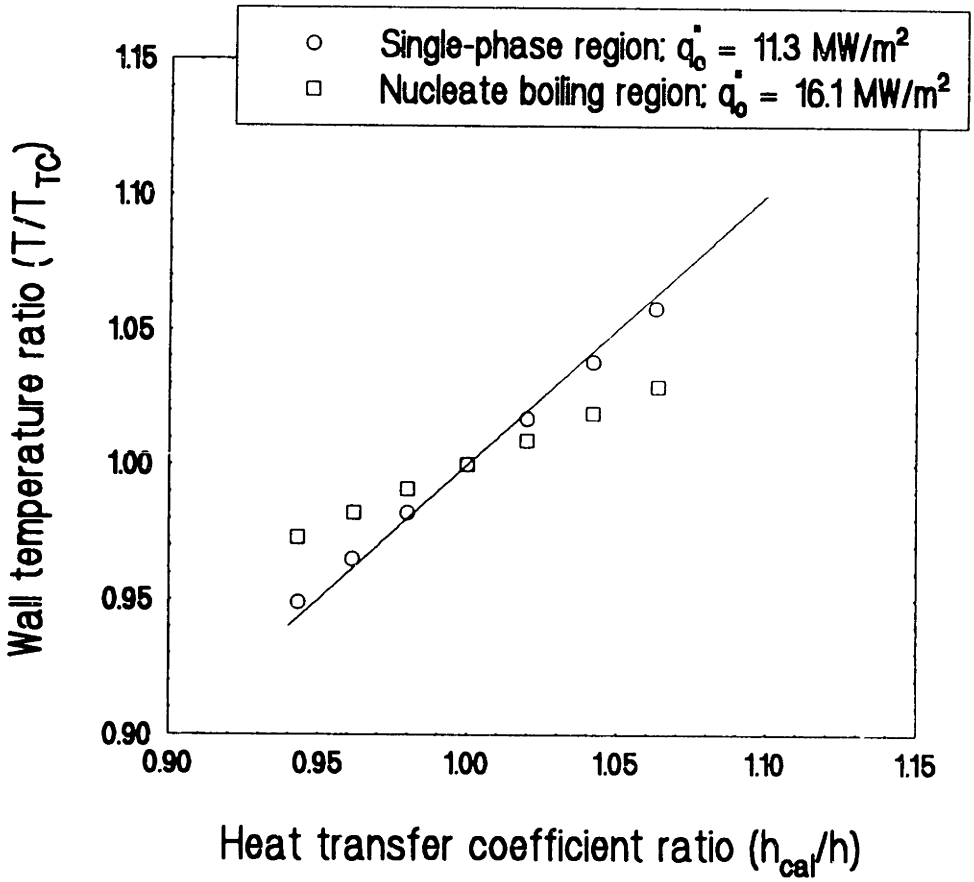

Figure 4-12: Sensitivity analysis results

4.4 Comments

Proposed conduction analyses convert experimental heat flux input and outer wall temperature measurements to wall heat flux distributions and to heat transfer coefficients for single-phase and nucleate boiling regions without the use of correlation's. The wall heat flux distribution is of interest to thermal hydraulics since the incident heat flux is apparatus specific while heat transfer models should be independent of geometry outside the coolant-wall interface. Thus the present modeling reports the total peaking factor (defined by Equation (4.26)).

It is postulated that local basis assumption holds for heat transfer. Thus, local wall temperature and bulk temperature are used in order to obtain local heat flux. The resulting relationships are assumed to apply whether or not there is significant variation of heat flux in the azimuth direction. No account is taken of developing velocity and coolant temperature distributions. This is done in order to simplify the problem. It will be shown in the next chapter that it is possible to obtain reasonable values of heat transfer coefficients with this local basis assumption. However, for other test section geometry, for example for a very short length test section, this assumption may not be valid.

Chapter 5

Heat Transfer Results

Fifty two high heat flux experimental runs are presented in this chapter. Results of analysis for single-phase convection and nucleate boiling regions are presented. The aggregate measured and deduced data will be presented first. Particular runs will be discussed in detail to illustrate the approach used for determining the values deduced.

5.1 Single-Phase Region

Table 5.1 lists the measured variables as recorded for the single-phase region.

The test sections are identified by numbers that are the same as in [23]. Each test specimen has two sides (A and B) coated with alumina and tungsten. Experiments were performed using heat deposition on each side (A and B) of the test section.
Table 5.2 lists runs and major thermal hydraulic parameters for single-phase region deduced from measurements and the computer model analysis.

Table 5.1: Measured Variables for Single-Phase Region

Experimental Run Number	Test Section ID	Velocity m/s	Power kW	Inlet T_{bulk} °C	Exit Pressure MPa
1	TS21B	3.65	2.5	23	3.01
2	TS21B	3.65	3	23	3.01
3	TS28B	4.34	2.5	25	2.98
4	TS28B	4.34	5.2	25	2.98
5	TS28B	4.34	7	25	2.98
6	TS28B	4.34	11	25	2.98
7	TS26A	5.74	5	22	2.92
8	TS26A	5.74	7.2	22	2.92
9	TS26A	5.74	11.25	22	2.92
10	TS23B	10.2	3.5	21	2.62
11	TS23B	10.2	4.5	21	2.62
12	TS23B	10.2	6.5	21	2.62
13	TS23B	10.2	7	21	2.62
14	TS29B	13.6	3.5	19	2.31
15	TS29B	13.6	5	19	2.31
16	TS29B	13.6	8	19	2.31
17	TS29B	13.6	12	19	2.31
18	TS29A	15.2	2	19	2.17
19	TS29A	15.2	3	19	2.17
20	TS29A	15.2	6	19	2.17
21	TS29A	15.2	9	19	2.17
22	TS29A	15.2	12	19	2.17
23	TS27B	19.4	6.5	19	1.79
24	TS27B	19.4	7.5	19	1.79
25	TS27B	19.4	13	19	1.79
26	TS27B	19.4	17.5	19	1.79

The distinguish between single-phase and nucleate boiling regions is made based on the inner wall temperature calculations results using computational modeling technique presented in Chapter 4 of this thesis. It is decided that if maximum inner wall temperature is less than saturation temperature we have single-phase heat transfer region, if not (T_w - T_s) we are in the nucleate boiling region.

Table 5.2: Synopsis of Reduced Data for Single-Phase Region: Major Thermal Hydraulic Variables

Run Number	Velocity m/s	Outer Wall Tempe-rature (TC2) °C	Outer Wall Tempe-rature (TC4) °C	Peaking Factor in Axial Direction	Total Peaking Factor	Maximu m Local Heat Flux MW/m^2	Heat Transfer Coefficient $kW/(m^2 K)$
1	3.65	130	85	0.967	0.830	2.1	20
2	3.65	190	126	1.373	1.192	3.6	21
3	4.34	85	50	0.589	0.513	1.3	21
4	4.34	140	75	0.602	0.582	3.0	30
5	4.34	180	100	0.637	0.613	4.3	29
6	4.34	250	145	0.614	0.587	6.7	28
7	5.74	150	75	0.799	0.838	4.2	38
8	5.74	200	100	0.841	0.893	6.4	39
9	5.74	240	120	0.702	0.791	8.9	39
10	10.2	90	48	0.865	1.023	3.6	52
11	10.2	120	60	0.962	1.145	5.2	54
12	10.2	147	78	0.958	1.140	7.4	54
13	10.2	170	90	1.044	1.226	7.3	52
14	13.6	62	39	0.677	0.836	2.9	60
15	13.6	115	70	1.261	1.566	7.8	61
16	13.6	170	90	1.380	1.843	14.7	75
17	13.6	225	120	1.282	1.700	20.4	74
18	15.2	38	30	0.537	0.686	1.4	66
19	15.2	62	38	0.518	0.654	2.0	64
20	15.2	105	52	1.013	1.418	8.5	86
21	15.2	160	70	1.243	1.832	16.4	100
22	15.2	225	115	1.470	2.058	24.7	86
23	19.4	100	50	1.081	1.619	10.5	105
24	19.4	140	75	1.520	2.202	16.5	95
25	19.4	215	112	1.426	2.051	26.7	103
26	19.4	265	140	1.331	1.893	33.1	104

Values of peaking factors, local heat flux and heat transfer coefficient in Table 5.2 were obtained with the of the computational modeling method presented in the previous chapter (see also Figure 4-7).

Thermocouple readings of TC2 and TC4 versus incident heat flux are shown in Figures 5-1 and 5-2. From these figures it is very difficult to see the difference between data points corresponding to different velocities (except for the very low and extremely high values). But with the help of computational modeling described in Chapter 4, it was found to be possible to separate these data points according to their actual velocities. As one can see, the heat transfer coefficient values obtained from computational modeling can be sorted according to their velocities. Again it should be noted that the value of flow velocity was not an input parameter used in computational modeling (see Figure 4-7).

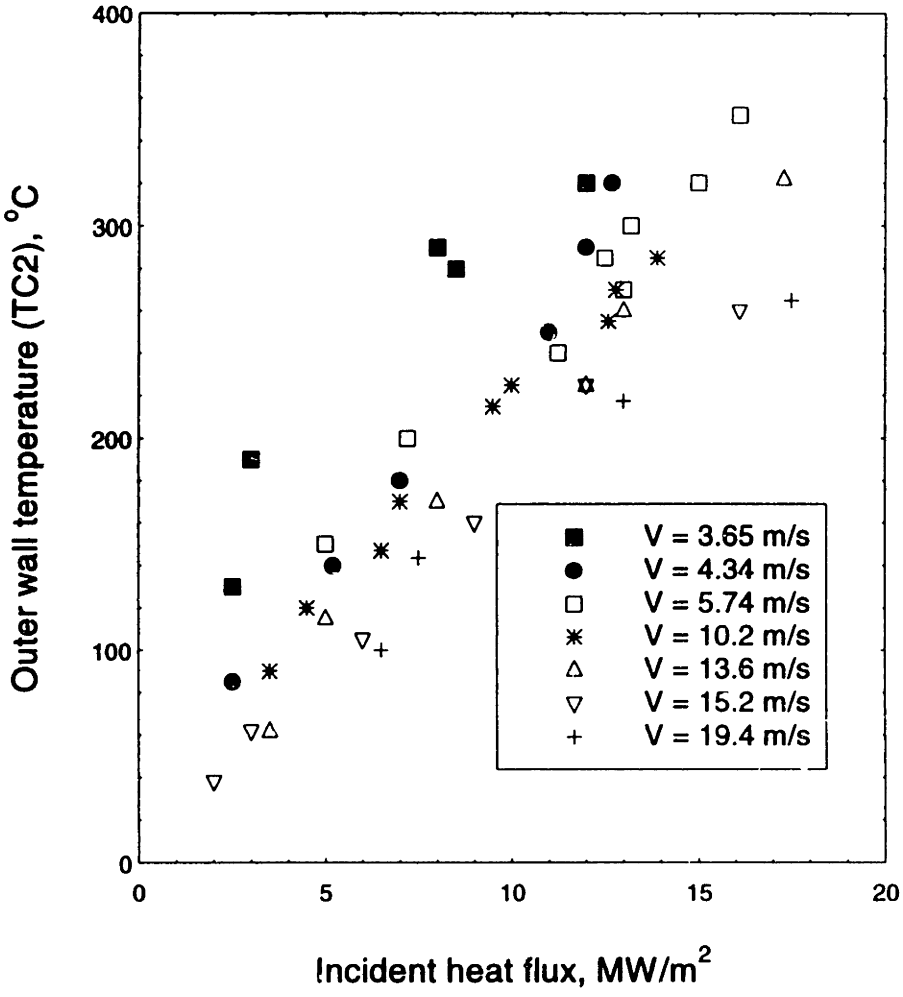

Figure 5-1: Outer wall temperature (TC2) vs. incident heat flux for various velocities

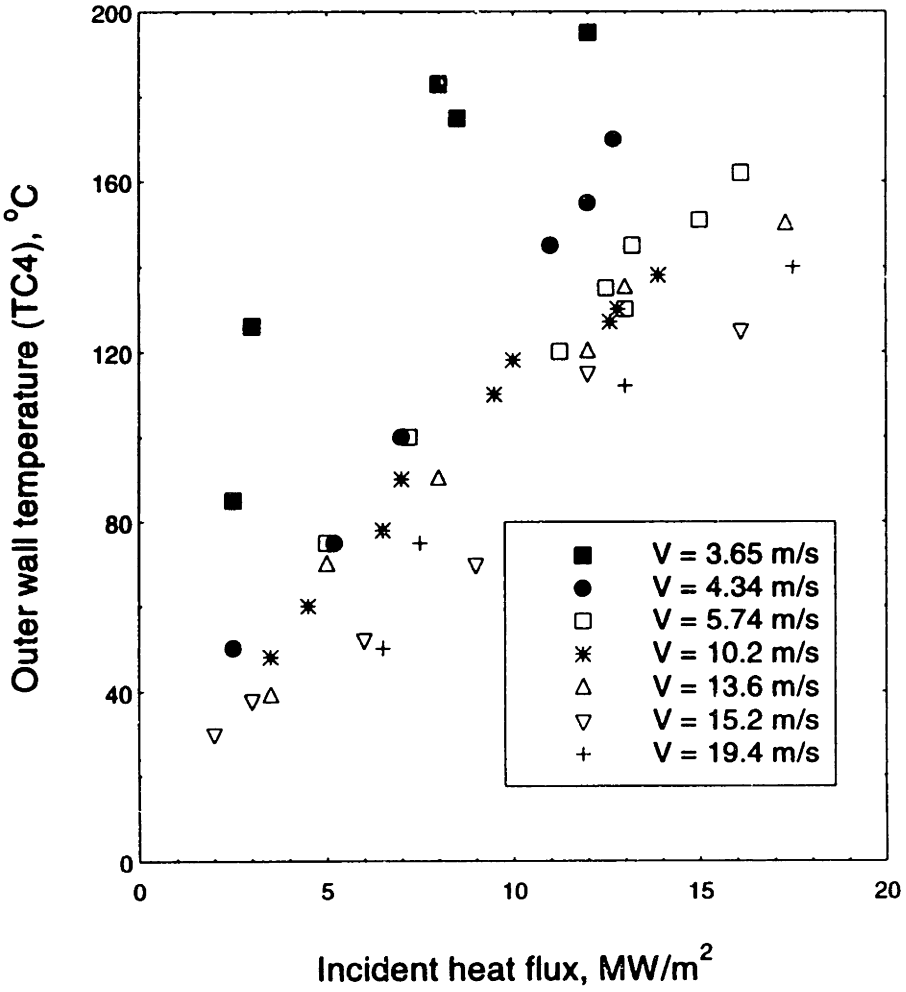

Figure 5-2: Outer wall temperature (TC4) vs. incident heat flux for various velocities

Values of heat transfer coefficients obtained from computational modeling were compared with the different correlations described in Chapter 1. These correlations are: Sieder-Tate correlation (Equation (1.4)); Dittus-Boelter correlation (Equation (1.1)) with all property parameters evaluated either at bulk or film temperatures; and Petukhov correlation (Equation (1.2)). Results of this comparison are shown in Figures 5-3 to 5-5. From results presented on these figures, two major conclusions can be made. First, for the single-phase convection region (no boiling present over the whole perimeter of the flow passage) - the Petukhov correlation with its viscosity correction multiplier is the best one. Second a conclusion can be made that the computational modeling, presented above, is also correct. This is because the Petukhov correlation is one of the most reliable and its good agreement with the experimental results adds confidence to the model. In computational modeling presented in Chapter 4, the heat flow in the radial direction through the wall was ignored. Because of the good agreement with Petukhov's correlation it was decided that this simplification was appropriate and that the wall temperature profile in the azimuthal direction can be used to get the real inner wall temperatures.

Heat transfer coefficients versus maximum local heat flux obtained from experimental data using the computational modeling for different values of flow velocities are presented in Figures 5-6 and 5-7. From these figures it is again clear that the Petukhov correlation is applicable to fusion reactor divertor conditions.

The uncertainty in measurement of the incident heat flux is 5%. The uncertainty in measurement of the surface temperature is 1%. Thus, based on Figure 4-12 and on the basis of the computational modeling, the uncertainty in the heat transfer coefficient is 6%. However, the calculations employed simplifying assumptions which may add some systematic error. By comparison to the HEATING7.2 calculations, as seen in Figures 4-3 and 4-8, there might be 10% error in the calculated values of heat transfer coefficients. This can be checked by comparing the agreement of the predicted values of heat transfer coefficients with the Petukhov correlation. A comparison of experimental values of heat transfer coefficients for single-phase region with the values obtained with the help of Petukhov correlation is presented in Figure 5-8. The agreement between calculated and experimental results was found to be in the range of $\pm$ 15%.

The influence of local wall temperatures on the value of heat transfer coefficient is shown in Figure 5-9, where experimental values of heat transfer coefficient are plotted versus flow velocity. The influence of the local wall temperature is not large. Thus, an assumption that there is no difference between values of heat transfer coefficient for different parts of the inner wall perimeter for single-phase region is valid.

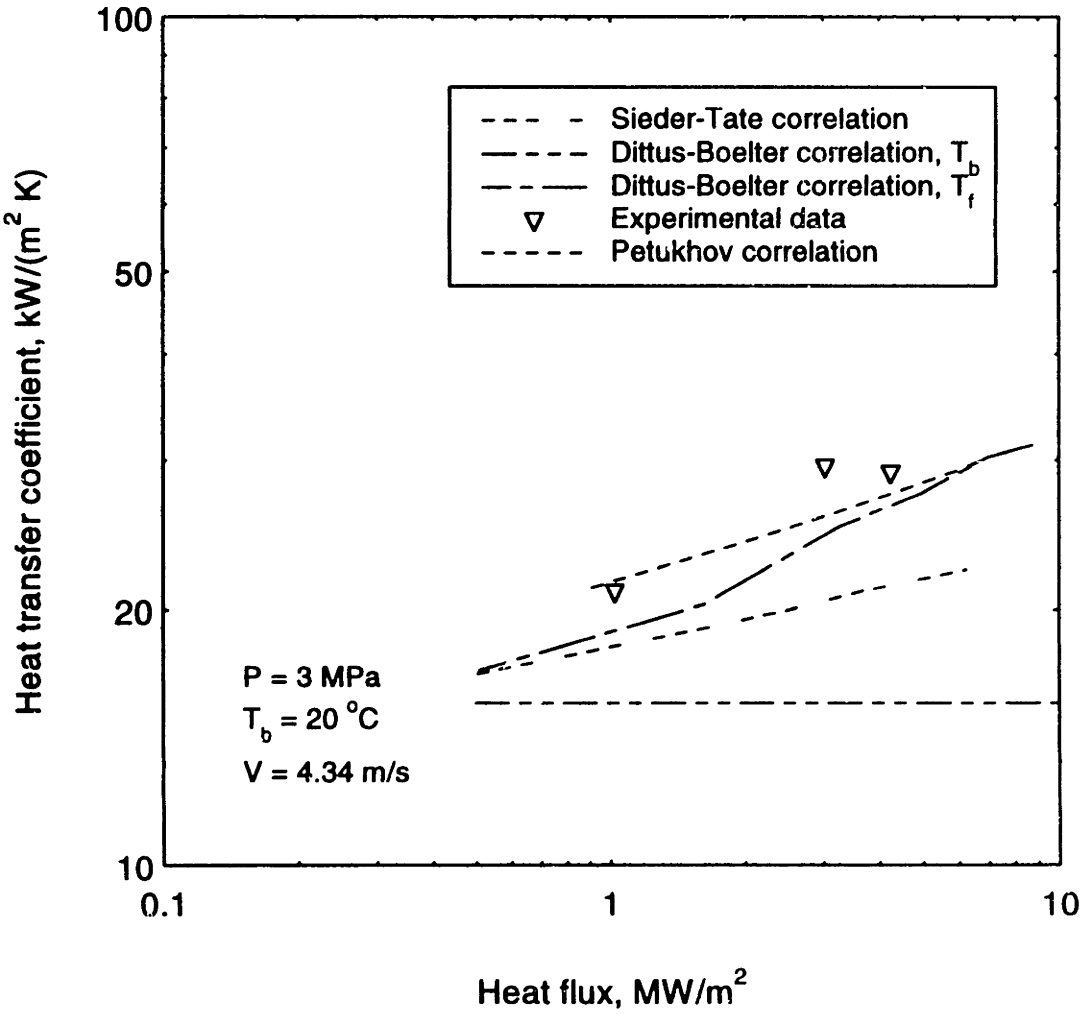

Figure 5-3: Single-phase heat transfer coefficient vs. maximum local heat flux

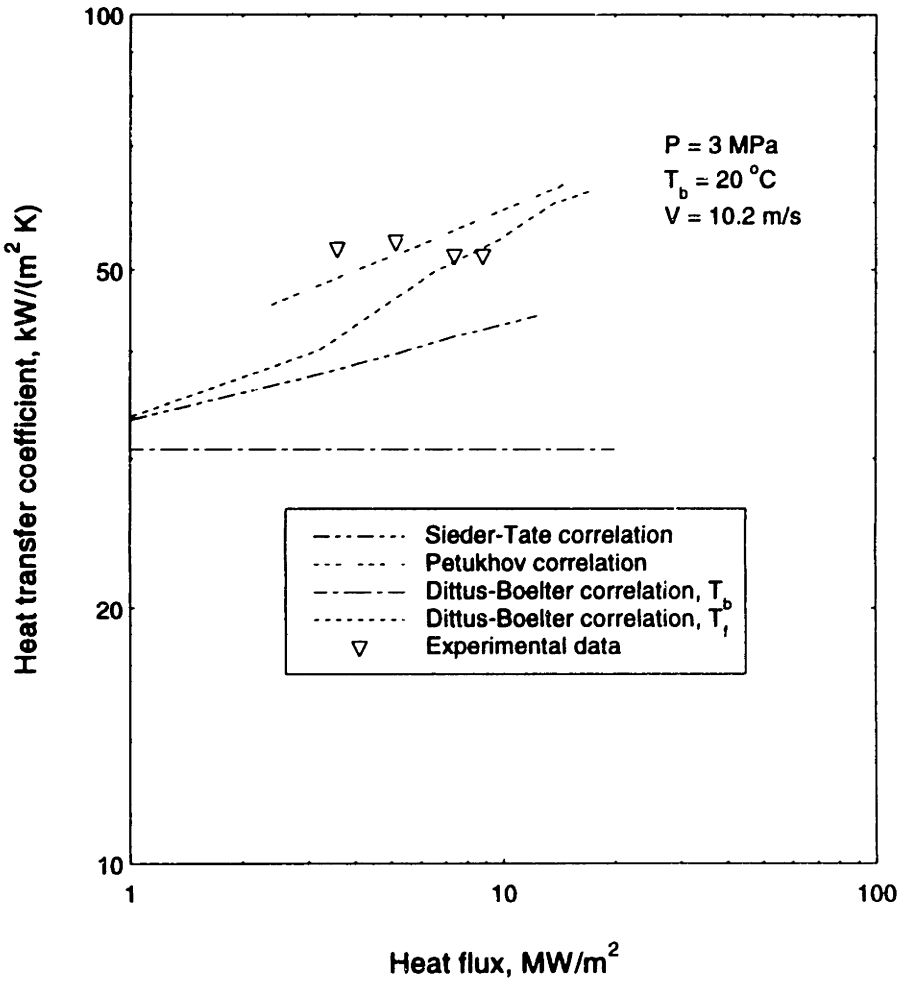

Figure 5-4: Single-phase heat transfer coefficient vs. maximum local heat flux

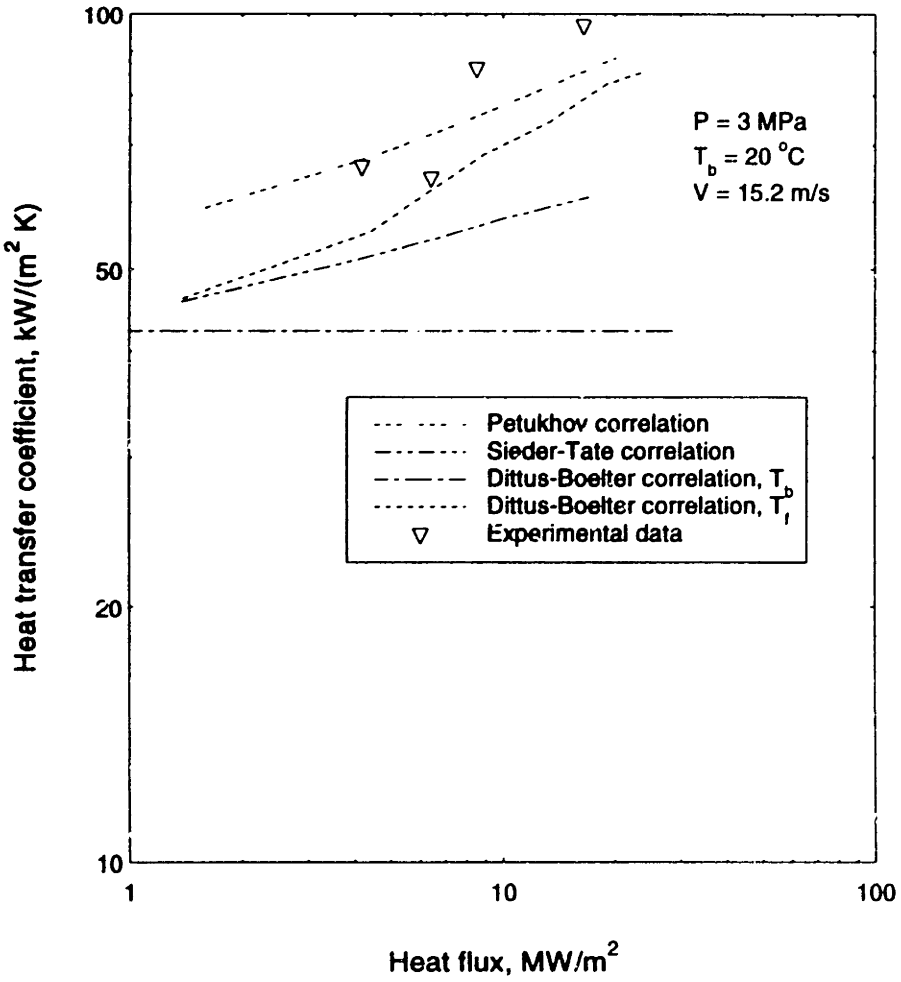

Figure 5-5: Single-phase heat transfer coefficient vs. maximum local heat flux

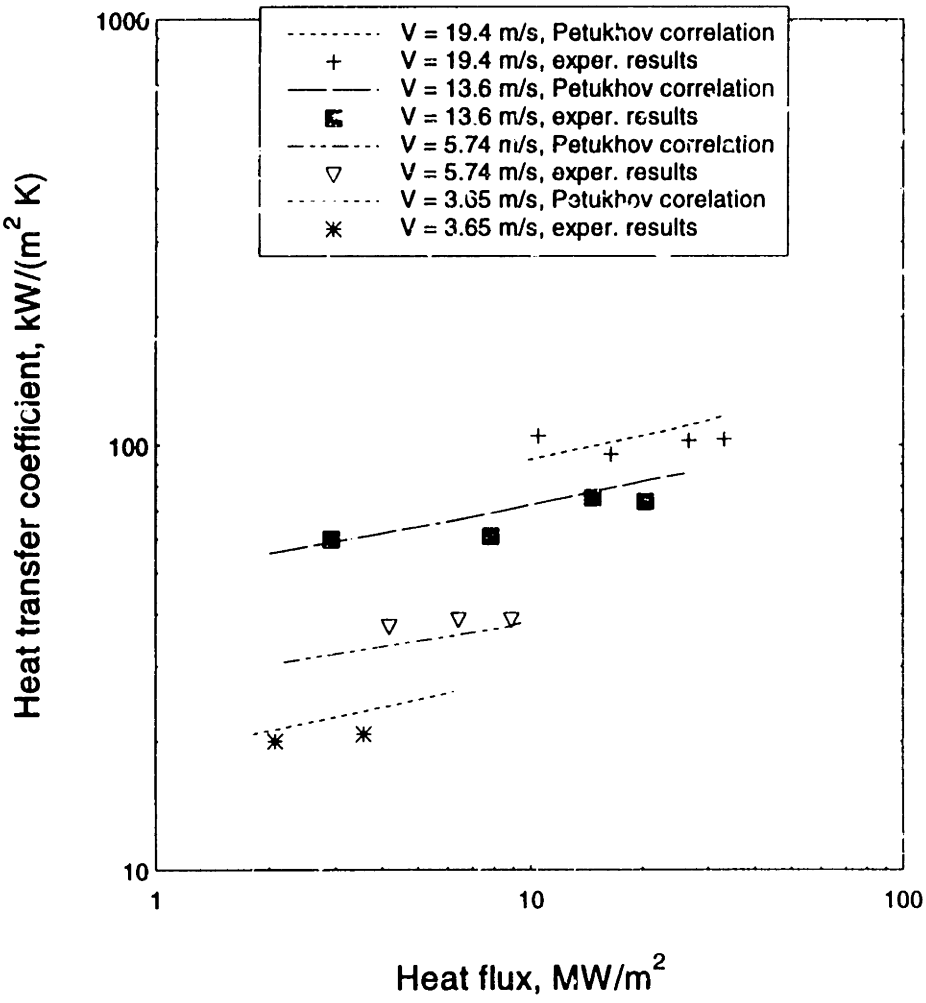

Figure 5-6: Heat transfer coefficient as a function of maximum local heat flux.

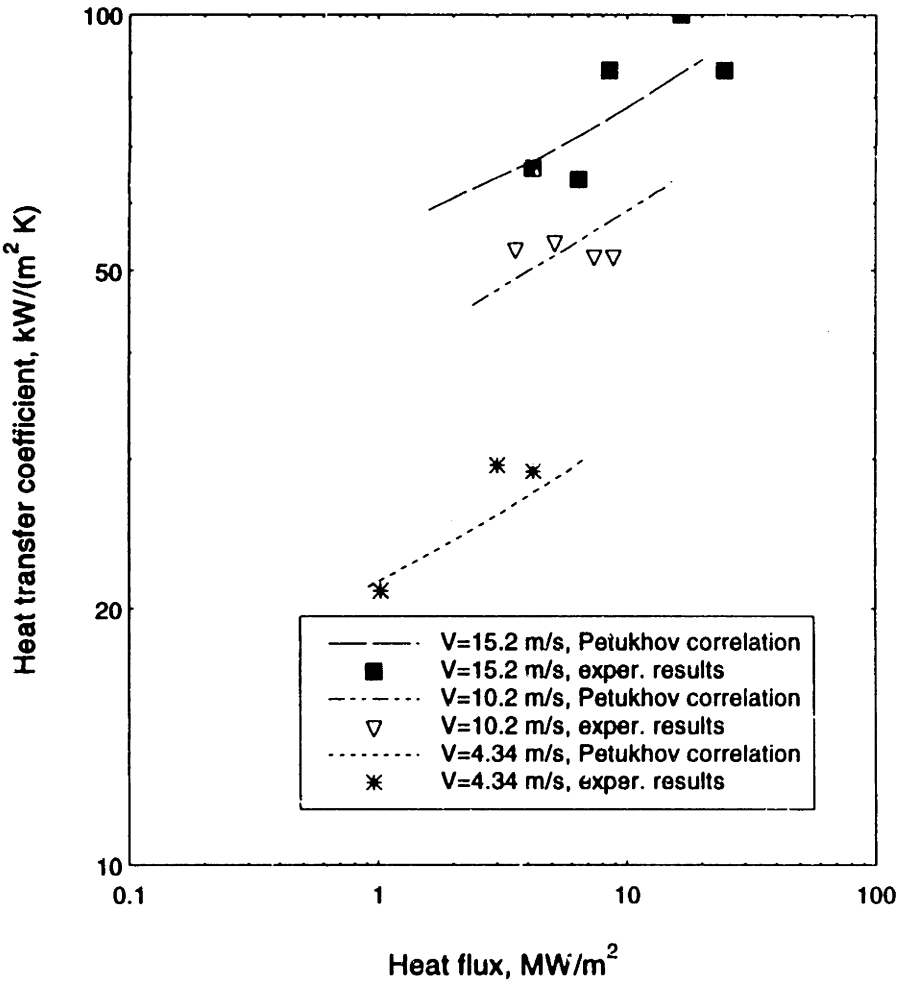

Figure 5-7: Heat transfer coefficient as a function of a maximum local heat flux

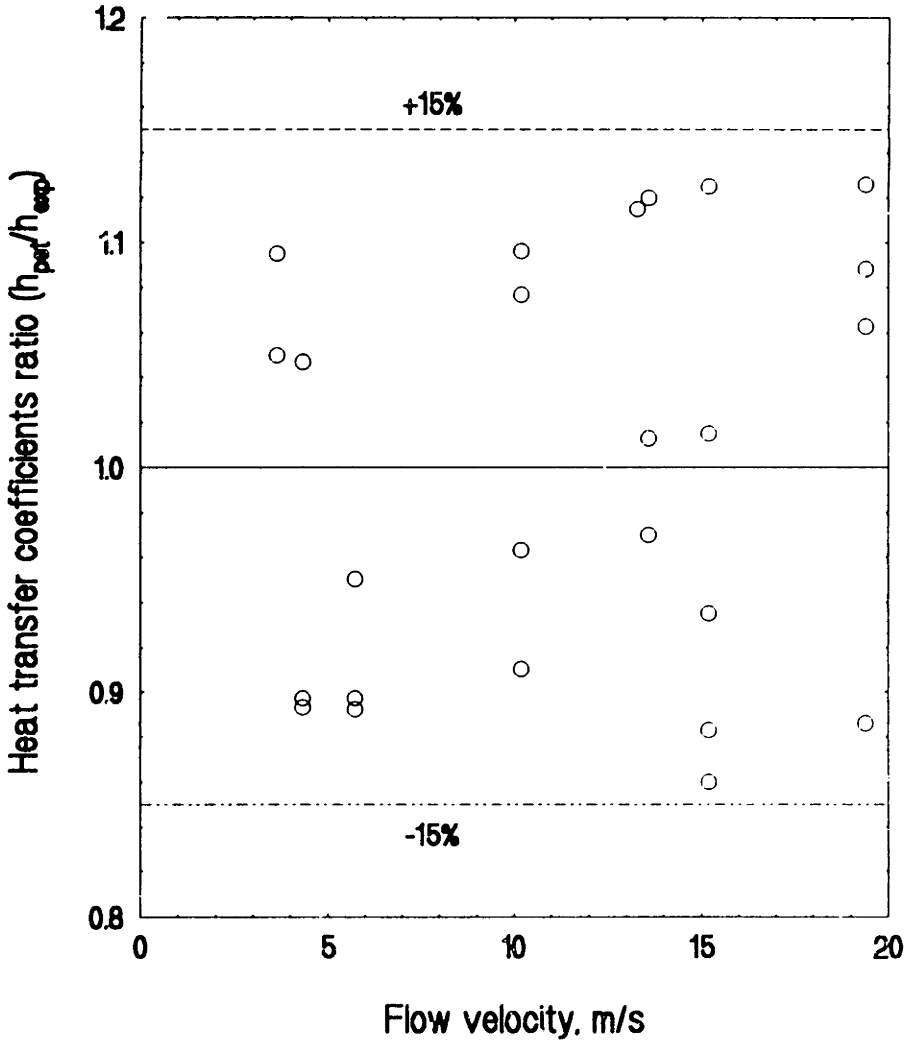

Figure 5-8: Heat transfer coefficient ratio vs. flow velocity

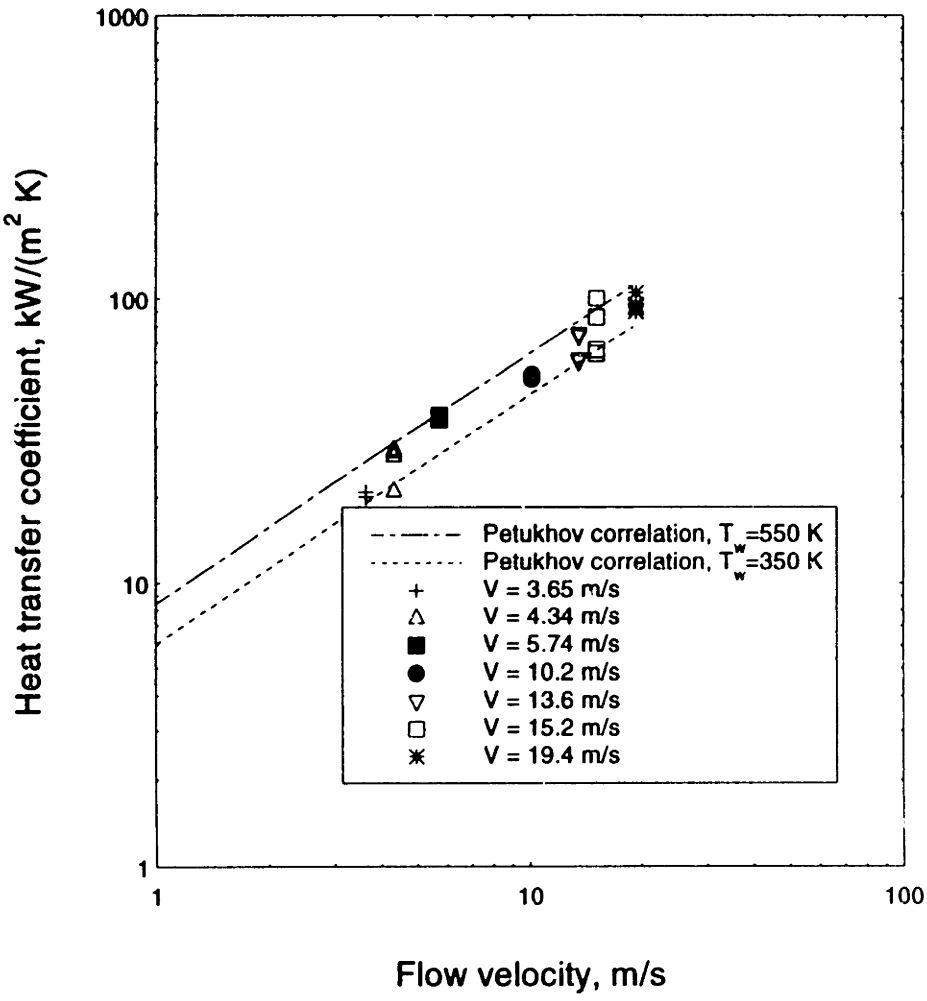

Figure 5-9: Heat transfer coefficient vs. flow velocity

5.2 Nucleate Boiling Region

5.2.1 Interpretation of the Results

Table 5.3 lists the measured variables as recorded for the nucleate boiling region.

Table 5.4 lists runs and major thermal hydraulic parameters for nucleate boiling region deduced from measurements and the computer model analysis.

Table 5.3: Measured Variables for Nucleate Boiling Region

Experimental Run Number	Test Section ID	Velocity m/s	Power kW	Inlet T_{bulk} °C	Exit Pressure MPa
1	TS21B	3.65	5.4	23	3.01
2	TS21B	3.65	8.5	23	3.01
3	TS21B	3.65	8.0	23	3.01
4	TS21B	3.65	12.0	23	3.01
5	TS28B	4.34	11.6	25	2.98
6	TS28B	4.34	12.0	25	2.98
7	TS28B	4.34	12.0	25	2.98
8	TS28B	4.34	12.7	25	2.98
9	TS26A	5.74	12.2	22	2.92
10	TS26A	5.74	13.0	22	2.92
11	TS26A	5.74	12.5	22	2.92
12	TS26A	5.74	13.2	22	2.92
13	TS26A	5.74	15.0	22	2.92
14	TS26A	5.74	16.1	22	2.92
15	TS23B	10.2	8.0	21	2.62
16	TS23B	10.2	9.5	21	2.62
17	TS23B	10.2	10.0	21	2.62
18	TS23B	10.2	12.6	21	2.62
19	TS23B	10.2	12.6	21	2.62
20	TS23B	10.2	12.6	21	2.62
21	TS23B	10.2	13.9	21	2.62
22	TS29B	13.6	12.6	19	2.31
23	TS29B	13.6	13.0	19	2.31
24	TS29B	13.6	17.3	19	2.31
25	TS29A	15.2	13.9	19	2.17
26	TS29A	15.2	16.1	19	2.17

Table 5.4: Synopsis of Reduced Data for Nucleate Boiling Region: Major Thermal Hydraulic Variables

Run Number	Outer Wall Tempe-rature (TC2) °C	Outer Wall Tempe-rature (TC4) °C	Peaking Factor in Axial Direction	Total Peaking Factor	Maximum Local Heat Flux MW/m^2	Heat Transfer Coefficient for zone#2 (single-phase region) $kW/(m^2 K)$	Heat Transfer Coefficient Ratio $\left(\frac{\text{zone\#1}}{\text{zone\#2}}\right)$ zone#1-nucleate boiling region
1	260	155	1.100	1.058	5.7	20.8	1.10
2	280	175	0.822	0.924	7.9	20.8	1.49
3	290	183	0.913	1.030	8.2	20.8	1.50
4	320	195	0.691	0.839	10.1	20.8	1.70
5	260	145	0.644	0.682	7.9	29.0	1.09
6	280	150	0.674	0.776	9.3	29.0	1.33
7	300	160	0.737	0.882	10.6	29.0	1.42
8	320	170	0.760	0.931	11.8	29.0	1.48
9	259	125	0.707	0.829	10.1	39.0	1.10
10	270	130	0.713	0.866	11.3	39.0	1.30
11	285	135	0.819	1.061	13.3	39.0	1.40
12	300	145	0.837	1.201	15.5	39.0	1.45
13	320	151	0.816	1.152	17.3	39.0	1.65
14	352	162	0.909	1.408	22.7	39.0	2.00
15	213	107	1.179	1.508	13.1	52.0	1.11
16	215	110	1.125	1.549	14.7	52.0	1.33
17	225	118	1.125	1.499	15.0	52.0	1.25
18	250	127	1.115	1.722	21.7	52.0	1.68
19	260	126	1.162	1.852	23.3	52.0	1.8
20	270	130	1.213	1.957	24.7	52.0	1.85
21	285	138	1.097	1.660	23.1	52.0	1.62
22	230	125	1.392	1.942	24.5	75.0	1.09
23	260	135	1.501	2.185	28.4	75.0	1.18
24	322	150	1.512	1.991	34.4	75.0	1.46
25	250	120	1.362	1.951	27.1	86.0	1.07
26	263	125	1.255	1.844	29.7	86.0	1.10

The values of peaking factors, local heat flux, heat transfer coefficient and heat transfer coefficient ratio in Table 5.4 were obtained using the modeling technique presented in Chapter 4.

Thermocouple readings of TC2 and TC4 versus incident heat flux for the nucleate boiling region are shown in Figures 5-10 and 5-11. As in Figures 5-1 and 5-2 for the single-phase region, it is difficult to see the difference between data points corresponding to different velocities.

In contrast to single-phase results (see paragraph 5.1) it was found impossible to differentiate these data points according to their velocities as was done before for the single-phase region. But it was found that heat transfer coefficients (defined by Equation (4.1)) can be plotted as a single line versus local heat flux. These data points are plotted versus the maximum local heat flux in Figure 5-12.

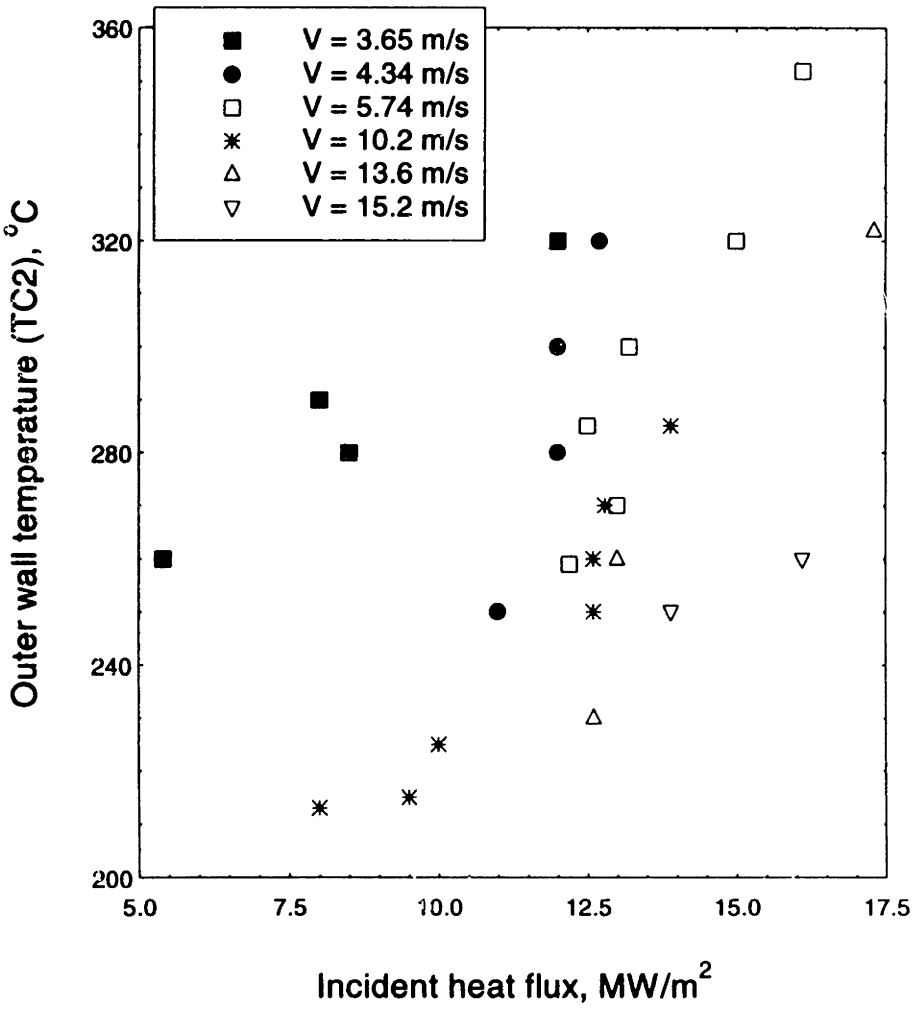

Figure 5-10: Outer wall temperature (TC2) vs. incident heat flux for nucleate boiling region

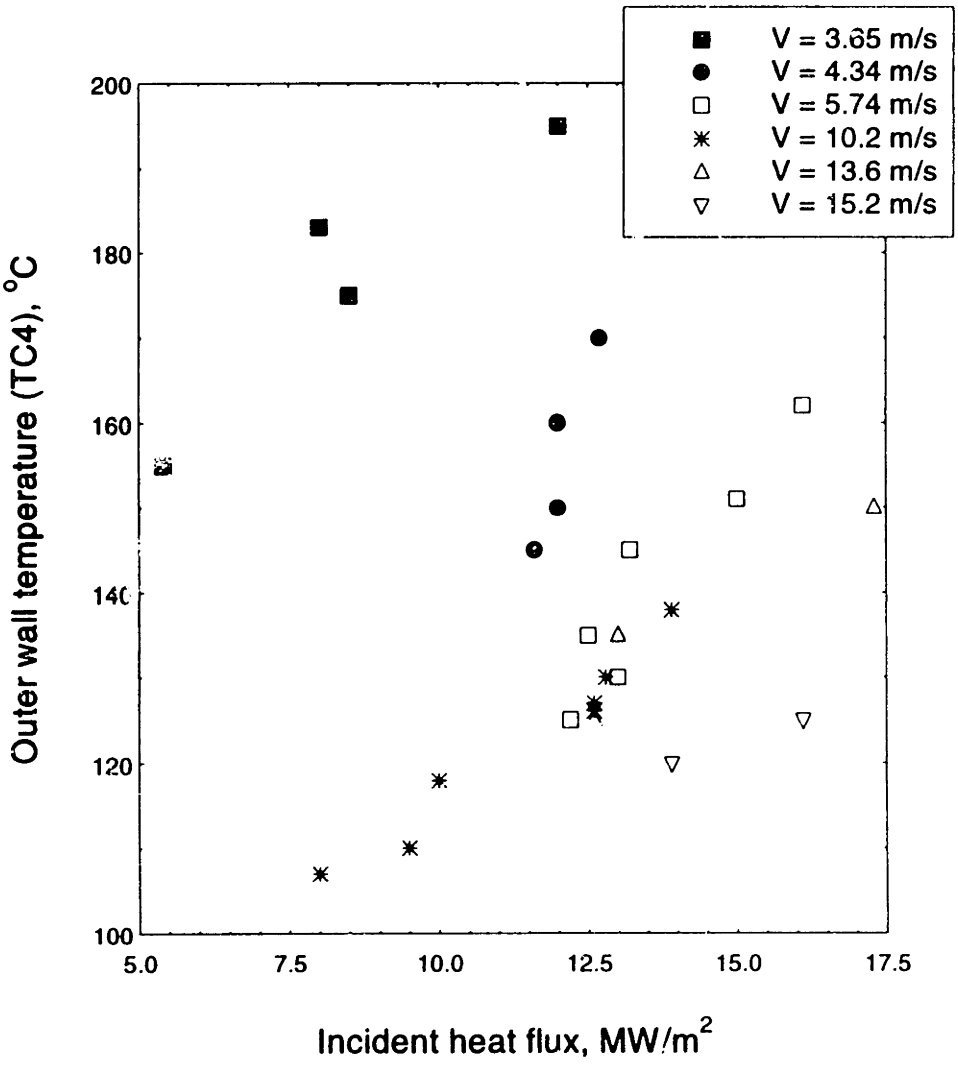

Figure 5-11: Outer wall temperature (TC4) vs. incident heat flux for nucleate boiling region

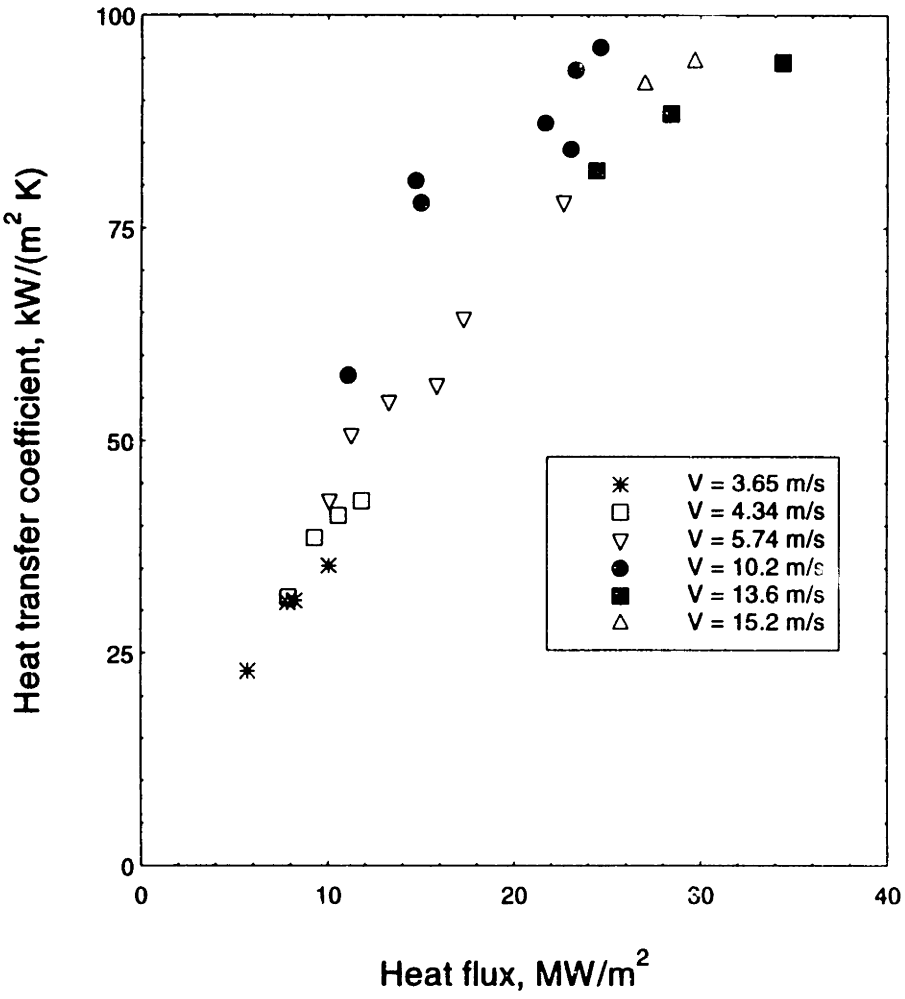

Figure 5-12: Local heat transfer coefficient vs. local heat flux

5.2.2 Discussion of Subcooled Nucleate Boiling Data

It was decided to compare the heat transfer coefficients presented in Figure 5-12 with the various correlations which were discussed in Chapter 1. In Figure 5-13 results are compared with the Jens-Lottes correlation (Equation (1.5)). From this figure it is clear that this correlation mostly overpredicts the values of heat transfer coefficients for high heat fluxes by 30%. Notice that the heat transfer coefficient values plotted on this figure are defined using wall temperature minus bulk temperature difference. That difference for our case is on the order of several hundred degrees. Therefore the heat flux is divided by a large number and there should not be a large difference between data points and correlation, if the last one is correct. Thus, we can conclude that the Jens-Lottes correlation does not adequately predict the heat transfer rate for our flow conditions.

The same conclusion can be made about Yin's correlation (Equation (1.7). This comparison is shown in Figure 5-14. The only difference from the previous figure is that Yin's correlation underpredicts the heat transfer coefficient values by 35% for high heat fluxes.

Experimental data comparison with the Shah correlation (Equation (1.19)) is presented in Figure 5-15. For low velocities (V < 5 m/s) the Shah correlation is quite correct. But it overpredicts heat transfer values for high velocities (V > 12 m/s) by 27%. Also Shah correlation predicts that as the velocity increases the value of heat transfer coefficient should also increase. Present experimental data do not show this trend. For those reasons this correlation cannot be recommended for high velocity flows (V > 12 m/s).

Chen's correlation (Equation (1.8)) is also appears to be inconsistent with experimental data. While for some data points it shows good agreement (see Figure 5-16), for others it does not, especially for high velocity data points (V > 10 m/s) it is overpredicting experimental results by 25%. Also it will be shown later in this chapter that the Chen correlation (as all other correlations mentioned above) does not predict the right slope of the curve wall heat flux versus wall superheat.

Analyzing the results presented in Figures 5-12 to 5-16 several preliminary conclusions can be made.

First, the Jens-Lottes correlation does not work well for divertor conditions because of the occurrence of suppression of nucleate boiling, and as was mentioned before in Chapter 1. The Jens-Lottes equation was derived for a moderate velocity case where there is no suppression of nucleate boiling phenomena.

Second, Yin's correlation underpredicts the experimental results because it was derived for a smaller tube diameter (3.6 mm). In Chapter 2 of this study it was found that the probability of nucleate boiling suppression increases as channel diameter decreases. Thus the second conclusion is consistent with previous analyses.

Third, while the Chen correlation is the best among those analyzed so far, it also does not have adequate performance versus experiment results for conditions of high heat and mass fluxes.

All the heat transfer results presented so far were based on heat transfer coefficients defined by Equation (4.1), using wall temperature minus bulk temperature difference. It is also desirable to consider heat transfer coefficient values defined as:

$$h = \frac{q_{local}}{(T_w - T_s)} \tag{5.1}$$

Results presented in Table 5-4 were recalculated using Equation (5.1). These recalculated data points are shown in Figure 5-17. It is interesting that now it becomes possible to separate different data points according to their velocities, while it was impossible when the heat transfer coefficient was defined

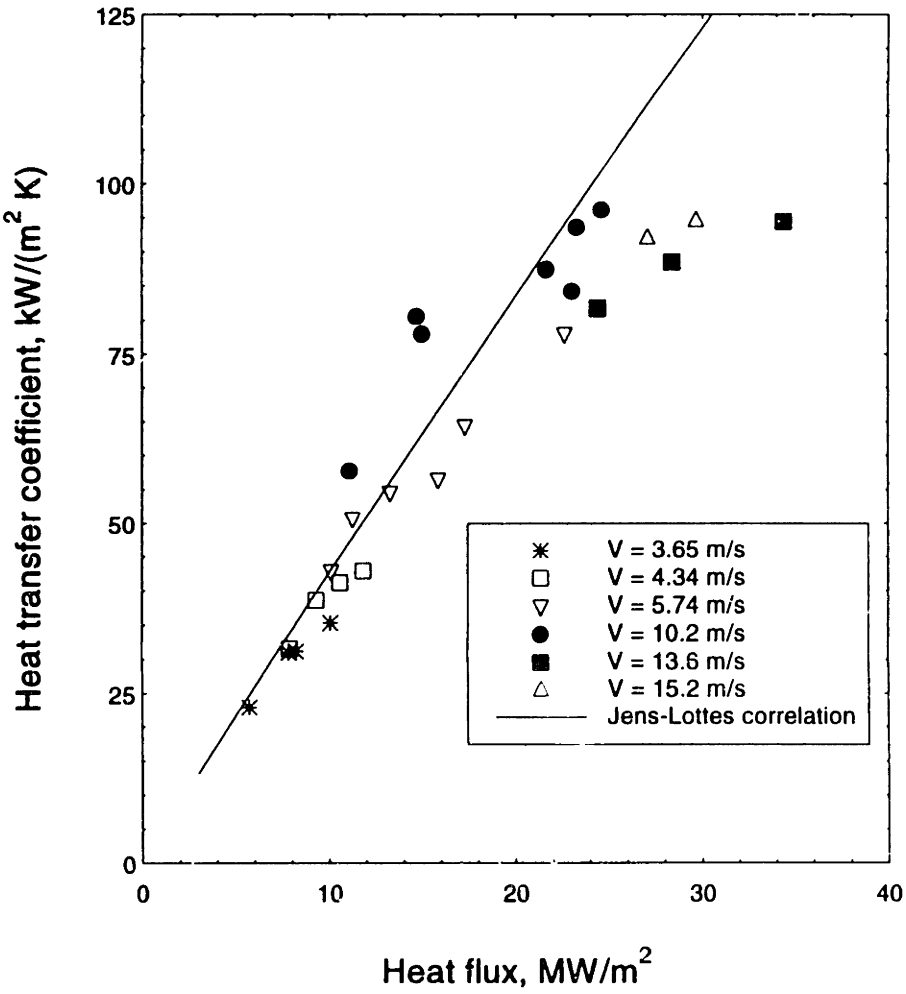

Figure 5-13: Local heat transfer coefficient vs. local heat flux ; comparison with Jens-Lottes correlation

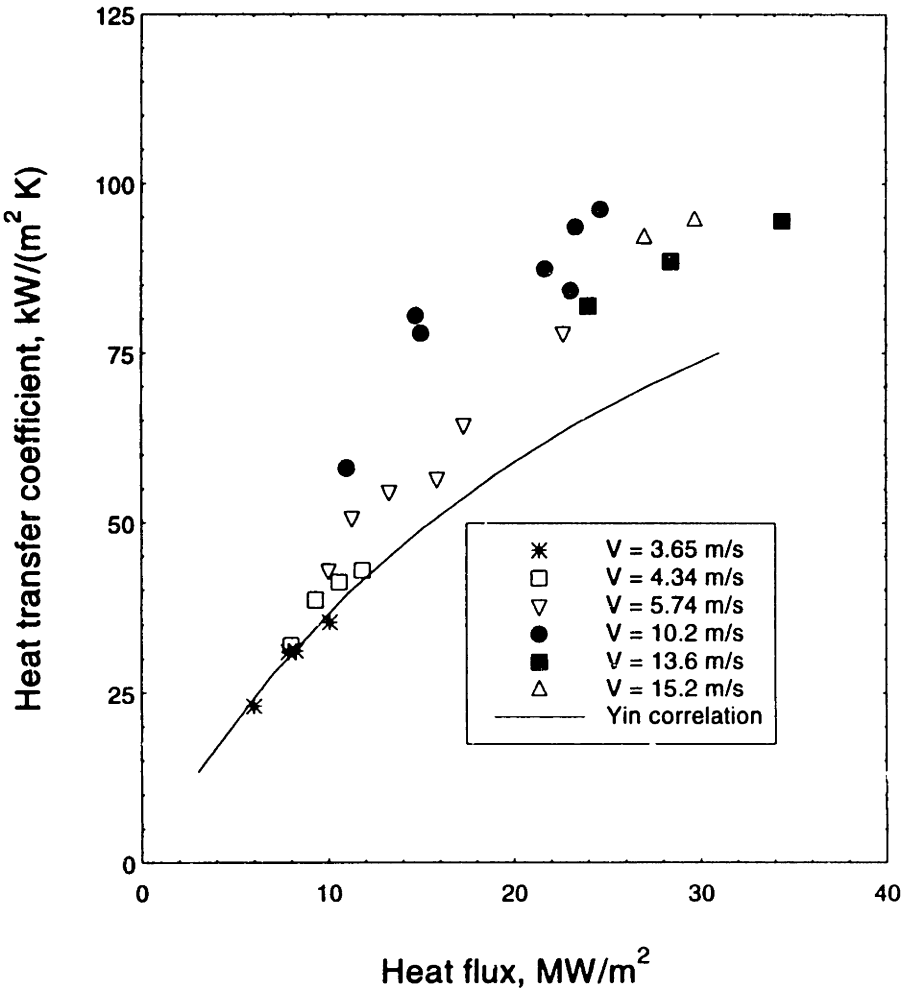

Figure 5-14: Local heat transfer coefficient vs. local heat flux; comparison with Yin's correlation

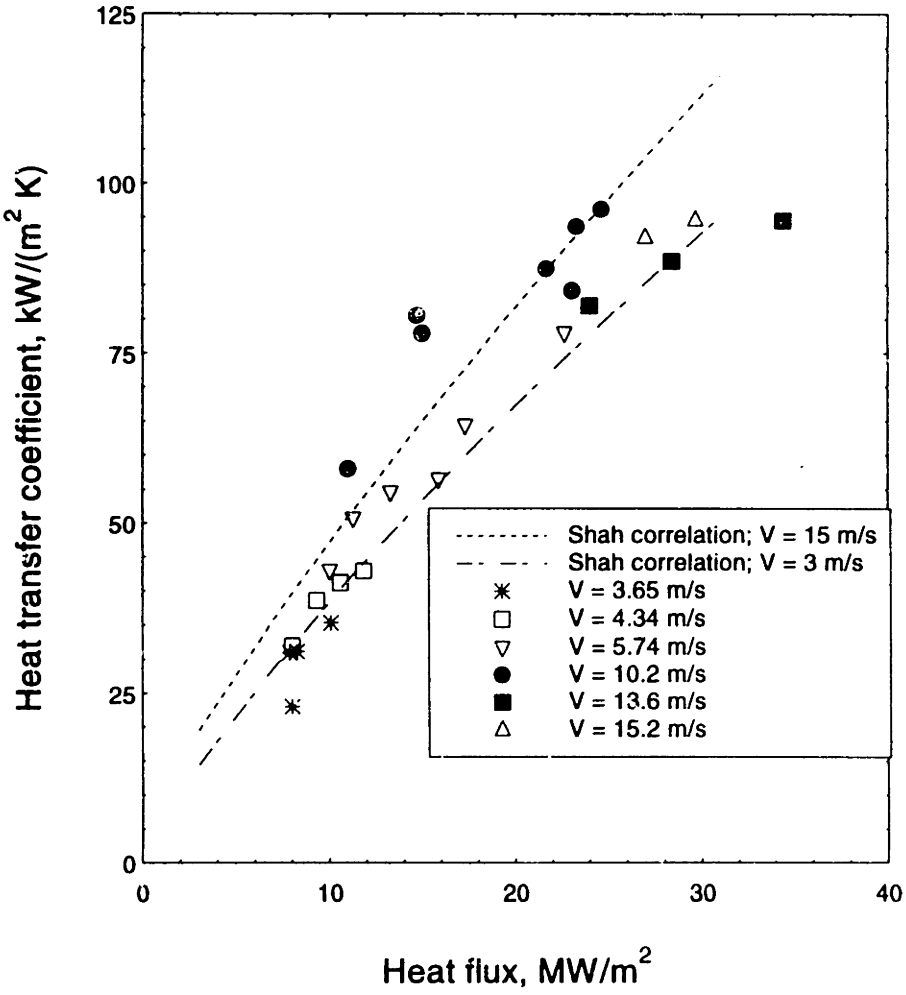

Figure 5-15: Local heat transfer coefficient vs. local heat flux; comparison with Shah correlation

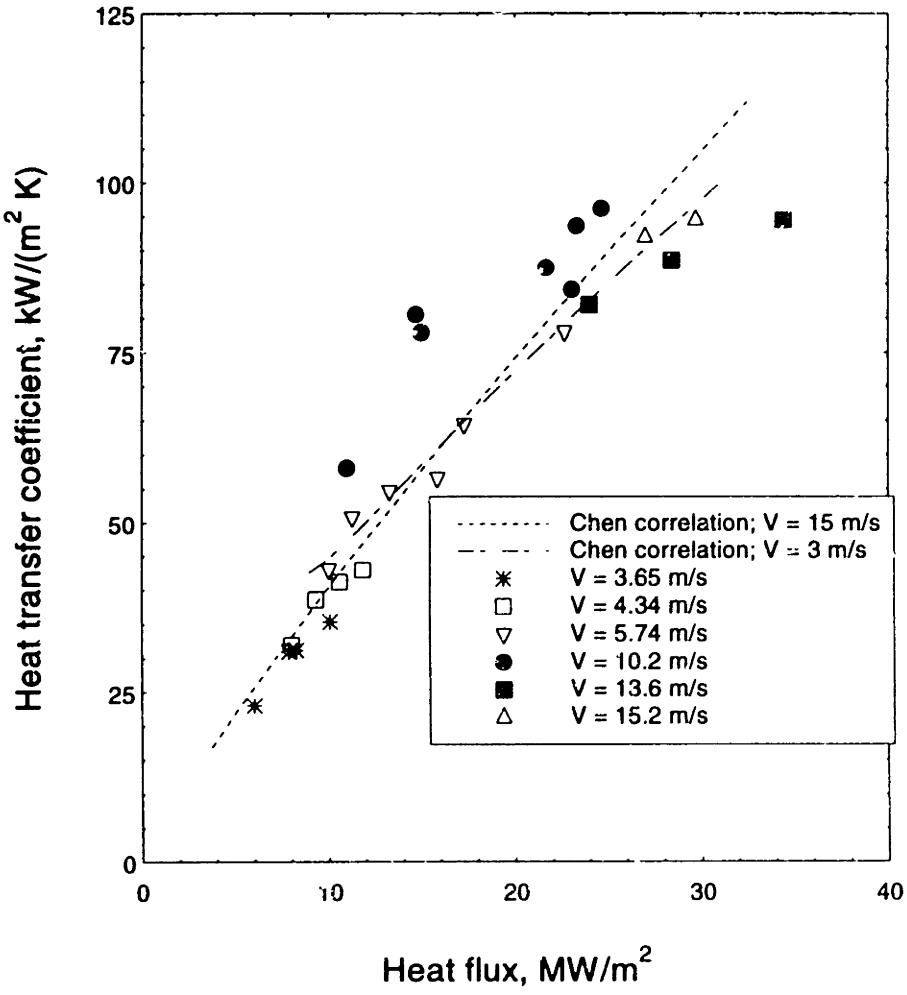

Figure 5-16: Local heat transfer coefficient vs. local heat flux; comparison with Chen correlation

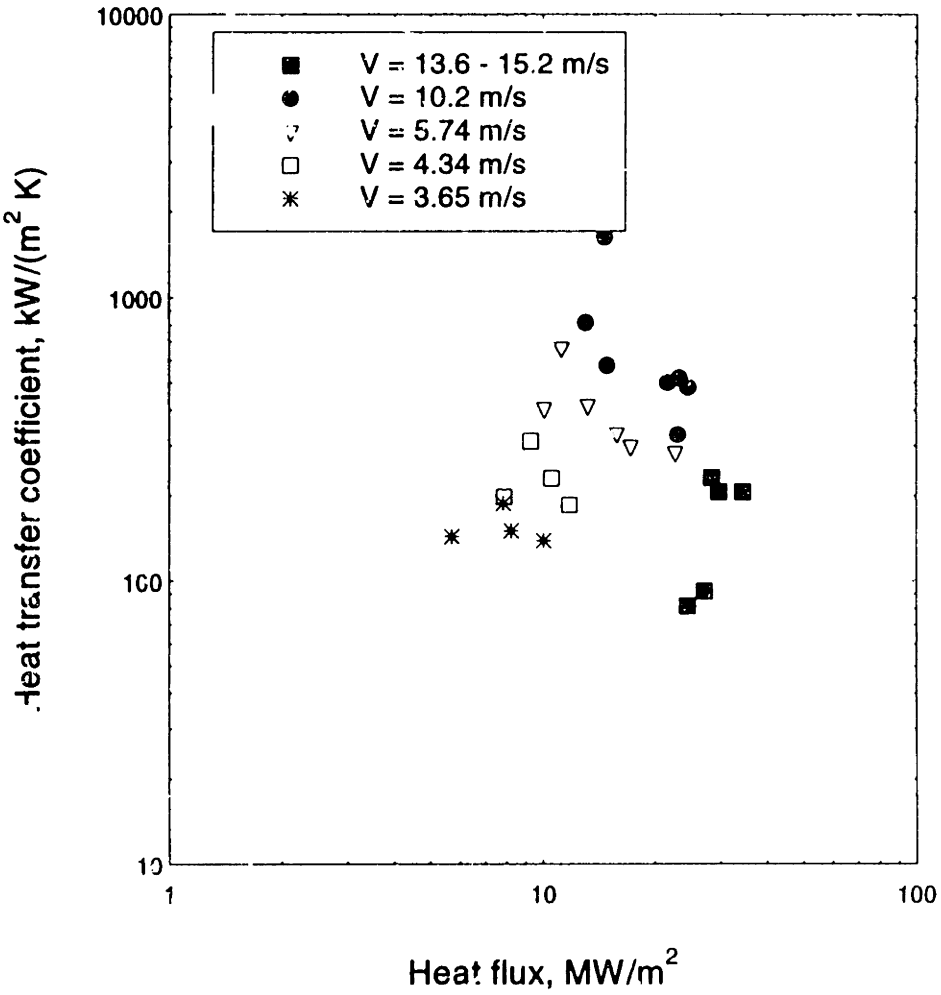

Figure 5-17: Local heat transfer coefficient based on wall superheat temperature difference vs. local heat flux

using the (T_w - T_b) temperature difference. This result again is what one expects to get. This is because there is no physical reason to use a heat transfer coefficient values defined by Equation (4.1) for the nucleate boiling region.

5.2.3 Development of Subcooled Nucleate Boiling Correlation

It was found that none of the correlations described above, neither (Eq.(1.5), (1.7), (1.8) nor (1.19)) had adequate performance versus the experimental results for conditions of high heat and mass fluxes (see Figures 5.13 to 5.16). That is our reason for creating a new nucleate boiling correlation applicable to fusion reactor divertor conditions. Experimental results showed that the Chen correlation (Eq.(1.8)) is unquestionably one of the better choices when compared with other correlations for subcooled nucleate boiling. However, because it was originally derived for saturated flow boiling, it needs corrections to the suppression factor (S) and to the forced convection correction multiplier (F). This should allow for the enhancement of the forced convective heat transfer mechanisms arising from the generation of vapor in the boundary layer next to the wall. Thus the F factor should be a function of the S factor and wall temperature.

An assumption was made that there are two mechanisms for nucleate boiling suppression. The first mechanism is due to the turbulence influence on steam bubble growth for high velocity flows. This mechanism was discussed in Chapters 1 and 2 of the present study. At high velocity, transverse velocity oscillations can be very high and the probability of turbulent vortex destroying vapor bubbles on the wall gets larger as the flow velocity increases.

The second mechanism is due to the high heat flux. This mechanism is discussed by Valle and Kenning [40]. They found that the total population of nucleation sites increases with increasing wall heat flux, the startup of new sites deactivated many of the sites active at lower wall heat flux (lower superheat). The activation of new sites tends to deactivate the old sites, according to [40] the influence declining over a distance of 2.5 bubble radius. Hence, many sites active at low wall superheat (low heat flux) become inactive at higher superheat (higher heat flux). An assumption is made that the total suppression factor in the nucleate boiling term is a function of both Reynolds number and heat flux, thus

$$S = S_v \; S_q \, (q_w / CHF) \tag{5.2}$$

where:
S_v = suppression factor due to velocity (i.e. Re)
S_q = suppression factor due to heat flux
CHF = Critical Heat Flux, (MW/m^2)
Given all of these factors the following form of the correlation can be proposed

$$q_w = F(S_v)(T_w / T_v)^n \, h_{vp} \, (T_w - T_b) + S \, h_{nb} \, (T_w - T_v) \tag{5.3}$$

where h_{vp} - single-phase heat transfer coefficient is to be calculated using the Petukhov correlation (Equation (1.2)) with a viscosity correction multiplier;
n - some coefficient that has to be determined;
h_{nb} - nucleate boiling heat transfer coefficient to be calculated using the original Chen correlation:

$$h_{nb} = 0.00122 k_f^{0.79} c_{pf}^{0.45} \rho_f^{0.49} (T_w - T_v)^{0.24} \frac{(P(T_w) - P(T_v))^{0.75}}{\sigma^{0.5} \mu_f^{0.29} \rho_g^{0.24} H_{fg}^{0.24}} \tag{5.4}$$

In order to develop correlations for F, S_v and S_q the following assumptions are made. It is assumed that for low velocity flows there is no suppression of nucleate boiling. Also, because correlations (Equations (1.5)

and (1.6)) developed for this case predict heat removal by vapor bubbles only (see Chapter 1), it is also assumed that for low velocity flow nucleate boiling dominates and convective contribution is not important. When no suppression of nucleate boiling exists, bubbles generated on the heated wall destroy the convective boundary layer and most of the heat is removed from the wall by vapor bubbles. Thus, based on the ranges of Equations (1.5) and (1.6) it is assumed that for Re = 5000 S_v value should equal to one. It is assumed also that the value of F is zero for a velocity up to 3 m/s and close to one for high velocity flows (V > 10 m/s). Also for local heat fluxes below CHF it is reasonable to assume that the value of S_q is equal to one. These assumptions make it possible to determine the value of suppression factor due to velocity (S_v). It is postulated that this equation should have the following form:

$$S_v(Re) = \frac{1}{1 + a\,Re^b} \tag{5.5}$$

where: a and b are coefficients that have to be determined.

Only two data points are needed to determine these coefficients. These points are obtained because we assumed that for small velocity (Re < 5000) $S_v(5000) = 1$ and we know that for large values of the Reynolds number, F = 1. Using original experimental data for high velocity runs (V > 10 m/s), Equations (5.3), (5.4) and the assumptions made above, it is possible to find coefficients a and b in Equation (5.5). The equation for suppression factor due to velocity is therefore found to be:

$$S_v(Re) = \frac{1}{1 + 1.52 * 10^{-16} (Re)^{3.37}} \tag{5.6}$$

The suppression factor calculated with the help of Equation (5.6) is compared with the suppression factor of the Chen correlation (Equation (1.11)) in Figure 5.18. From this figure it can be seen that since for some range of the Reynolds numbers the two equations predict similar results, Equation (5.6) can be used for further development of a subcooled nucleate boiling correlation. The difference is due to the fact that the Chen correlation originally was derived for saturated boiling. Thus, it cannot be directly applied over wide range of the Reynolds numbers for subcooled nucleate boiling case.

Now with the help of Equation (5.6) and with the assumption that F=0 for low velocity flows (V < 3 m/s), correlation for suppression factor due to heat flux can be developed for the low velocity case experimental results as follows:

$$S_q\left(\frac{q_w}{CHF}\right) = \frac{1}{1 + 1.41\left(\frac{q_w}{CHF}\right)^{29}} \tag{5.7}$$

An assumption is made that Equation (5.7) can be applied for the whole range of velocities considered in this study. The suppression factor due to heat flux is plotted versus relative local heat flux in Figure 5.19. From this figure one can see that for low values of local wall heat flux there is no suppression due to heat flux, and only when the heat flux is approaching CHF this kind of suppression occurs. This result is consistent with experimental and theoretical investigations of Valle and Kenning [40].

After these steps (developing correlations for suppression factors) it is finally possible to determine the equation for the F factor for the whole range of conditions used in the experiments. The acceptance criteria should be formulated as follows: all data points must fit well a single curve plotted in the coordinates F versus S_v. Also, it is assumed that, for the whole range of S_v, the value of F should be less than one. Using experimental results, the values of F are found. These data points are plotted in Figure 5.20.

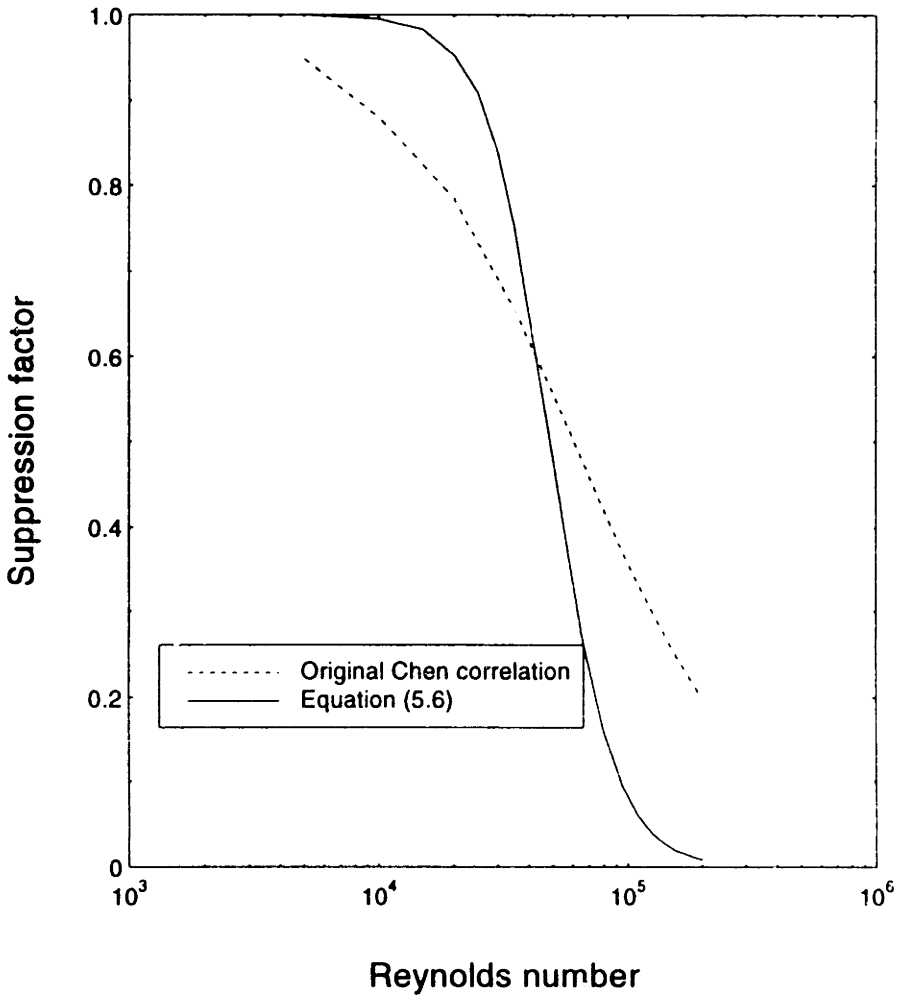

Figure 5-18: Suppression factor due to velocity as a function of the Reynolds number

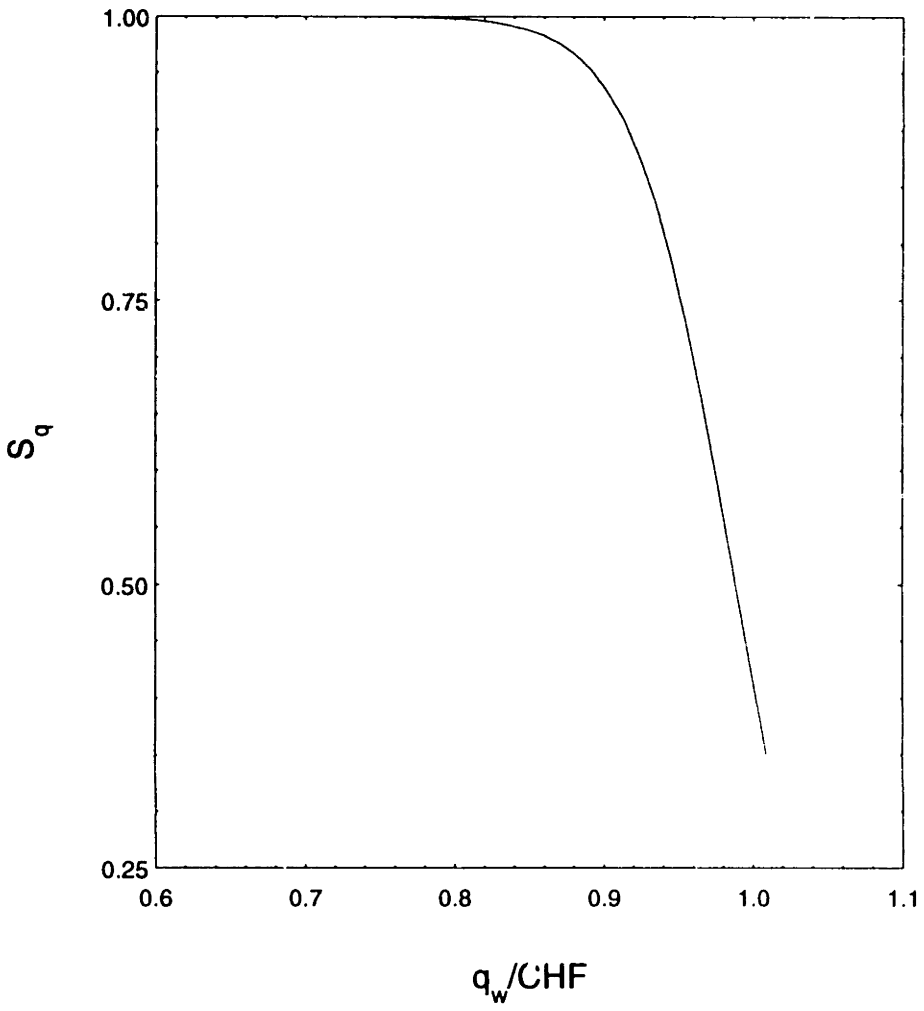

Figure 5-19: Suppression factor due to heat flux as a function of relative local wall heat flux

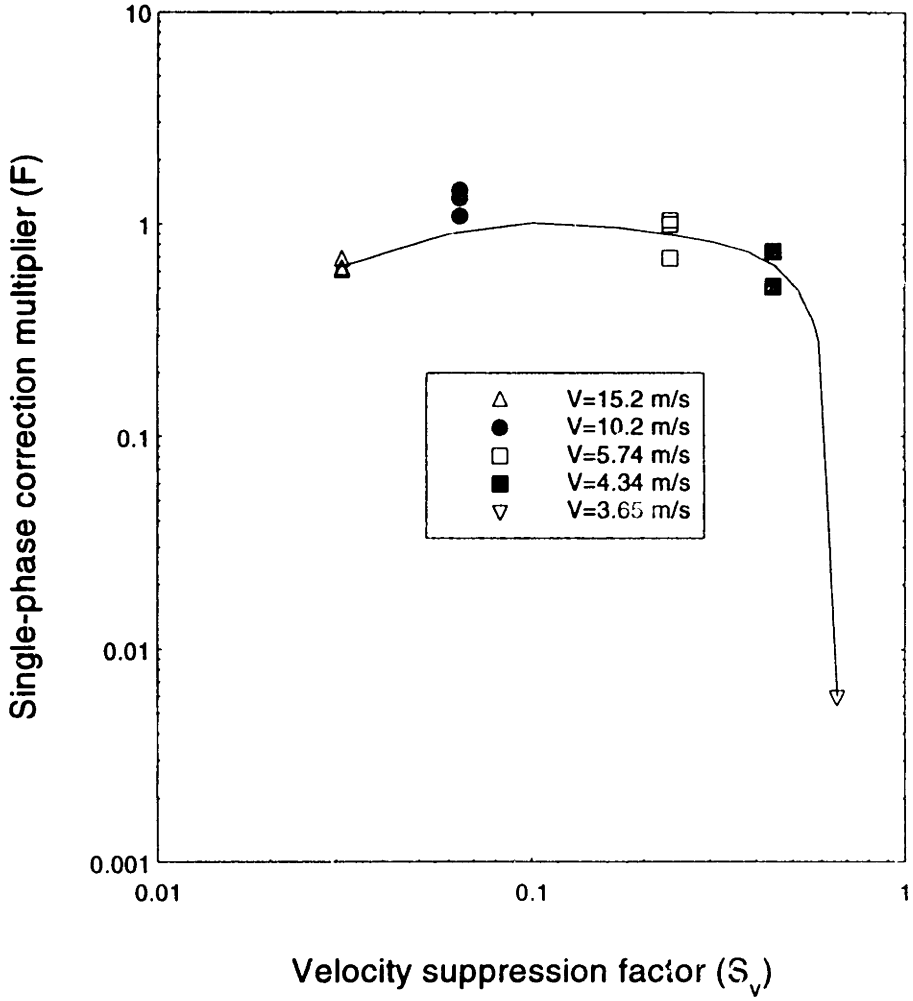

Figure 5-20: Single-phase correction multiplier (F) as a function of suppression factor due to velocity

It is found that the data points will form a single line if the value of coefficient n in Equation (5.3) is equal to two. A correlation for the F coefficient is found as follows:

$$F=(36.7S_v^{1.06}-37.2S_v^{0.5}-14.5\exp(S_v)+37S_v^{0.16}) \quad (5.8)$$

The data points shown in Figure 5.20 form a single line. Hence, acceptance criteria formulated above is satisfied. Now it is obvious that Equations (5.6) and (5.7) derived using only a small number of experimental data points are valid for the whole range of velocities and heat fluxes. Equation (5.8) can be applied for V = 4 to 15 m/s. For V < 4 m/s, F = 0. That means that for low velocities there is no nucleate boiling suppression and many vapor bubbles are generated on the heated wall. They destroy the boundary layer and prevent heat transfer via convection. Thus the final form of the subcooled nucleate boiling correlation proposed in this study is as follows:

$$q_w = F(S_v)\left(\frac{T_w}{T_s}\right)^2 h_{sp}(T_w - T_b) + S_v S_q h_{nb}(T_w - T_s) \quad (5.9)$$

where: $F(S_v)$, S_v, S_q are given in Equations (5.8), (5.6) and (5.7).

Comparisons of the proposed correlation with experimental results for different velocities are presented in Figures 5-21, 5-22, 5-23 and 5-24. For the value of CHF in Equation (5.7) results presented in Chapter 6 of this thesis are used (Tables 6.1 and 6.2). It is clear from these figures that the new correlation is more reliable than any of the other correlations tested for nucleate boiling region.

The agreement between calculated and experimental results was found to be in the range of $\pm$20% for P=3 MPa, bulk temperatures from 17 to 22 °C and 3-19 m/s velocity range. This comparison is presented in Figure 5-25. Data points shown in this figure are those used for developing the proposed correlation and other data points which were not used for correlation developing. The proposed correlation can be applied only if it predicts a wall heat flux greater than single phase convection, $q_w > h_{sp}(T_w - T_b)$; otherwise Equation (1.2) should be applied.

5.2.4 Subcooled Nucleate Boiling Correlation applied to Different Velocities, Pressures and Subcooling

The purpose of this investigation is to examine the proposed correlation's behavior for conditions different than was used for its derivation. Although this comparison cannot prove that the new correlation can be used out of its original range of parameters, the predictions of the correlation proposed above should be realistic. Also for its original range (subcooling and pressure), the new correlation (Equation (5.9)) predicts heat transfer coefficients between the Yin and the Chen correlations, and the same tendency should be observed for other values of pressure, velocity and/or subcooling.

The heat transfer coefficient is plotted versus flow velocity for low and high values of local heat flux in Figures 5-26 and 5-27. Heat transfer coefficients calculated by using the proposed correlation are higher than the Yin correlation calculations but lower than Jens-Lottes predictions. This is expected given that the Jens-Lottes correlation ignores suppression of nucleate boiling. When the velocity increases from 3 m/s to 11 m/s, the heat transfer coefficient should increase because of the role of single-phase convection. Within this range of velocities there is suppression of nucleate boiling. However, vapor bubble generation rate is decreasing, and the role of single-phase convection is increasing (bubbles cannot deform the boundary layer), especially at the higher velocities. It seems that within this range of velocities (from 3m/s to 11 m/s), partially suppressed nucleate boiling exists and there is a large single-phase convection contribution to heat removal from the wall. As the value of velocity increases, nucleate boiling becomes

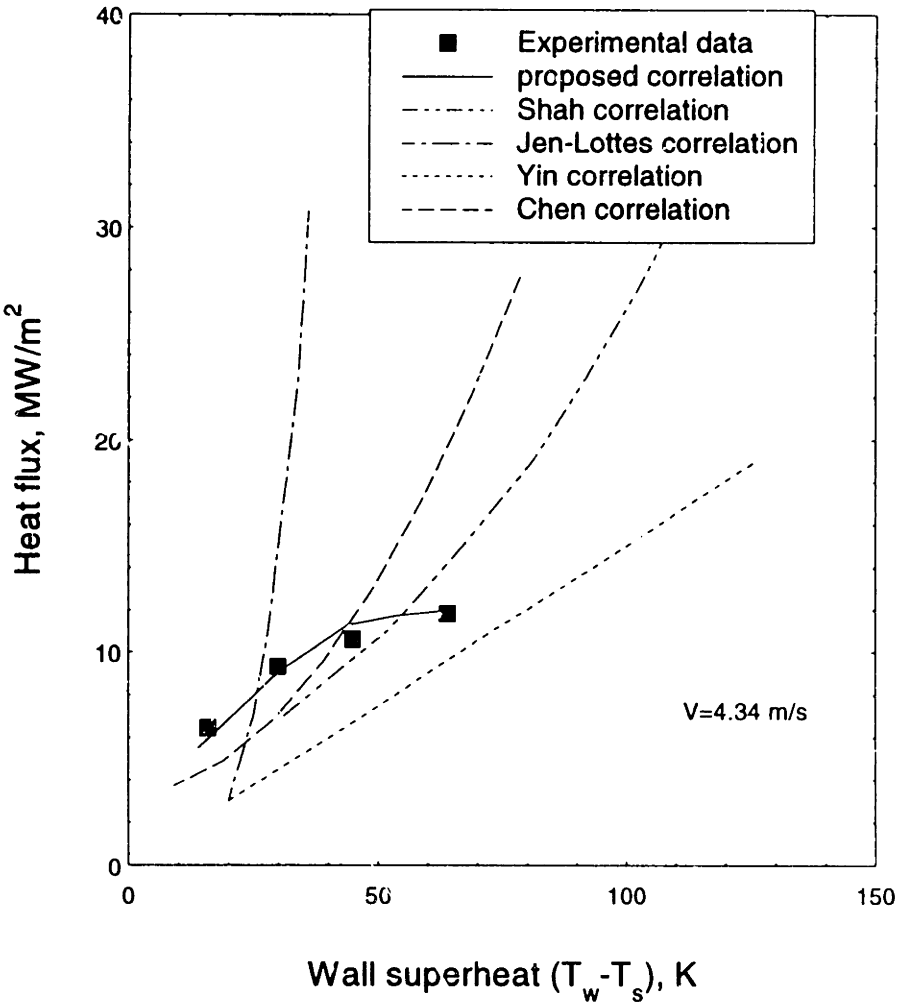

Figure 5-21: Local heat flux as a function of wall superheat

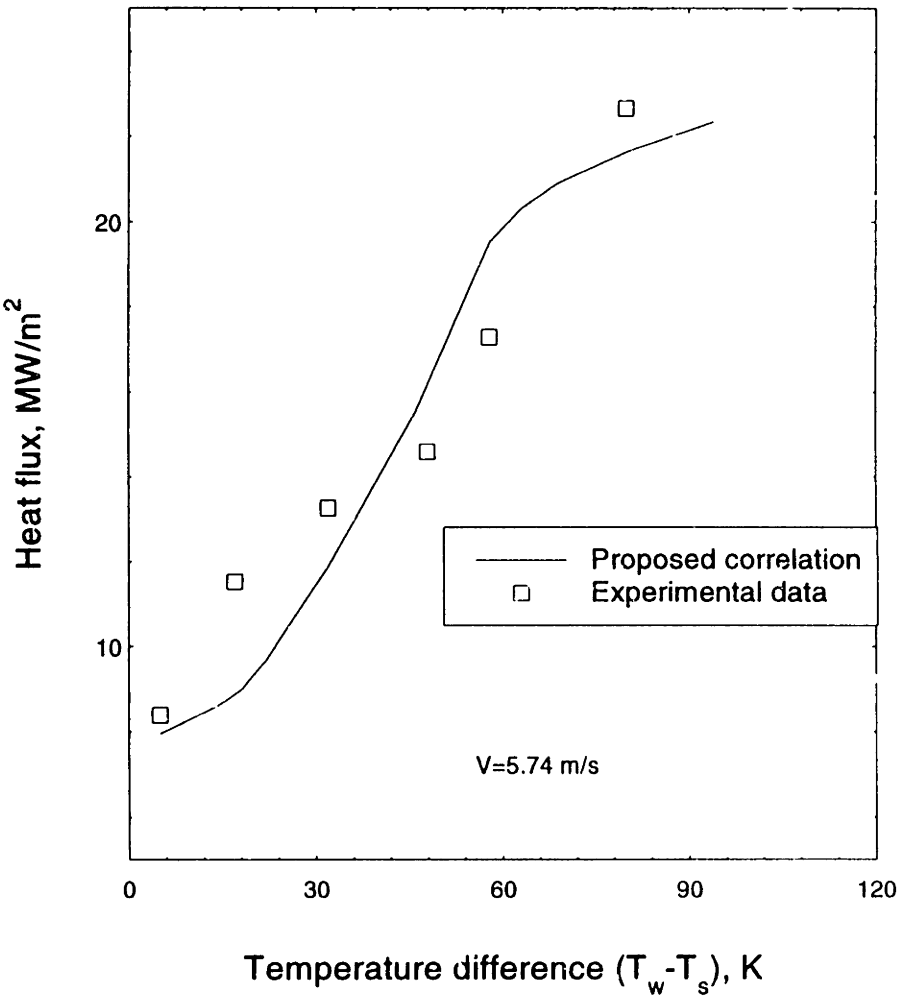

Figure 5-22: Local heat flux as a function of wall superheat

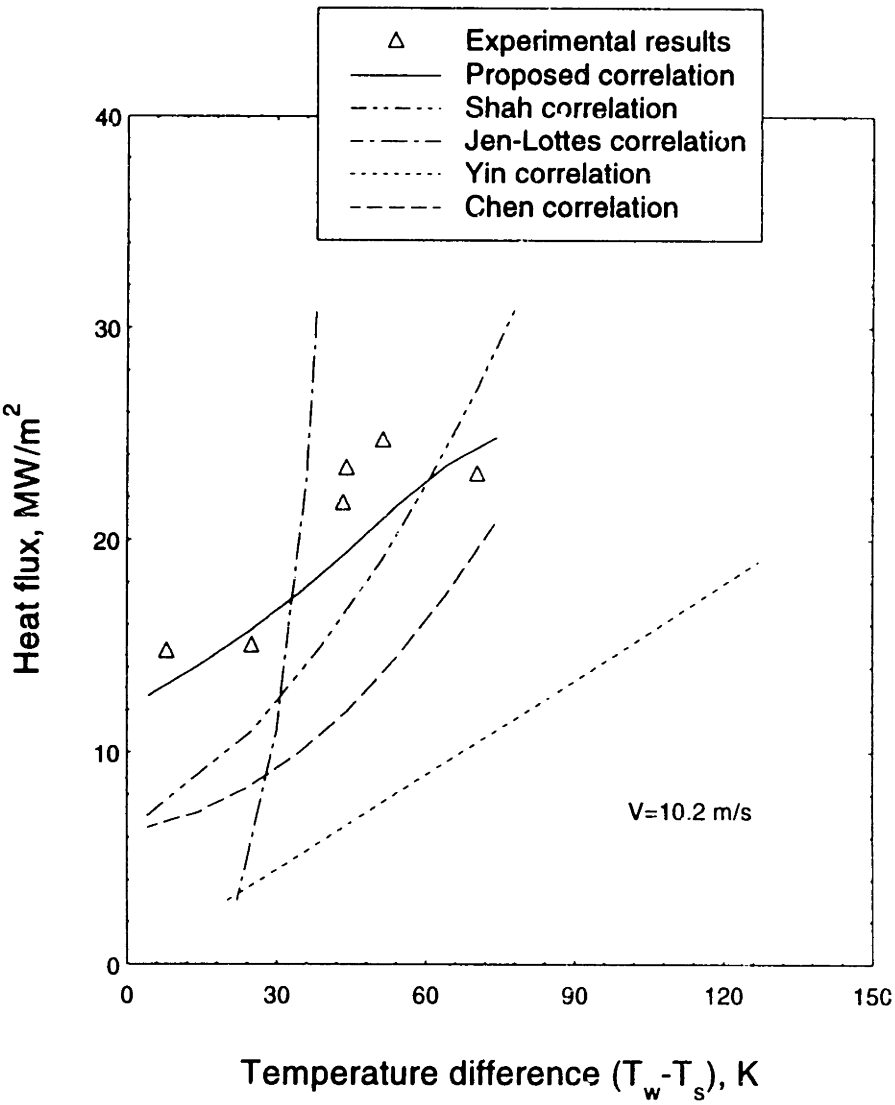

Figure 5-23: Local heat flux as a function of wall superheat

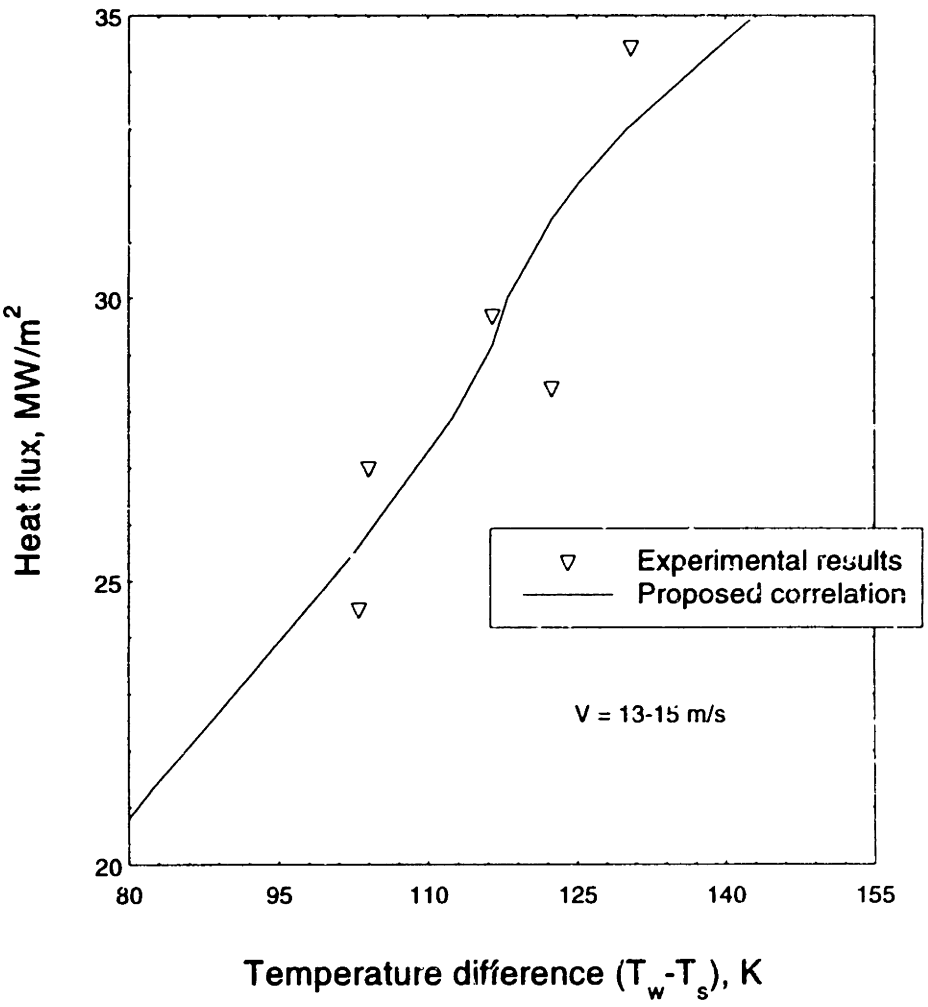

Figure 5-24: Local heat flux as a function of wall superheat

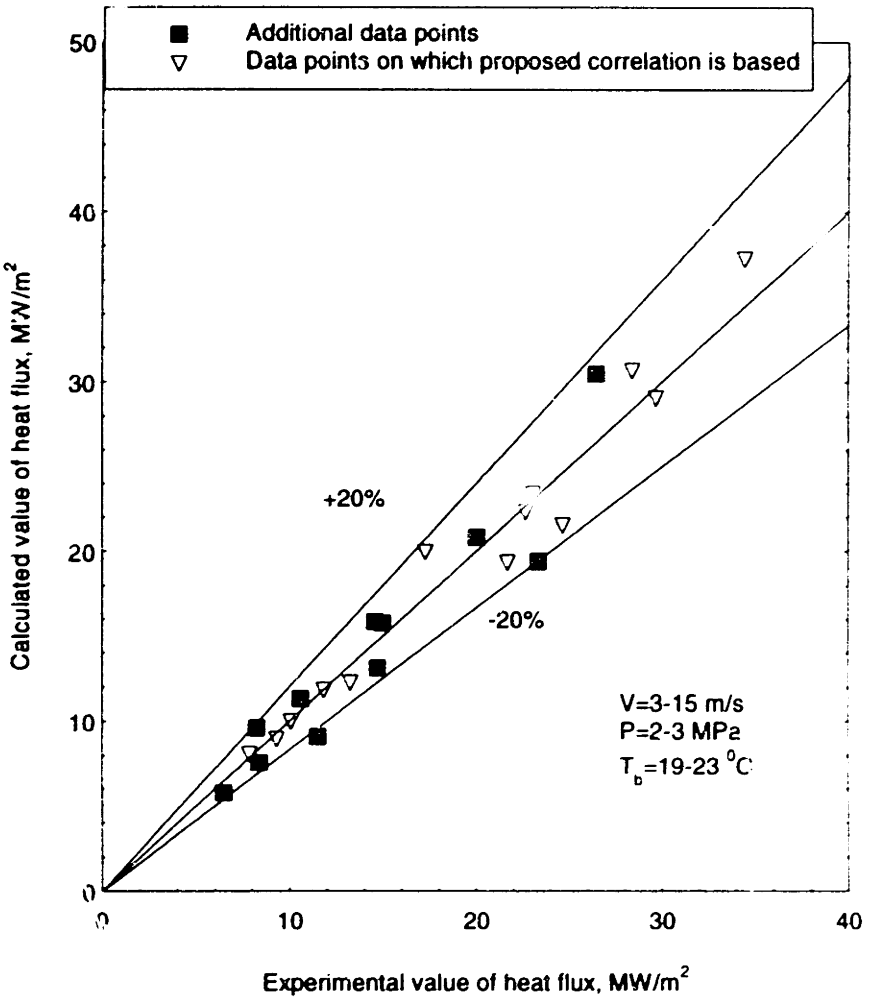

Figure 5-25: Comparison between experimental and calculated results

more suppressed and the total value of heat transfer coefficient may decrease when the nucleate boiling suppression becomes noticeable. However, at velocities sufficiently high, single phase heat transfer is capable of very efficient heat transfer and no nucleation occurs. This tendency can be observed in Figures 5-26 and 5-27.

Figure 5-28 shows the heat transfer coefficient plotted versus bulk water temperature using three different correlations (the proposed, Shah and Chen correlations) for an intermediate velocity of 9 m/s. Results of the proposed correlation are higher than the Shah correlation and are lower than the Chen correlation predictions. Hence, the proposed correlation behavior tested against different bulk temperatures seems reasonable and it can be used for preliminary design calculations for high velocity flow. It should be tested by additional experiments in order to be used.

It is also desirable to apply the proposed correlation (Equation (5.9)) for different values of pressure. Experimental data analysis presented in Chapter 2 shows that nucleate boiling suppression is a function of pressure. Therefore the proposed correlation has to be modified. This modification is done in the following way. As it was mentioned before, the subcooled nucleate boiling in high velocity flow involves different mechanisms. For heat fluxes less than CHF (q_w < 0.8 CHF) there are two heat transfer mechanisms: heat transfer via single-phase convection and heat transfer via nucleate boiling. The only data available for analysis are data from [20] where suppression of nucleate boiling was found for swirl flow at moderate velocities for a pressure range from 3 MPa to 15 MPa. Because it was found (see Chapter 2) that the suppression mechanism for high velocity smooth and swirl flows is the same, it is decided to use those data in the proposed correlation modification. Also, the data in [20] was obtained for relatively low velocities (V < 1 m/s). According to data analyzed in the present study, there is no heat transfer at low velocity case via single-phase convection. Thus, the proposed correlation (Equation (5.9)) is modified as follows:

$$q_w = F(S_v)\left(\frac{T_w}{T_s}\right)^2 h_{sp}(T_w - T_b) + S_P S_v S_q h_{nb}(T_w - T_s) \tag{5.10}$$

where: S_P = pressure correction factor and T is in K.

In order to obtain an expression for the pressure correction factor, data obtained in [20] are plotted as heat transfer coefficient ratio (experimental value of heat transfer coefficient / heat transfer coefficient for fully developed nucleate boiling obtained with the help of Equation (1.14)) versus pressure. This curve is shown in Figure 5-29. The following expression (Equation (5.11)) fits the experimental data presented in Figure 5-29.

$$\frac{h_{ex}}{h_{fnb}} = 0.33p_r^2 - 0.58\sqrt{p_r} + 1.07\frac{1}{p_r^2 + 1} \tag{5.11}$$

where: h_{ex} = experimental value of heat transfer coefficient;
h_{fnb} = fully developed nucleate boiling heat transfer coefficient;
p_r = reduced pressure (absolute pressure / critical pressure).

Because the original correlation was developed for pressure equal to 3 MPa it is desirable to make the pressure correction coefficient equal to one at this pressure. In other words, we use P = 3 MPa as a reference pressure. Using this approach and Equation (5.11), the pressure correction coefficient can be determined from the following expression:

$$S_P = 0.39p_r^2 - 0.69\sqrt{p_r} + 1.27\frac{1}{p_r^2 + 1} \tag{5.12}$$

The pressure correction factor versus pressure is presented in Figure 5-30. This correction is taking into account suppression changes due to changes in physical properties for different pressures. Of course, h_{nb} coefficient in Equation (5.10) is also a function of pressure, but it seems that it does not take into account suppression of nucleate boiling phenomenon (because the Chen correlation was developed for relatively low flow velocity case).

Figures 5-31 and 5-32 show heat flux as a function of wall superheat according to Jens-Lottes and Shah correlations predictions for different values of pressure. In Figure 5-33 the proposed correlation behavior with the pressure correction factor is shown for several pressures. As can be seen from these figures, the correlation predicts the same tendency at all three pressures. As the pressure is increased, the wall superheat value decreases. Also the proposed correlation with the pressure correction coefficient predicts reasonable values of heat flux for a given value of wall superheat. Because no experiments were done for pressure values other than 3 MPa, the proposed expression for pressure correction coefficient (Equation (5.12)) should be considered as an interim equation to be verified experimentally.

5.3 Comments

For the single-phase region, the Petukhov correlation (Equation (1.2)) is found to be applicable.

A subcooled boiling correlation (Equation (5.10)) for fusion reactor divertor conditions has been developed. Compared with experimental data used in developing the equation, and with other data points not used in developing the equations, the new correlation was found to be more reliable than any of the other correlations tested for nucleate boiling.

The proposed correlation predicts physically reasonable results for different velocities, pressures and subcooling when extrapolated outside of the experimentally tested range.

Since the proposed correlation distinguishes clearly between nucleate boiling and forced convection effects, it can be used as a starting point in understanding the suppression of nucleate boiling which exists at high velocities and for prediction of THN limit for high velocity high heat flux flows. This will be done in the next chapter of the present thesis.

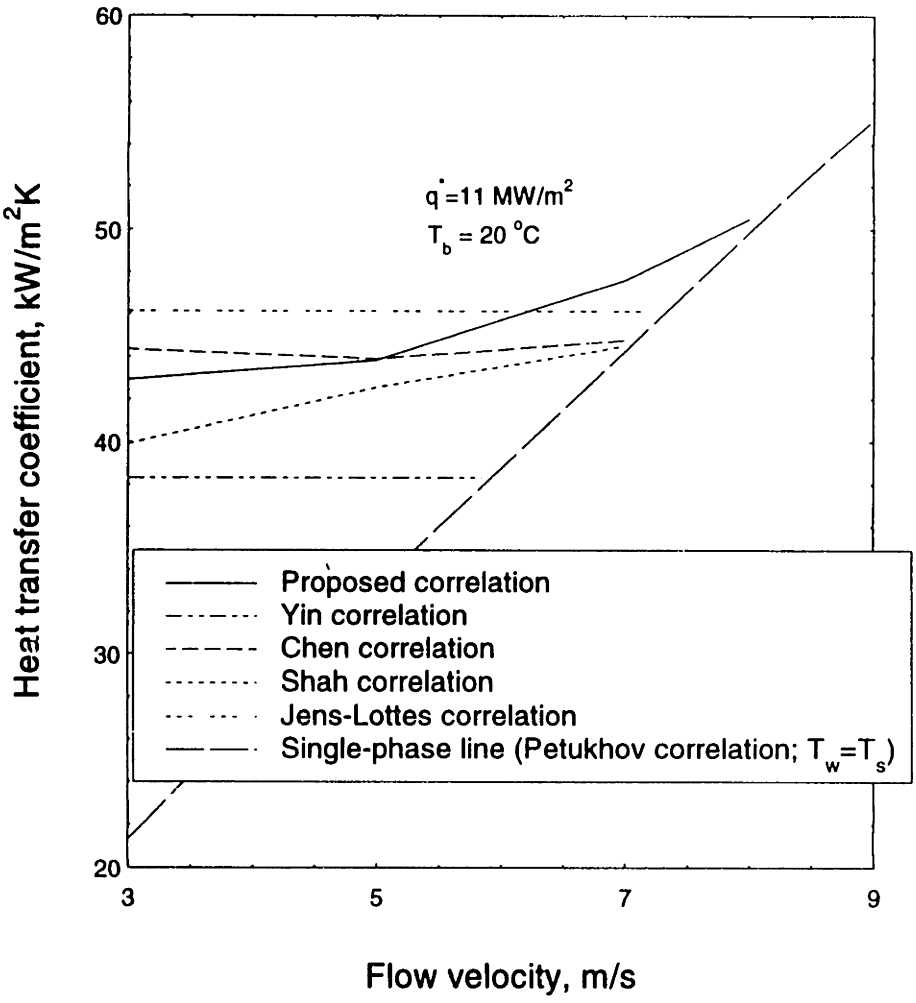

Figure 5-26: Heat transfer coefficient as a function of flow velocity

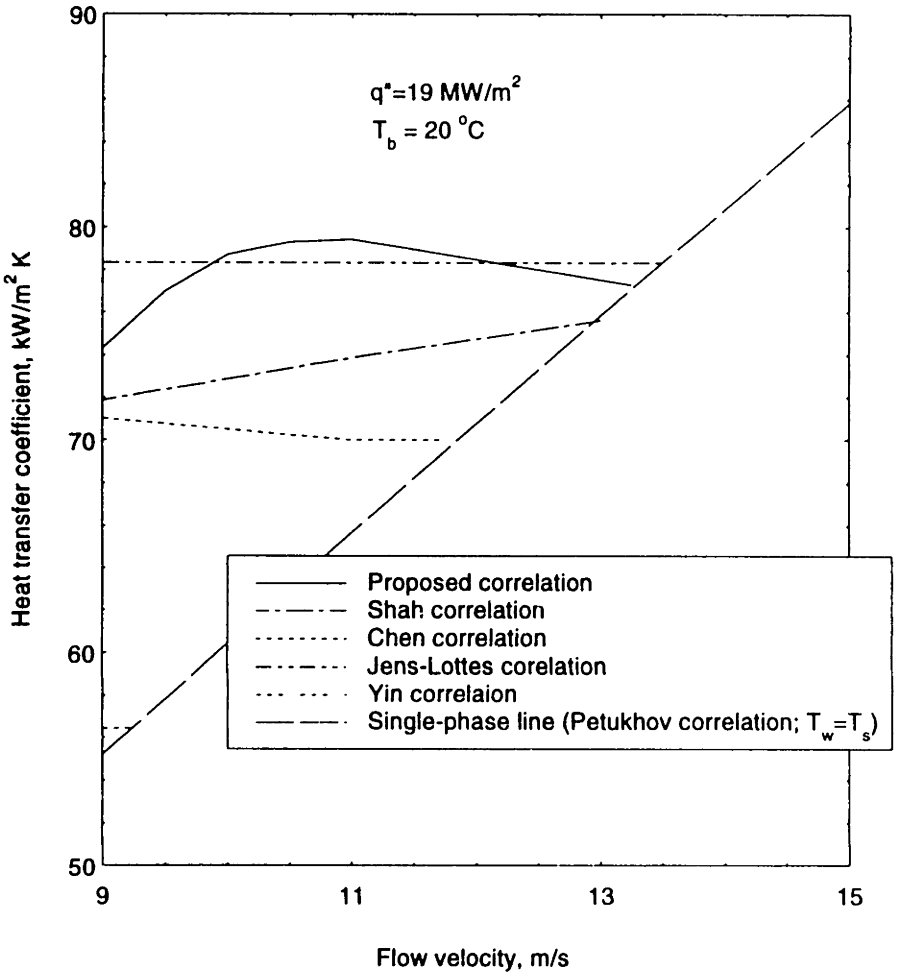

Figure 5-27: Heat transfer coefficient as a function of flow velocity

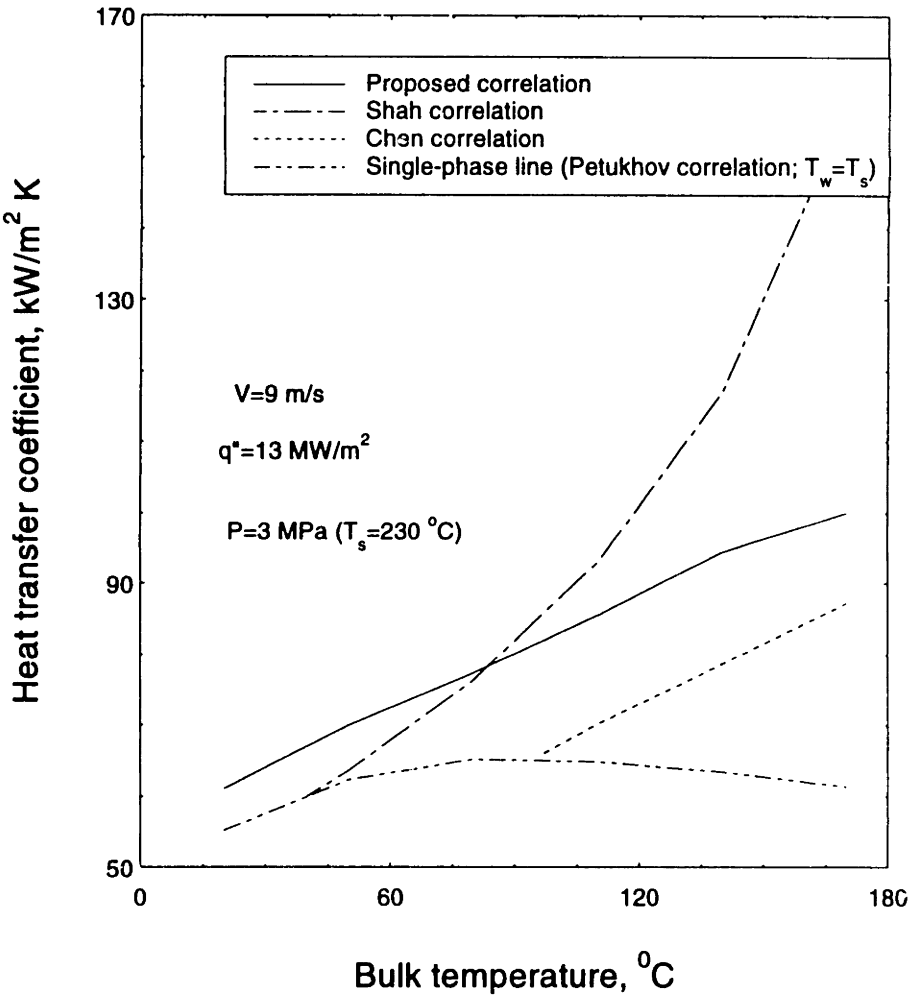

Figure 5-28: Heat transfer coefficient as a function of bulk temperature

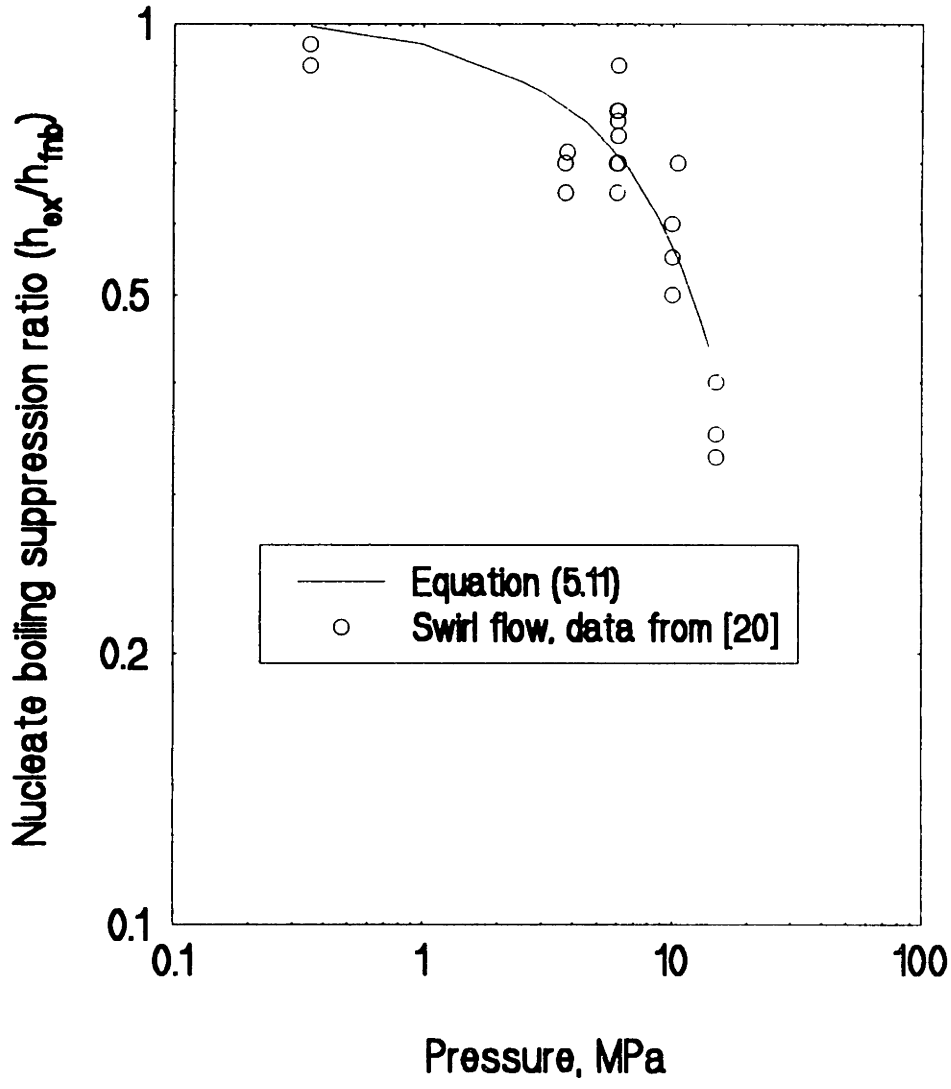

Figure 5-29: Nucleate boiling suppression ratio as a function of pressure

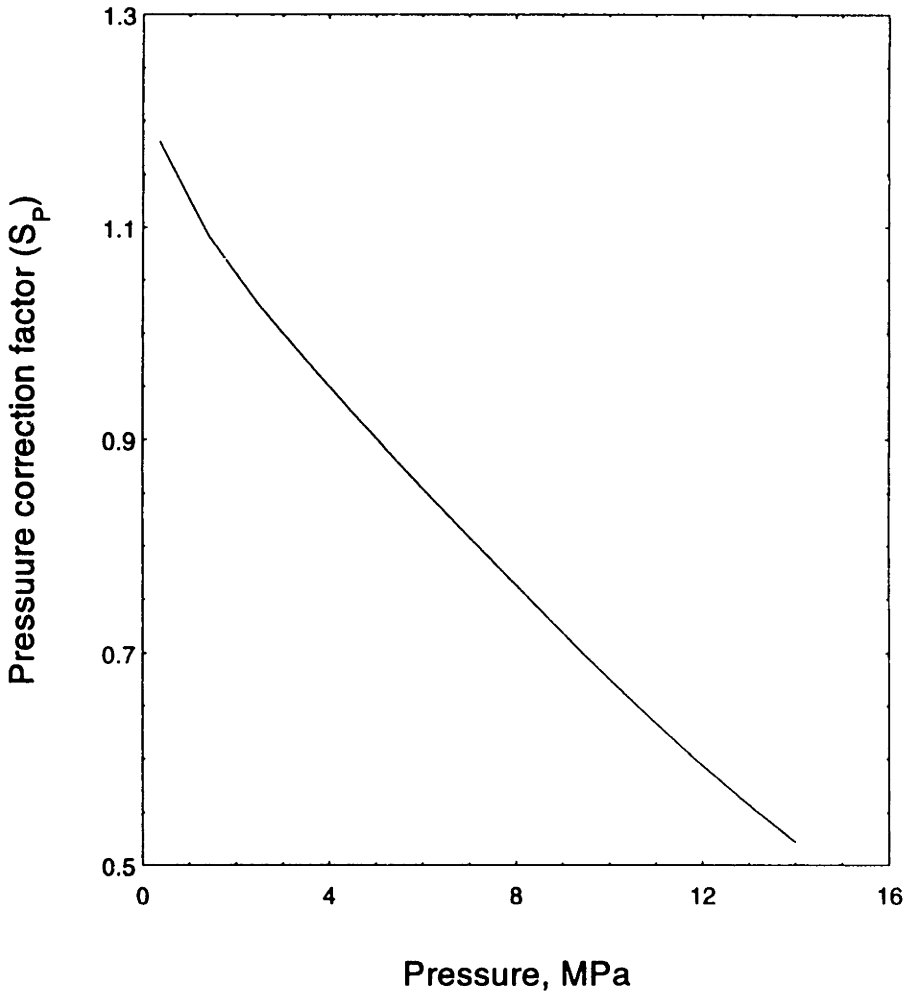

Figure 5-30: Pressure correction factor as a function of pressure

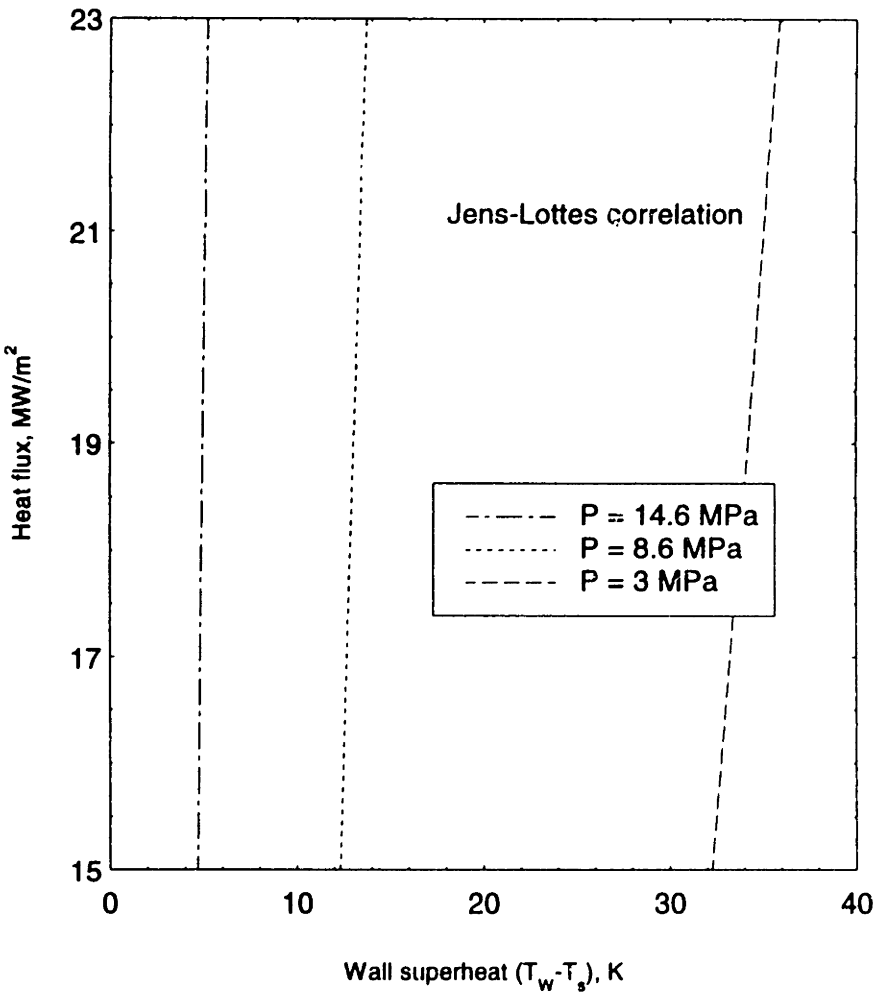

Figure 5-31: Local heat flux as a function of wall superheat

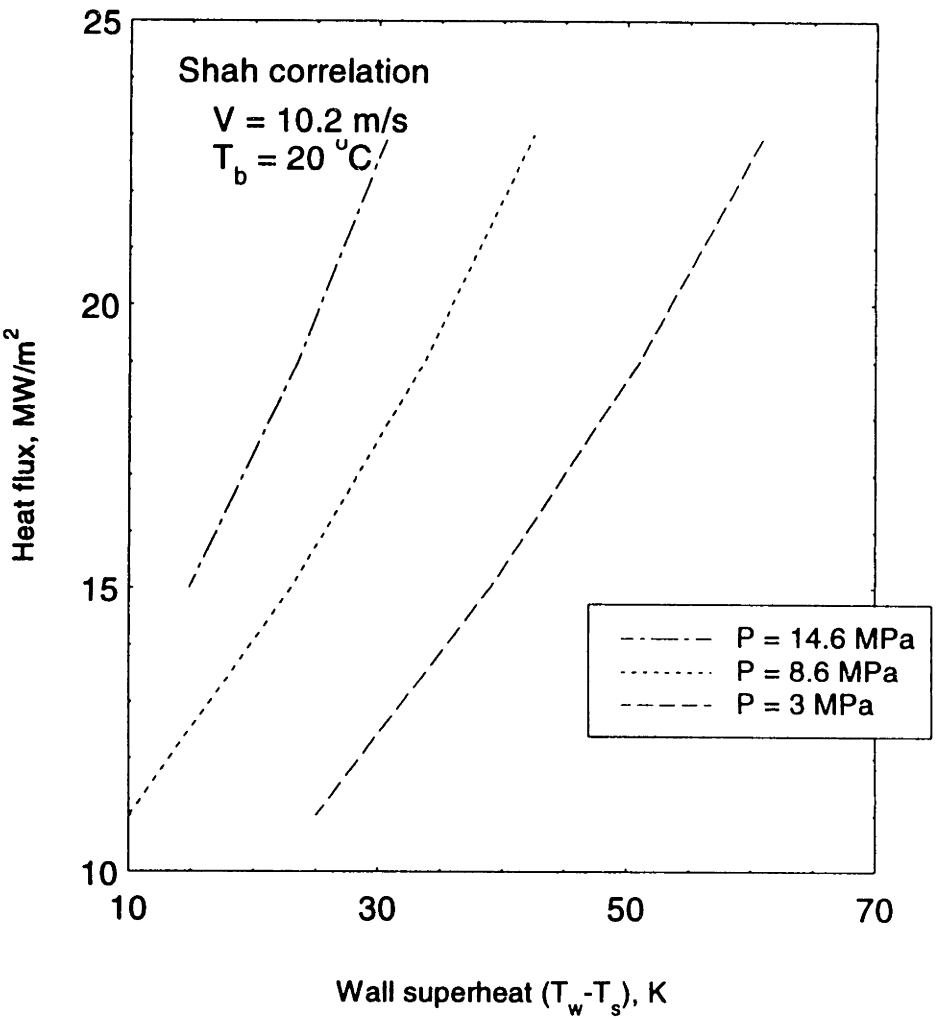

Figure 5-32: Local heat flux as a function of wall superheat

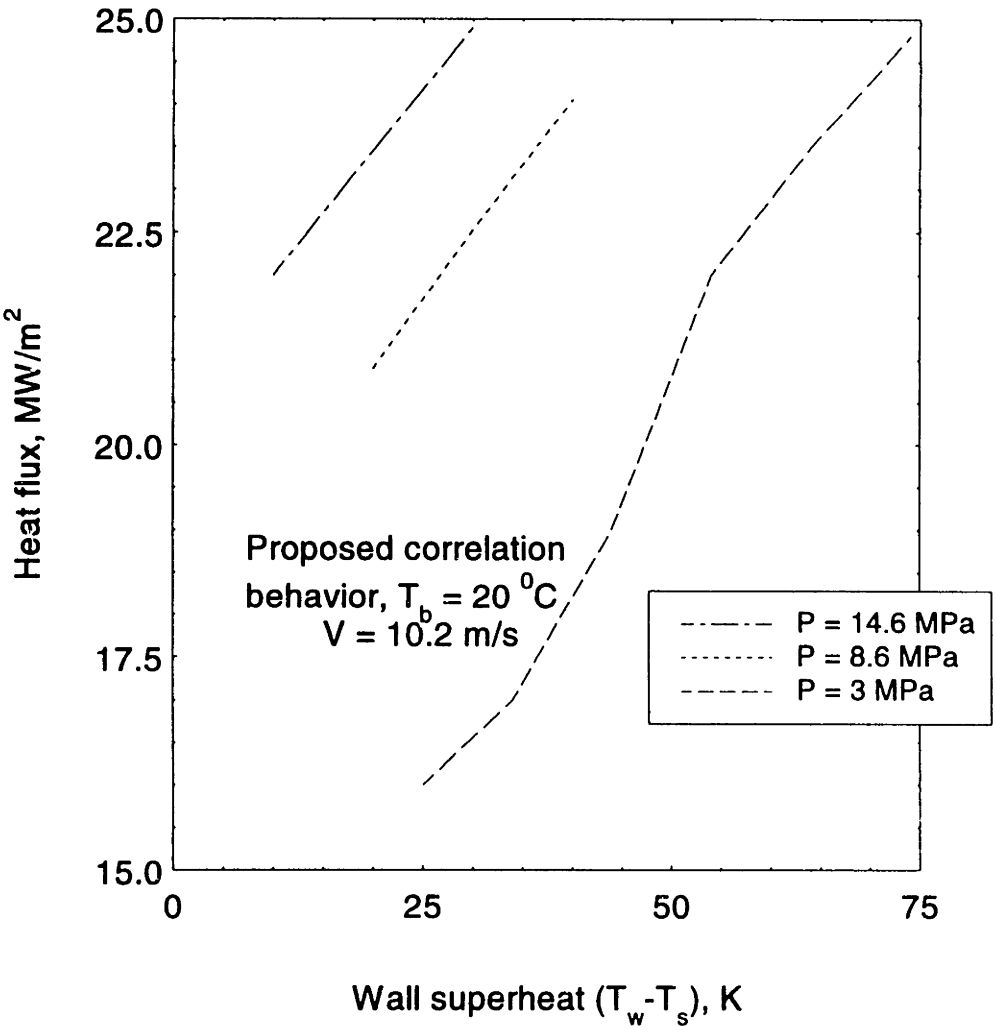

Figure 5-33: Local heat flux as a function of wall superheat

Chapter 6

A Framework for CHF and Post-CHF Predictions

This chapter is focused on examination of the limits on heat transfer at high heat fluxes when nucleate boiling is no longer possible. First, power-based Critical Heat Flux (CHF) estimates are validated using thermocouple measurements and the computational technique presented in Chapter 4. Next, an investigation of CHF data is performed. Finally, a Temperature of Homogeneous Nucleation (THN) limit and a Heat Flux limit for subcooled liquid in the post-CHF region are defined and correlations are developed for their estimation. Critical Heat Flux (CHF) can apparently occur when the wall temperature reaches the THN limit. A limit of this nature can occur only under conditions of very high mass and heat fluxes. Since a new proposed correlation was found to be more reliable than any of the other correlations for nucleate boiling, it is proposed to use it for prediction of a THN limit for fusion reactor high heat flux components. THN or classical CHF limits may not be real limits with respect to the possibility of having high wall temperatures (temperature excursions). In some cases the heat flux that can be removed by subcooled liquid from a vapor film is greater than the wall heat flux. This phenomena can occur only under conditions of a very high mass flux and a very high bulk subcooling.

6.1 Interpretation of the Results

The previous chapter presented the results of all the test runs for which no failures of the test section (i.e., overheating and destruction of the heater) were observed . This chapter deals with only those test runs which resulted in failure of the test section. These results were also presented by Hechanova [23]. However, in the present study only the initial data obtained in [23] are used. These data are used for heat flux estimates only using the computational modeling presented in Chapter 4 of the present study. This is the main difference between the present and Hechanova analyses because in [23] the HEATING7.2 conduction code combined with certain heat transfer correlations was used to determine coolant-side wall temperatures and local heat fluxes. The disadvantages of this methodology were already discussed in Chapter 4.

Although visualization of the failure mechanism, such as burnout, is beyond the scope of this study, inference can be made given the consistency of thermal hydraulic parameters. For all of the test runs analyzed the coolant-side wall temperature was well above the saturation temperature. Thus, it is assumed that heating failure is not due to a fault in the manufacturing of the heater (e.g., uneven surface coating) or in the electrode connection (e.g., poor contact).

Seven data points in the present study are deduced from measurements, the computer model analyses and used to bench mark of CHF (or near CHF) data. These bench mark data are given in Table 6.1.

Another eleven CHF data points from Hechanova's [23] investigation will also be used in order to determine possible mechanisms for CHF occurrence. For these runs it is impossible to use the computational modeling presented in Chapter 4 because some thermocouple measurements were not made (TC4 was not in use). The bench mark CHF data for which HEATING7.2 modeling was used by Hechanova in order to obtain local heat fluxes are given in Table 6.2.

The data of Tables 6.1 and 6.2 are plotted in Figure 6.1. Both computational modeling techniques (Chapter 4 and HEATING7.2) give similar CHF predictions. This enhances our confidence in the ideas presented in Chapter 4. A maximum tungsten temperature when inner wall temperature is equal to the THN value (325 °C) is less than 850 °C. For this value of tungsten temperature mechanical heater fault cannot occur. As the velocity goes up the CHF value also mostly increases. This consistency of measured and calculated thermal hydraulic parameters also implies that heater failure is due to CHF occurrence, not to a fault in manufacturing and/or poor electrode connection.

Table 6.1: Bench Mark Cases for Critical Heat Flux Data

Test Section ID	Flow Velocity, m/s	CHF, MW/m^2	Max. Inner Wall Temperature, °C
TS21B	3.65	10.1	304
TS28B	4.34	11.8	295
TS26A	5.74	19.9	299
TS23B	10.2	23.1	295
TS29B	13.6	28.4	318
TS29A	15.2	29.6	312
TS27B	19.4	33.1	325

Table 6.2: Bench Mark Cases for Critical Heat Flux Data [23]

Test Section ID	Flow Velocity, m/s	CHF, MW/m^2
TS15A	5.89	20.0
TS15B	5.72	14.1
TS16B	0.63	15.6
TS17A	2.55	12.5
TS18B	0.265	20.6
TS19B	11.3	28.4
TS20B	10.3	20.5
TS24B	10.6	21.8
TS25B	7.39	20.2
TS27A	4.49	18.0
TS28A	5.52	19.6

6.2 Discussion of CHF Data

When critical heat flux occurs in subcooled flow there are certain resemblances to pool-boiling critical heat flux, as already noted in Chapter 1. A number of detailed mechanisms for this type of critical heat flux can be suggested.

(a) Near-wall bubble crowding and vapor blanketing.
A kind of bubble boundary layer builds up at the heated wall. This becomes so dense that it effectively prevents fresh subcooled liquid from reaching the surface.

(b) Liquid film vaporization.
Vapor bubbles grow and depart the surface to form a vapor blanket and CHF occurs as a result of vaporizing the thin liquid film attached to the wall, see Celata et al. [39].

(c) Overheating at nucleation sites.
At very high heat fluxes, nucleation sites, which are locally dry, heat up so much during the bubble growth phase that they cannot be rewetted properly when the bubble has departed.

(d) Temperature of Homogeneous Nucleation (THN) limit.
Suppression of nucleate boiling on the coolant wall surface allows very high wall temperatures and CHF based on homogeneous nucleation, (discussed in Chapters 1,2 and 5).

It seems probable that all of these mechanisms can occur: the first one can happen in moderate heat flux at low subcooling. This mechanism is a usual one for saturated pool boiling.

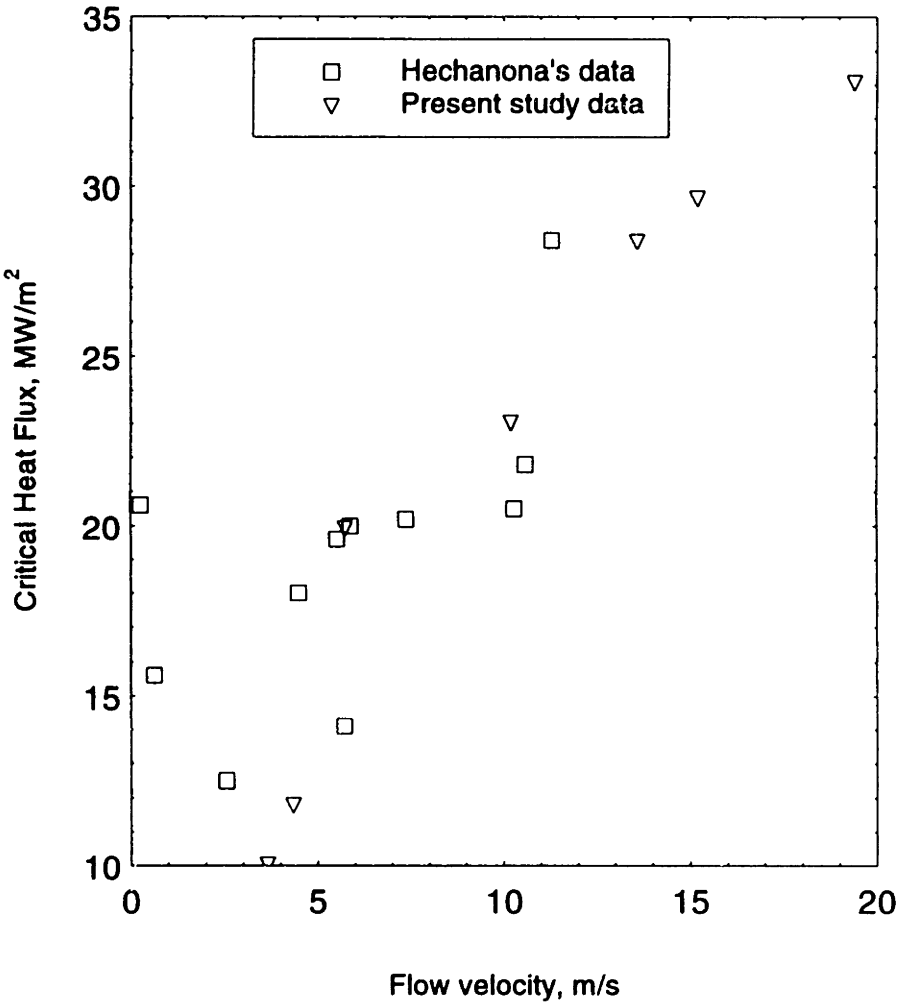

Figure 6-1: Critical heat flux as a function of flow velocity

In order to verify the second (b) possible mechanism data points from Tables 6.1 and 6.2 are plotted in Figure 6.2 as Stanton number versus Peclet number. These coordinates allow us to display the Saha and Zuber bubble departure criterion [41]. This well known bubble departure correlation [41] for distinguishes two regions: hydrodynamically-controlled and thermally-controlled bubble departure. These regions are distinguished using the Peclet number. The Onset of Significant Voids (OSV) or bubble departure is determined using the Nusselt or Stanton numbers as follows:

$$Pe = \frac{GDc_{pf}}{k_f} \tag{6.1}$$

$$Nu = \frac{q'' D}{k_f (T_s - T_b)} \tag{6.2}$$

$$St = \frac{q''}{Gc_{pf} (T_s - T_b)} \tag{6.3}$$

For $Pe < 70{,}000$, bubble departure is thermally-controlled and occurs when $Nu > 455$.
For $Pe > 70{,}000$, bubble departure is hydrodynamically-controlled and occurs when $St > 0.0065$.

It is clear from Figure 6-2 that all data points except those for very low velocity ($V < 0.6$ m/s) fall below the line $St = 0.0065$. Hence, according to the Saha-Zuber correlation vapor bubbles are not expected to leave the surface. Furthermore, in such a highly subcooled coolant with little thermal boundary layer development, the ability of a bubble layer to exist away from the wall is doubtful since any vapor that forms should condense very close to the wall. The bubble departure criterion is surpassed only for low velocity flow data ($V < 0.6$ m/s). For these cases the thermal boundary layer has a much better opportunity to develop and behave as suggested by Celata et al. [39]. CHF predictions for these low velocity cases found by Hechanova [23] suggests that this mechanism (b) is plausible in that region.

It seems possible that mechanism (c) can occur when nucleate boiling is not highly suppressed and wall temperatures are high, but below THN. For this case bubbles stay on the heated wall, but their total number is small because of nucleate boiling suppression. Thus, they cannot form a bubble layer near the wall and they also cannot prevent subcooled liquid movement toward the heated surface. Thus, if the wall temperature is below THN, the only possible mechanism is overheating at nucleation sites (c).

Figure 6-3 shows the maximum inner wall temperature as a function of flow velocity. From this figure it is clear that for velocities less than 10 m/s the inner wall temperature is high but below THN, hence the only possible mechanism for this case is overheating at a nucleation site. However, for velocities greater than 10 m/s the inner wall temperature exceeds THN. Thus, for these cases CHF due to THN limit (d) is likely.

Figure 6-4 shows critical heat flux as a function of flow velocity for velocities less than 11 m/s. In this velocity region we expect that the only possible mechanism for CHF is overheating at nucleation sites (c). A Canadian look-up table [24] and Hechanova's [23] correlation (Equation (1.20)) are also shown in this figure. It seems that both Canadian look-up table and Hechanova correlation underpredict CHF for flow velocities greater than 5 m/s and predict well in the velocity range from 2.5 m/s to 5 m/s. A possible explanations for these occurrences will be discussed in the next section of this study.

CHF results for flow velocities greater than 11 m/s are plotted in Figure 6-5. We expect that, for these velocities, CHF is caused by the THN limit. Thus, for this case CHF estimation can be made making use of Equation (5.9). In order to use this equation we must set wall temperature (T_w) equal to the THN and local wall heat flux in Equation (5.7) equal to CHF ($q_w/CHF=1$, $S_q= 0.41$). CHF due to the THN limit

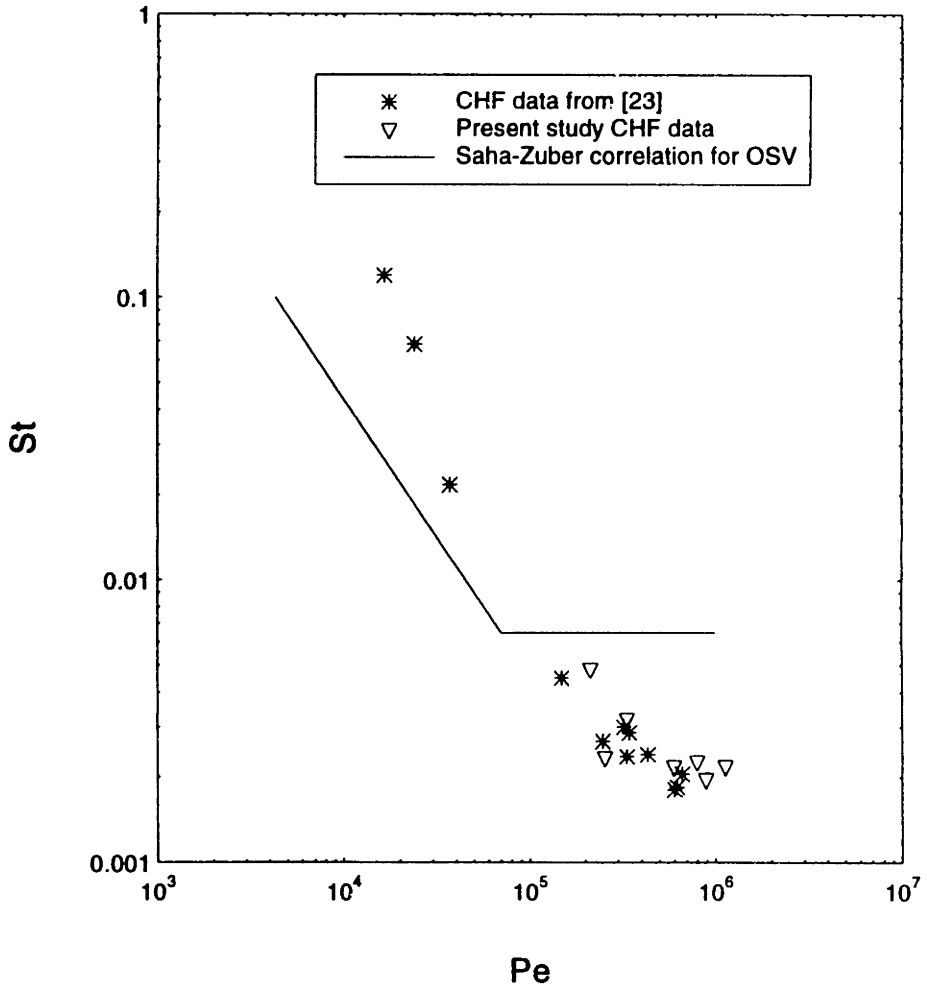

Figure 6-2: Stanton CHF number as a function of Peclet number

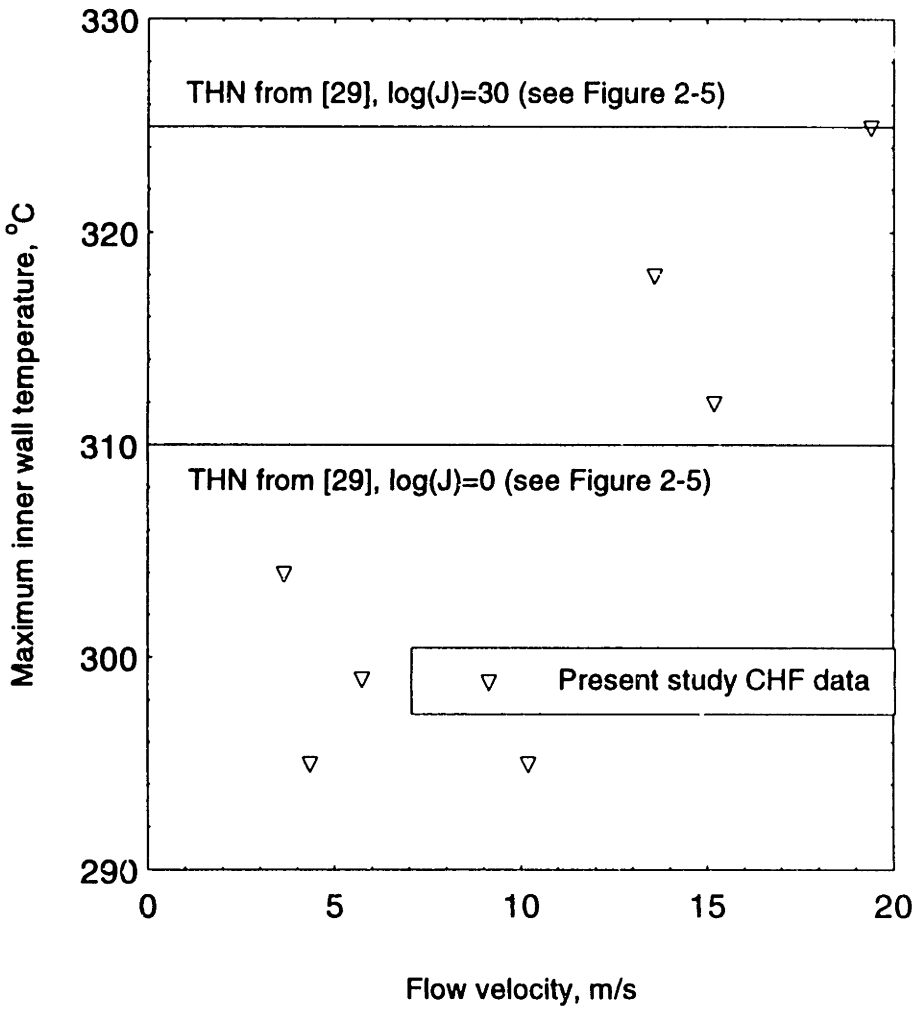

Figure 6-3: Maximum inner wall temperature as a function of flow velocity

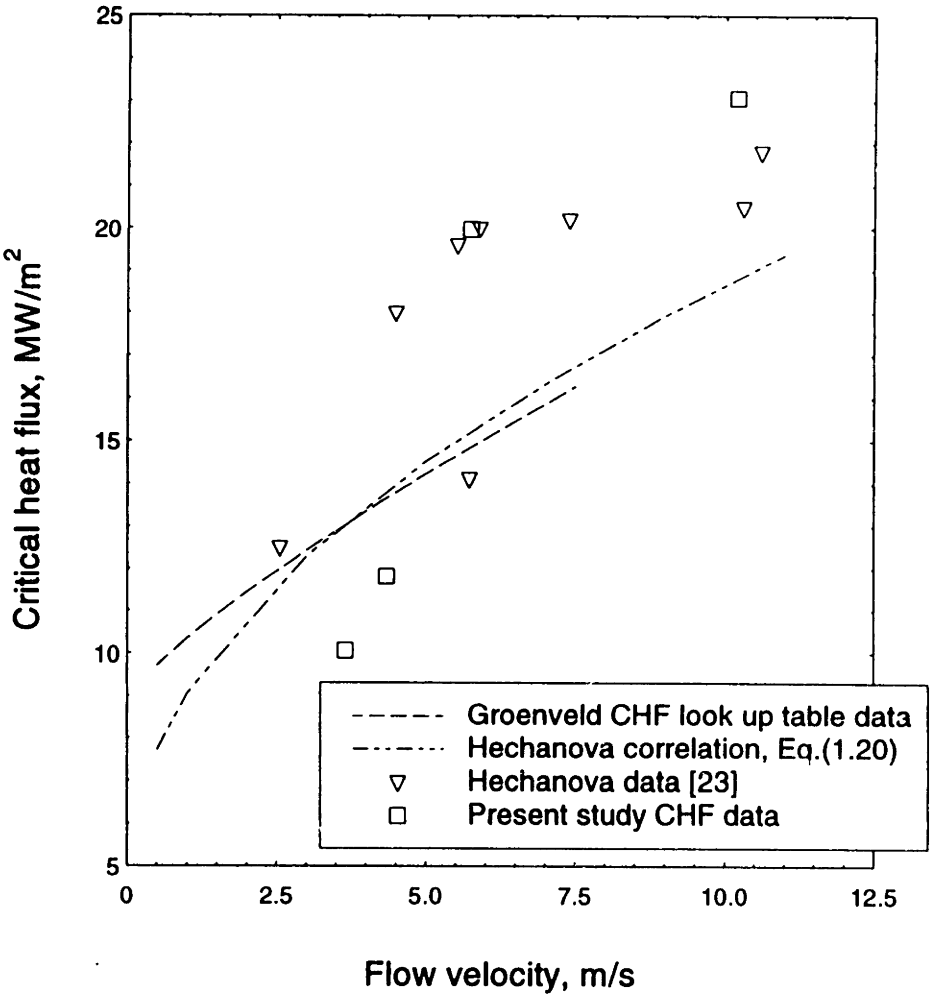

Figure 6-4: CHF in overheating at nucleate site

is determined as follows:

$$CHF_{THN} = F(S_v)\left(\frac{THN}{T_s}\right)^2 h_{sp}(THN - T_b) + 0.41 S_v h_{nb}(THN - T_s) \qquad (6.4)$$

CHF due to THN line is plotted in Figure 6-5. It is clear from this figure that CHF predictions with the help of Equation (6.4) are reasonable. Data extrapolations from the Canadian look-up table [24] cannot be used for this range of velocities. The CHF mechanism here is different from that for the range of velocities in the data of the look-up table.

All CHF data points plus the Canadian look-up table data and the CHF_{THN} correlation (Equation (6.4)) are shown in Figure 6-6. It is obvious from this figure that Canadian look-up table [24] can be used for CHF predictions in the range of velocities up to 5 m/s and Equation (6.4) can be used in the range of velocities greater than 11 m/s. The question remains is "what correlation should be applied in the intermediate range of velocities?" The answer to this question will be developed in the next section of this chapter.

6.3 Heat Flux Limit for Subcooled Liquid in Post-CHF Region

In order to give an answer to the last question of the previous section let us assume that the local wall heat flux is greater than CHF. In other words, let us consider the post-CHF region. While the high velocity, low temperature liquid is present in the center of the channel, the wall is covered by a thin film of vapor. For this case the local wall heat flux can be represented in the form of a sum:

$$q_w = q_v + q_l \qquad (6.5)$$

where: q_v represents the evaporation of liquid at the interface between liquid and vapor;
q_l is heat flux from convection to liquid at the liquid-vapor interface.
The radiation component is neglected here.

For the general case, the heat flux removed by the subcooled liquid (q_l) can be determined as:

$$q_l = h_c(T_s - T_b) \qquad (6.6)$$

where h_c = heat transfer coefficient.
The next question to be answered is "how is this heat transfer coefficient to be calculated?"

In order to answer this question it is necessary to take a look at the geometry of the vapor-liquid interface. A study of the characteristics of the vapor layer produced by film boiling has been reported by Bradfield et al. [42]. This study confirms the great influence that liquid velocity and subcooling have on vapor film thickness. Observations for liquid velocities greater than 6 m/s and high subcooling indicate that ripping and bumping instabilities exist which are attributed to vapor films whose thickness is of the same order of magnitude as the surface roughness.

Dougall and Rohsenow [43] found that vapor-liquid interface structure is not smooth but irregular. These irregularities occur at random locations but appear to retain their identity to some degree as they pass up the tube with velocities of the same order as that of the liquid core.

If the vapor-liquid interface is not smooth, it is likely that some vapor moves in a transverse flow direction from the vapor film to the bulk subcooled liquid. Therefore, we cannot make the assumption that the value of heat transfer coefficient in the equation (6.6) can be obtained from typical correlations for turbulent flows.

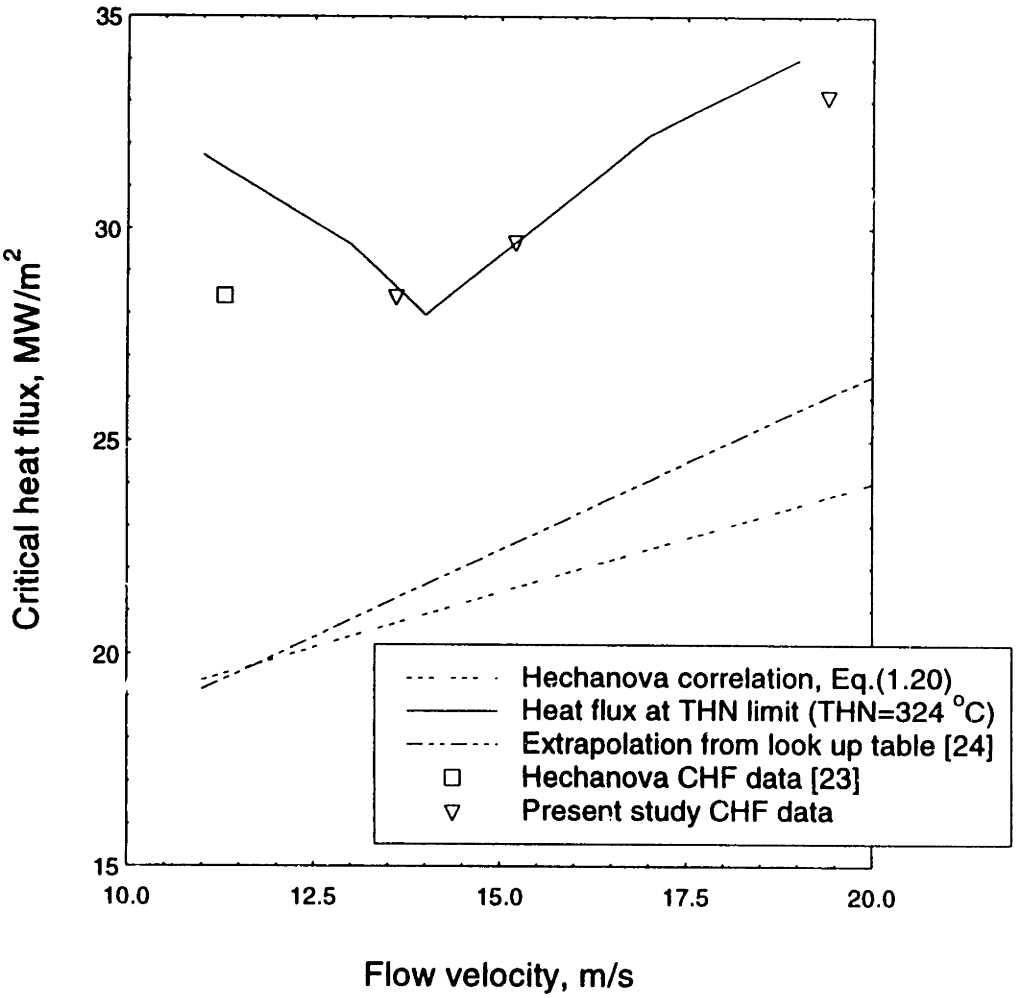

Figure 6-5: CHF due to Temperature of Homogeneous Nucleation (THN) limit

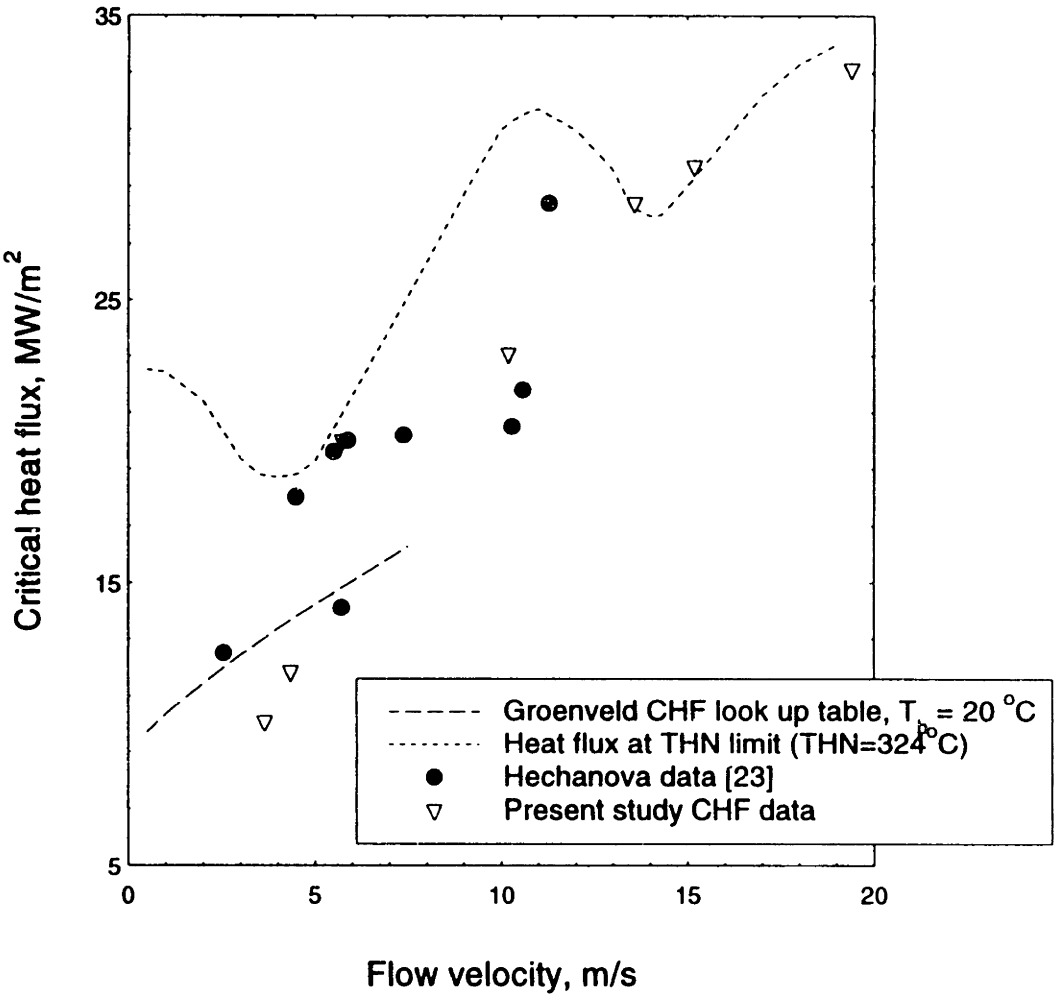

Figure 6-6: Critical heat flux as a function of flow velocity

This is because the movement of vapor in transverse direction should enhance heat transfer by convection from the vapor film to subcooled liquid. It is known that for subcooled flows in the presence of nucleate boiling on a heated wall the value of pressure drop is higher than for non-boiling case. Equation (6.7) is recommended in Russian Codes [13] for this case.

$$\frac{\Delta P_{nb}}{\Delta P_{sp}} = 1 + 5.38\left(\frac{q''}{H_{fg}\rho_g V}\right)^{0.7} \tag{6.7}$$

where: ΔP_{nb} = Pressure drop for subcooled nucleate boiling case;
ΔP_{sp} = Pressure drop for single-phase case;
V = Velocity of subcooled liquid.

Now we can assume that the vapor-liquid boundary in the film boiling case plays the role of the heated wall in nucleate boiling case. Because the boundary is rough, bubbles can leave this film in the transverse direction. Hence, we can apply Equation (6.7) for this case assuming that ΔP_{sp} is the value of pressure drop in the case where there is no vapor flow from the liquid-vapor interface inside the bulk liquid and ΔP_{nb} is the value of pressure drop when there is transverse vapor flow inside the subcooled liquid in the transverse direction. With the assumption that Reynolds analogy is valid for our case, the pressure drop ratio in equation (6.7) is the same as heat transfer enhancement factor. Thus, the heat transfer coefficient in equation (6.6) can be determined as:

$$h_c = \left(1 + 5.38\left(\frac{q_l}{H_{fg}\rho_g V}\right)^{0.7}\right) h_{sp} \tag{6.8}$$

Where: h_{sp} = Single-phase heat transfer coefficient, evaluated using Equation (1.2).
With the use of Equations (6.6) and (6.8), the heat flux removed by subcooled liquid from a vapor film can be calculated as follows:

$$q_l = h_{sp}\left(1 + 5.38\left(\frac{q_l}{H_{fg}\rho_g V}\right)^{0.7}\right)(T_s - T_b) \tag{6.9}$$

The values of heat flux transferred to the subcooled liquid as obtained from equation (6.9) are shown in Figure 6-7. It is interesting that for low velocities (V < 4 m/s) this heat flux is lower than Canadian look-up table [24] CHF predictions, but for high velocities this heat flux is higher. When $q_l > q'' >$ CHF then we have non-steady state conditions on a heated wall. Because wall heat flux exceeds CHF we have film boiling. Due to vapor penetration into the subcooled liquid, heat transfer increases and heat flux removed from vapor becomes greater than the wall heat flux. Hence the vapor film is condenses. When there is no vapor film, there is no heat transfer enhancement and with wall heat flux greater than CHF film boiling occurs again. So, the only possibility to get stable film boiling on a heated wall is to exceed the value of subcooled liquid heat flux (Equation (6.9)). Hence, there is another limit - Heat Flux Limit for Subcooled Liquid. Only when heat flux is greater than this limit can we have stable film boiling on a heated wall and extremely high wall temperatures which high heat flux component devices cannot maintain. That is our explanation of Divavin [27] experimental results (see Chapter 1). It is shown in [27] that it is possible to exceed local CHF by as much as 80% before causing global distruction of a tube. Similar observations were reported by Gotovskii [44]. Fukuyama [45] experimental results for high velocity flow of highly subcooled Freon-113 show that a sharp reduction of heat transfer coefficient during transition to film boiling can be eliminated with the combined effects of high mass flux and high subcooling.

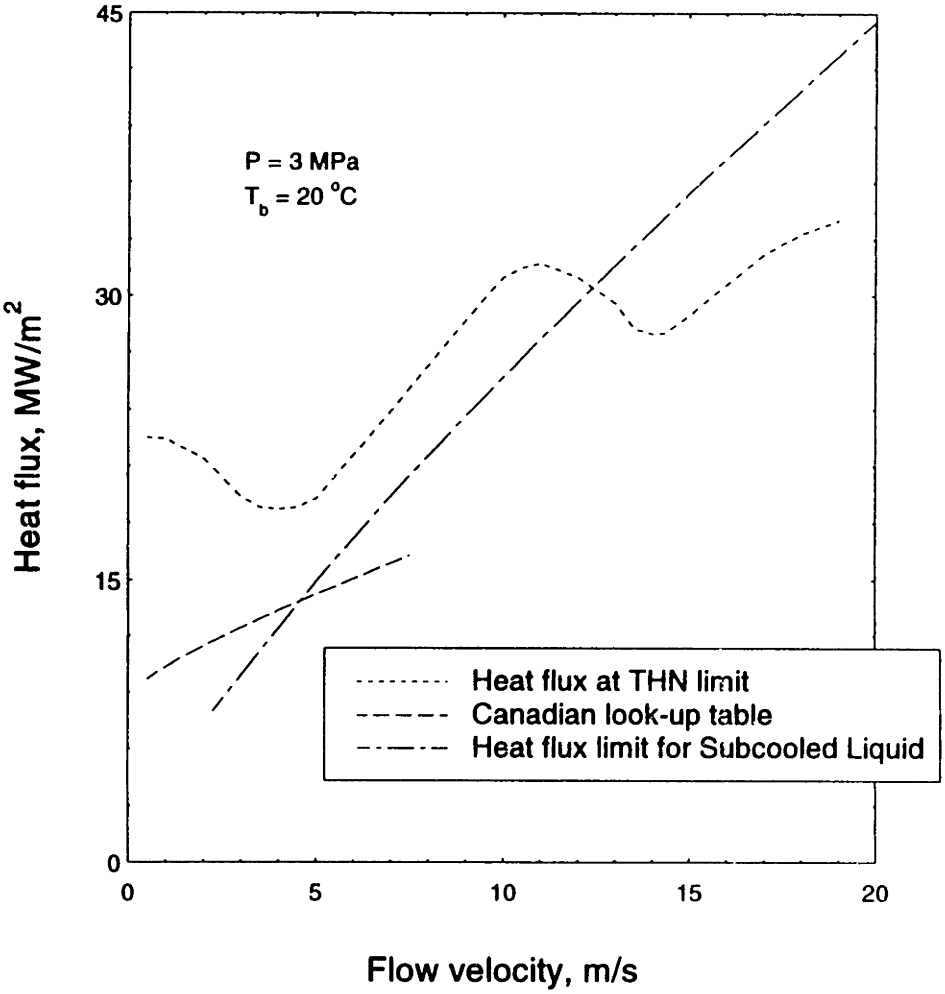

Figure 6-7: Heat Flux Limit for Subcooled Liquid in post-CHF region

Two regions of film boiling can exist in some cases for high velocities and high subcooling. In the first region (region AB in Figure 6-8) we can have non-steady state film boiling. In this region as it was stated before we have subcooled liquid vaporization and vapor film condensation. This region can exist only when $q_l > q'' > CHF$. When $q'' > CHF$ we can have stable film boiling on a heated wall (region BC in Figure 6-8). In comparison with the previous region here there is no steam condensation. Thus we should expect a sharp reduction in the heat transfer coefficient that may cause overheating of a tube. If $q_l < CHF$ we should have only this film boiling region (classical film boiling). These regions are shown in Figure 6-8.

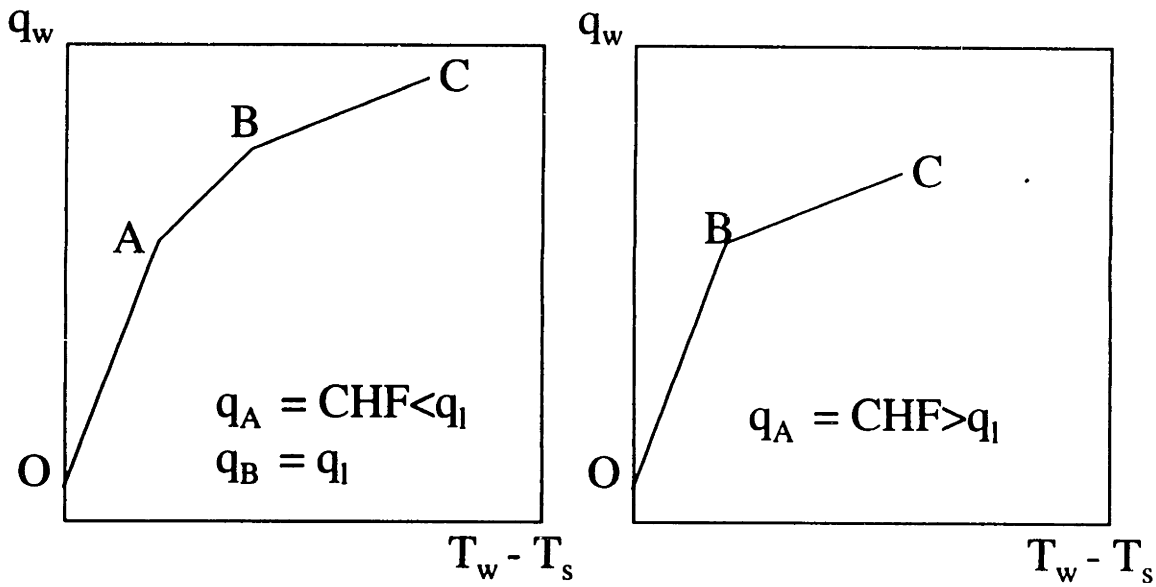

OA - nucleate boiling region
AB - Unstable film boiling region
BC - Stable film boiling region

Figure 6-8: Film boiling regions

Figure 6-9 shows the Heat Flux Limit for Subcooled Liquid and CHF data. Now it becomes clear why Canadian look-up table [24] does not predict correct CHF values. These CHF data points can represent the extension of the post-CHF data points. Since the vapor film is stable only when the Heat Flux Limit for Subcooled Liquid is reached, it is difficult to determine CHF from thermocouples reading and we have an apparent CHF disappearance or in other words there is no sharp reduction in the heat transfer coefficient because of the transition from nucleate to film boiling. By CHF occurrence we mean the transition from single-phase convection plus nucleate boiling to film boiling.

The question remains " why are data points for high velocities (V > 11 m/s) below the Heat Flux Limit for Subcooled Liquid? " Possible explanation is that Equation (6.9) is derived on the assumption that Reynolds analogy is valid. Also it is based on Equation (6.7) which was not derived for extremely high velocities.

Results of calculations using Equation (6.9) for the Heat Flux Limit for Subcooled Liquid for different pressures are shown in Figure 6-10. The enhancement ratio (E_{fb}) is defined as:

$$E_{fb} = \frac{h_c}{h_{sp}} = 1 + 5.38\left(\frac{q_l}{H_{fg}\rho_g V}\right)^{0.7} \tag{6.10}$$

The value of heat flux limit for subcooled liquid (q_l) is found numerically from Equation (6.9). It is well known from heat transfer enhancement studies of single phase flow [4] that the enhancement ratio at a liquid boundary layer is usually in the range from one to two. It is therefore assumed here that it is physically unrealistic to have enhancement ratio defined by Equation (6.10) greater than three. From results in Figure 6-10 we can conclude that this criterion is satisfied for water pressure greater than 1 MPa but is not satisfied for water pressure less than 1 MPa. Mathematically this is because the lower vapor density at lower pressures leads to higher level of enhancement. From the physical point of view this is correct, because at low vapor density the vapor volume agitation is large, hence, more heat transfer enhancement. But from a realistic point of view it is difficult to imagine cases where the heat transfer enhancement ratio is greater than ten. Thus, Equation (6.9) is recommended only for water pressure greater than 1 MPa.

The maximum heat flux for nucleate boiling is proportional to $E_{nb}\ h_{sp}\ (T_w - T_b)$, where E_{nb} is the enhancement ratio for nucleate boiling region. If we compare the last expression with Equation (6.9) it is clear that in order to have $q_l > CHF$, the enhancement factor for film boiling (E_{fb}) must be greater than enhancement factor for nucleate boiling region (E_{nb}). For low velocities there is no nucleate boiling suppression, and a large nucleation rate causes a very high E_{nb}. For high velocities there is nucleate boiling suppression. At extremely high heat flux the vapor film on the heated wall begins to play the role of a vapor source. In other words the heat transfer rate of film boiling is enhanced and at high heat fluxes and velocities it is enhanced more than nucleate boiling before CHF occurrence.

6.4 Development of CHF Correlations

The preceding subsections indicate that different mechanisms may control the CHF occurence at different flow velocities. The following procedure is recommended to assess heat flux limits. First, the likely CHF mechanism should be determined. This can be done with the help of the Canadian look-up table [24] and Equation (6.11) for the THN type of CHF.

$$CHF_{THN} = F(S_v)\left(\frac{THN}{T_s}\right)^2 h_{sp}(THN - T_b) + 0.41 S_v S_P h_{nb}(THN - T_s) \tag{6.11}$$

Equation (6.11) and a previous Equation (6.4) differ in that there is a pressure correction multiplier in Equation (6.11). This multiplier should be determined with the use of Equation (5.12). Thus, in comparison with Equation (6.4), Equation (6.11) can be applied for different values of water pressure. The Canadian look-up table provides CHF values due to overheating at a nucleation site - CHF_{OV}.

Equation (6.11) provides CHF due to the THN limit. Comparison between these two heat fluxes (CHF_{OV} and CHF_{THN}) should be made over the whole flow velocity range. The critical heat flux will be the minimum of these two heat fluxes.

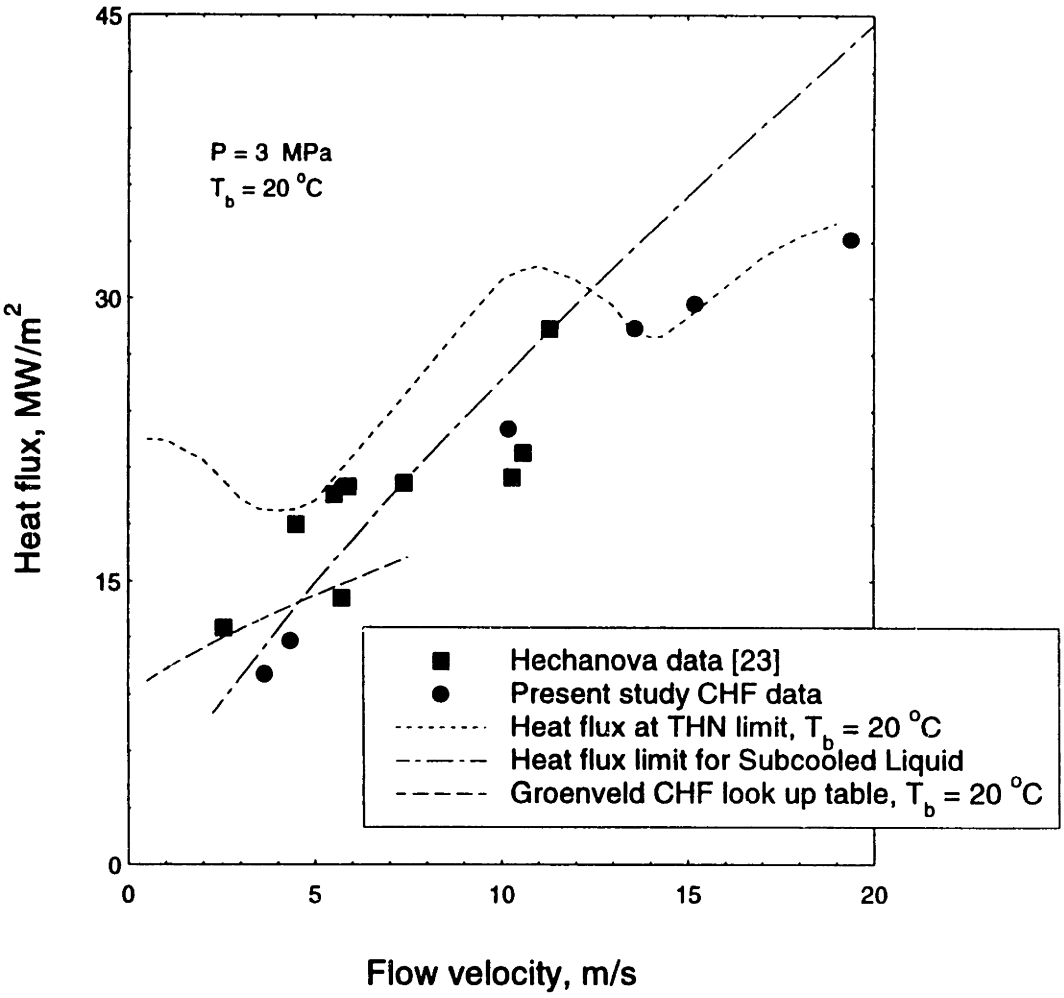

Figure 6-9: Critical heat flux as a function of velocity

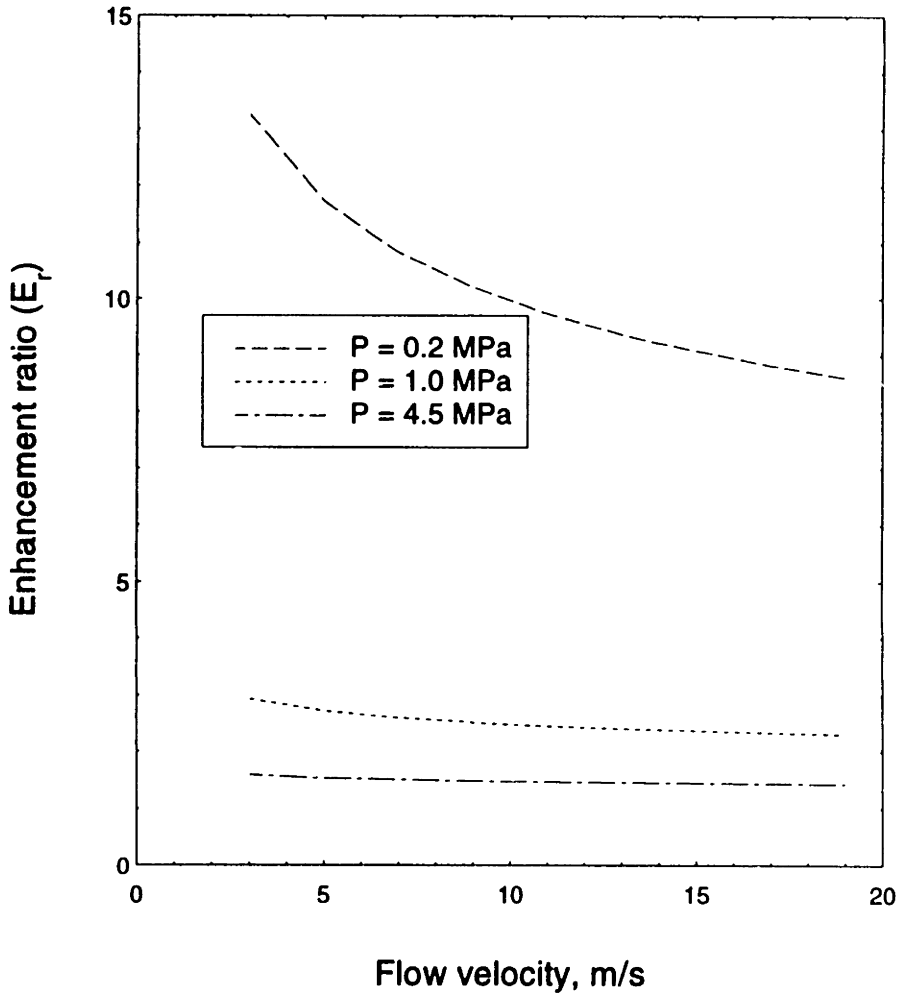

Figure 6-10: Enhancement ratio in post-CHF region as a function of flow velocity

$$CHF = \text{Minimum } \{ CHF_{OV}, CHF_{THN} \} \quad (6.12)$$

Note that the Canadian look-up table [24] covers all possible values of subcooling, but flow velocities only up to 7.5 m/s. It is being adopted here that extrapolations may be done for velocities greater than 7.5 m/s.

The next step is to compare the heat flux obtained by Equation (6.12) with heat flux limit for subcooled liquid determined by equation (6.9). The following equation is proposed in order to evaluate the heat flux limit for a cooling channel.

$$q_{limit} = \text{Maximum } \{ CHF , q_l \} \quad (6.13)$$

The value of CHF is obtained from Equation (6.12). Results of this procedure are shown in Figure 6-11 for P = 3 MPa. Note that Figure 6-11 is a modified version of Figure 6-9. It is clear from Figure 6-11 that the procedure recommended predicts reasonable results (within $\pm$ 25%) for heat flux limit. Once this limit is reached a wall temperature excursion to extremely high values is expected.

In order to verify the proposed procedure let us consider the data from different values of pressure and subcooling for the flow velocity range from 2 to 20 m/s. Hechanova [23] provided a good review of CHF data as related to fusion reactor divertor conditions. We shall use his CHF data base for smooth flow in uniform heated tubes (D > 5 mm) in order to verify the equations proposed in this study. The data base for non-uniform heated channels will not be used here because for these cases only the incident heat fluxes were reported and, as it was shown before in Chapter 4, the appropriate peaking factors values are not known. Swirl flow CHF data base will not be used in the present study because correlations developed here are based on experimental results for smooth flows may not be used directly for the swirl flow case.

Results for low pressure (P = 0.2 MPa) are shown in Figure 6-12. As mentioned before, the heat flux limit for subcooled liquid cannot be evaluated for this pressure. As expected THN limit is greater than CHF values predicted by Canadian look-up table. For low pressure case (P < 1.5 MPa) THN limit is not a real limit and can be ignored. Canadian look-up table [24] predicts CHF values satisfactorily.

Results for P = 1 MPa are shown in Figure 6-13. As for P = 0.2 MPa the THN limit again can be ignored. However, the heat flux limit for subcooled liquid has to be taken into account for velocities greater than 5 m/s. Same conclusion about this heat flux limit was made for P = 3 MPa (see Figure 6-9). Data points for this pressure show good agreement with proposed procedure for heat flux limit evaluation.

As the pressure goes up for a low subcooling case, THN limit must be taken into account. Results from Figure 6-14 for P = 3 MPa, T_b = 145°C prove this point. Because at a high bulk temperature the heat flux limit for subcooled liquid is very low, it can be ignored. Most of the data points shown are located just between CHF_{OV} and CHF_{THN}. Same conclusions can be made about results shown in Figure 6-15 for the same pressure and lower subcooling (T_b = 180 °C). From both of the two last figures it is clear that Canadian look-up table predict low values of CHF than experiments show. However, it still can be applied for a conservative calculations.

Results for P = 4.5 MPa show very good agreement with Canadian look-up table predictions and Equation (6.11) for the THN limit. (see Figure 6-16). Here in spite of high subcooling (T_b = 150 °C) for V < 5 m/s we have CHF due to overheating at a nucleation site and the Canadian look-up table [24] predicts CHF values very close to experimental values. For V > 5 m/s CHF is due to THN limit and Equation (6.11) predicts very reasonable values of CHF_{THN} .

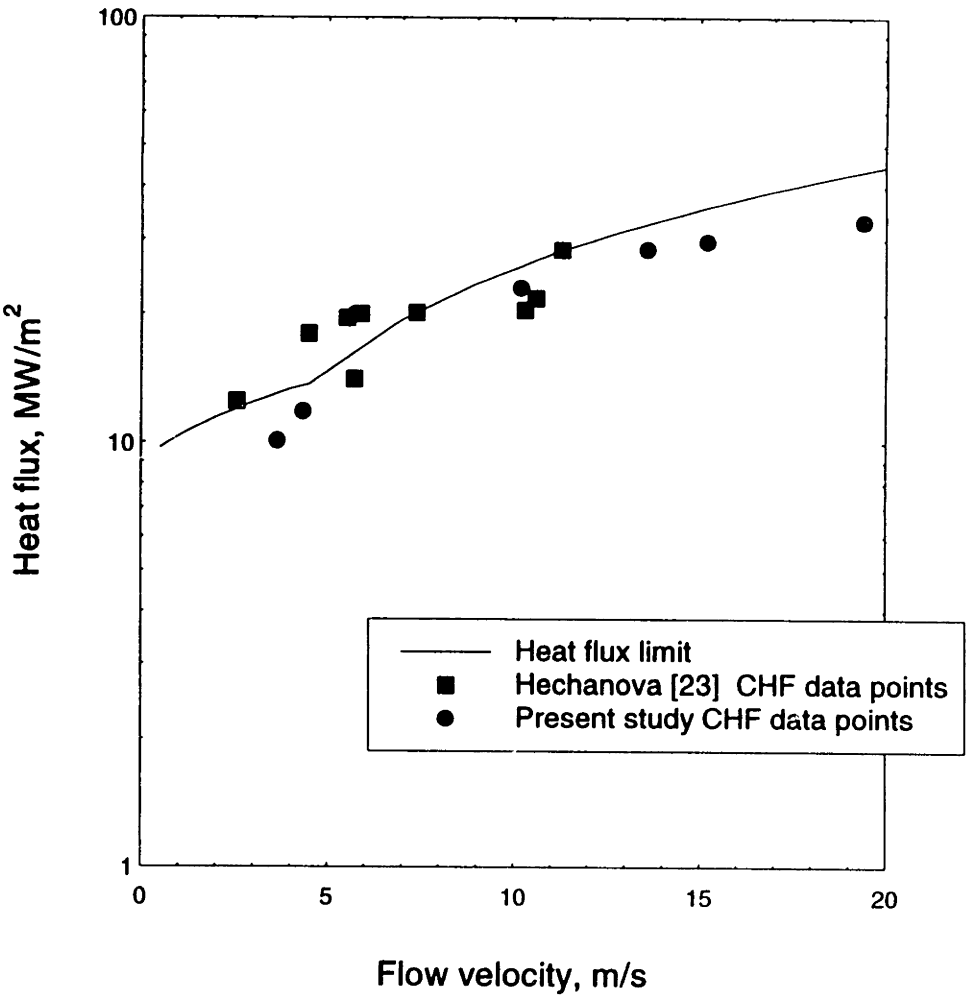

Figure 6-11: Heat flux limit (Equation (6.13)) as a function of flow velocity

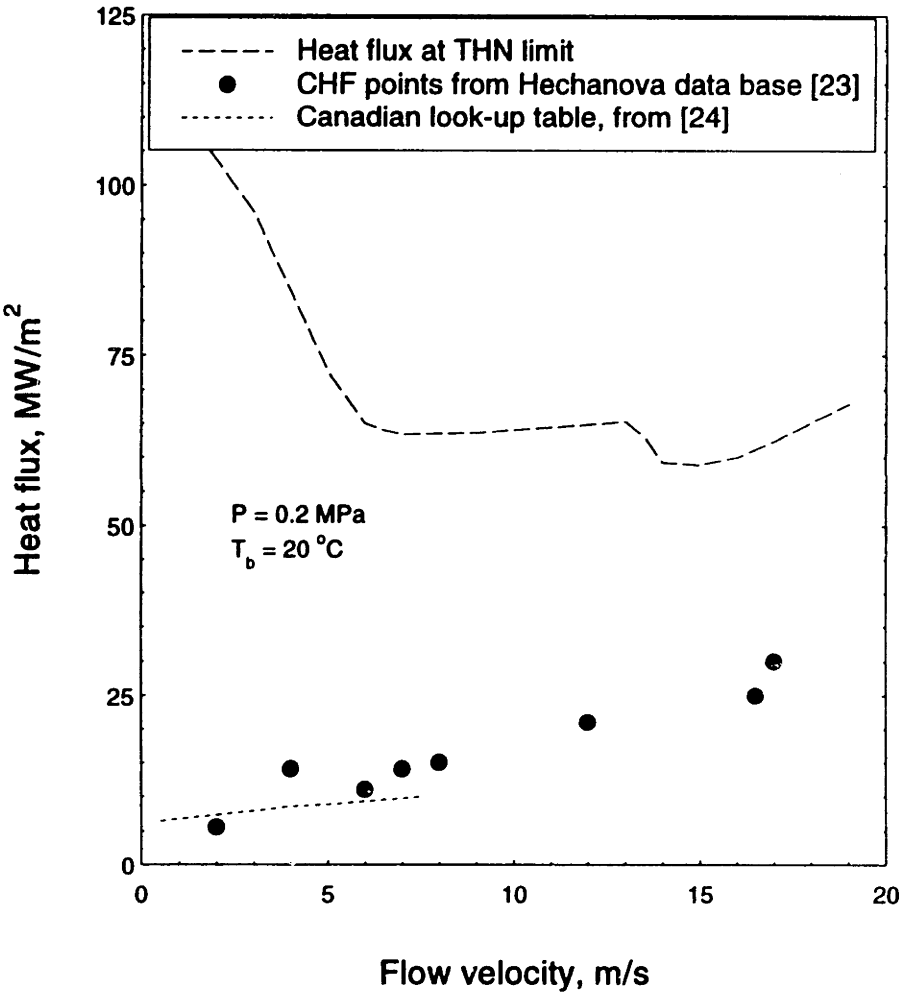

Figure 6-12: CHF as a function of flow velocity

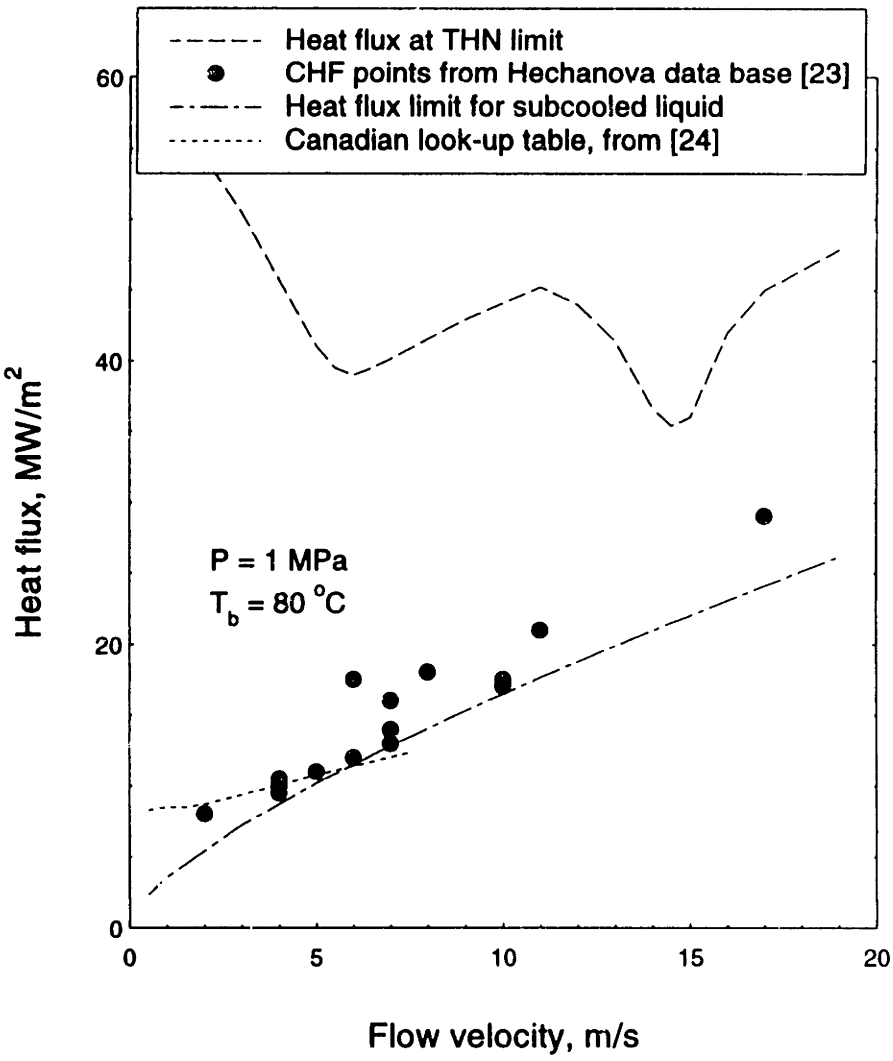

Figure 6-13: CHF as a function of flow velocity

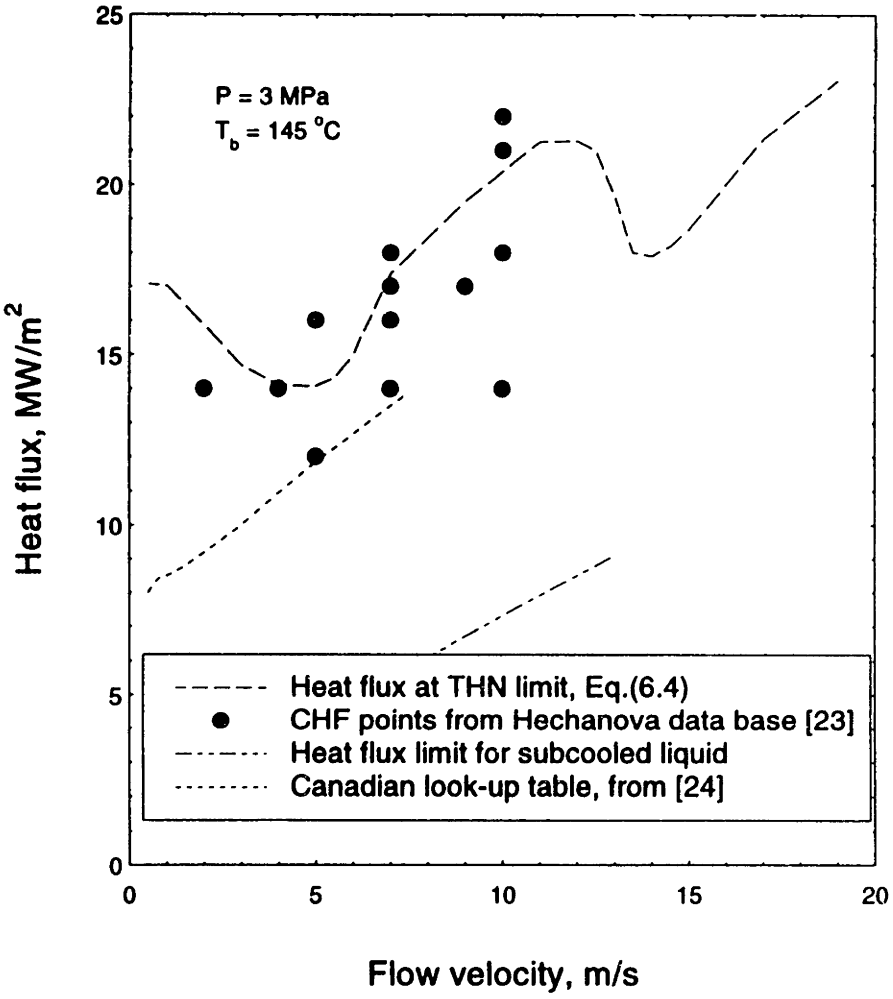

Figure 6-14: CHF as a function of flow velocity

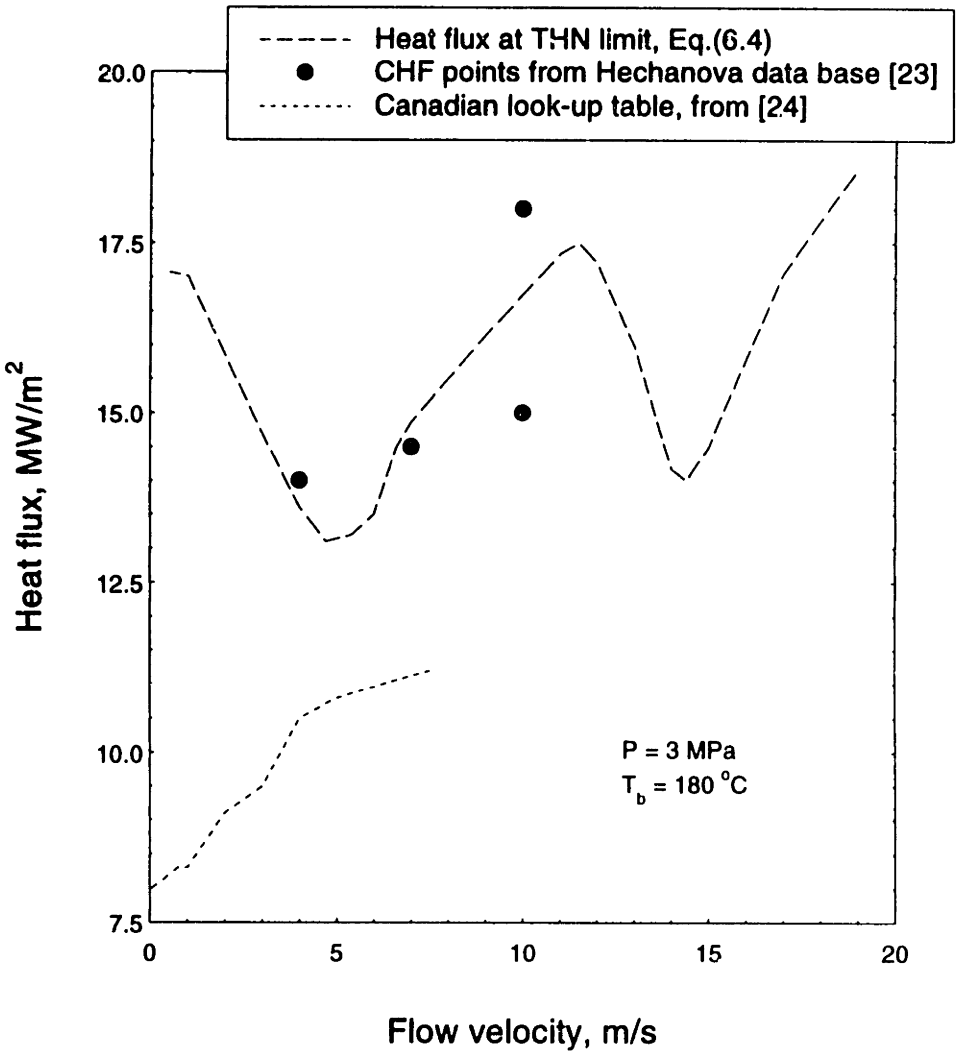

Figure 6-15: CHF as a function of flow velocity

Analyzing the results from the Canadian look-up table, some strange behavior of CHF versus velocity appears for some values of pressure and subcooling. Usually for classical CHF values as velocity increases so does the value of CHF. Strange behavior is found for P = 3 MPa and bulk temperatures from 200 to 215 °C for the velocity range from 2 to 5 m/s. At these values of subcooling where DNB must occur, CHF decreases as velocity increases. The only possible explanation from our point of view is that in this range we do have CHF due to THN limit. Comparison of THN predictions (Equation (6.11)) and Canadian look-up table [24] CHF values is shown in Figures 6-17 and 6-18. Results from these figures prove that our assumption that for this range of parameters CHF is due to THN limit is correct.

For higher pressure (P = 7 MPa) and low subcooling CHF is also due to THN, but here there is no such behavior of CHF versus flow velocity. Equation (6.11) here also works well. Canadian look-up table [24] CHF predictions and predictions for THN limit (Equation (6.11)) are shown in Figure 6-19. Again, the correlations developed predict very reasonable results even though the range of pressure and subcooling is out of the experimental range for which correlations were originally developed.

The closest comparative CHF study to the experimental range of the present study is an unpublished study made in Russia by Gotovskii [44] (CHF data are presented in Appendix of the present study). Results of this study are shown in Figure 6-20. A modified version of Figure 6-20 is Figure 6-21 in which heat flux limit (q_{limit}) evaluated with the help of Equations from Eqn.(6.11) to Eqn.(6.13) is shown as a function of flow velocity. One can see that these equations result in very reasonable results. For low velocities (V < 2.5 m/s) the Canadian look up table [24] governs the curve q_{limit} versus flow velocity. For the velocities from 2.5 m/s to 6 m/s CHF occurs due to the THN limit and for the velocities greater than 6 m/s the heat flux limit for subcooled liquid must be chosen as a wall temperature excursion limit.

As one can see from Figures 6-17, 6-18, 6-19 and 6-21 the Hechanova correlation (Equation (1.20)) predicts reasonable results but does not take into account different CHF mechanisms. For low subcooling and moderate velocities it seriously underpredicts the value of CHF.

Canadian look-up table [24] CHF values and predictions for THN limit for different values of pressures are shown in Figure 6-22. At low pressures THN limit can be disregarded, but it should be taken into consideration at high pressures (P > 2 MPa). The same values are shown in Figure 6-23 for different values of subcooling. From this figure one can see the importance of the THN limit for low subcooling.

The proposed procedure for heat flux limit evaluation was applied to all CHF data shown in the present chapter (present study, Hechanova CHF data, CHF data bank [23], Gotovskii [44]). A comparison between experimental CHF results and the heat flux limit for subcooled liquid (Equation (6.9)) for the region where this heat flux (q_l) is a limit is shown in Figure 6-24. The same comparison for all possible heat flux limits (CHF_{OV}, CHF_{THN} and q_l) is shown in Figure 6-25. The data points show good agreement with the procedure, since 75% of the data falls within $\pm$ 20% of the predicted value.

No wall temperature oscillations were detected for CHF experimental data (CHF data of the present study and Hechanova [23] CHF data). Usually these oscillations are present after the point of transition from nucleate boiling to film boiling (CHF point) [45]. It is very difficult to detect them with the help of thermocouples placed at the outer surface because heat conduction can eliminate them. That may explain why during the experiments no oscillations were detected. Inner wall temperature oscillations will produce strain and stress oscillations. We believe these oscillations could destroy the contact between the alumina isolation layer and/or the tungsten layer. This is our explanation why at relatively low surface temperatures (less than 850 °C) we have flashing or arcing on the test section heater. That is why we assume these data correspond to the CHF occurrence.

It is found using the procedure proposed that for ITER design conditions (V = 10 m/s, P = 3.5 MPa, T_b = 50 °C) the heat flux limit (q_{limit}) is equal to 27 MW/m^2. That is greater than a nominal peak heat flux (15 MW/m^2) from Table 1.1. For dynamic gas target divertor conditions (V = 10 m/s, P = 4 MPa,

T_b = 150 °C) the heat flux limit (q_{limit}) is equal to 17 MW/m^2. However, the desired burnout safety margin (see also Table 1.1) would be 1.8 for the normal divertor [2] and 3.4 for the dynamic gas target divertor [3]. This margin may be adequate, but that decision require more analysis of the possible uncertainties than can be addressed here.

6.5 Comments

When high velocity, low temperature liquid is present in the center of the channel, at high heat flux the wall is expected to be covered by a thin film of vapor. The liquid-vapor interface has an irregular and rapidly fluctuating shape. The temperature excursion which would be expected to occur in film boiling (boiling through a film of vapor) is precluded here since the film is so thin and since the high velocity cold liquid is so effective in condensing actions.

Critical Heat Flux can occur when the wall temperature reaches the THN limit. This happens for high velocity flow due to an influence of turbulent vortices on the steam bubble growth. Equation (6.11) is proposed to calculate CHF due to THN limit.

Critical Heat Flux can occur without accompanying high wall temperatures. Only after exceeding the Heat Flux Limit for Subcooled Liquid in Post-CHF region high wall temperatures are expected. Equation (6.9) is recommended in order to evaluate Heat Flux Limit for Subcooled Liquid in Post-CHF region. In some cases this heat flux can be a real limit.

When inner wall temperatures are below the THN value Critical Heat Flux occurs due to overheating at a nucleation site. Canadian look-up table [24] is recommended for this particular mechanism.

Equations (6.12) and (6.13) are proposed in order to evaluate the heat flux limit for high velocity flows. However, continuing validation and improvement of CHF correlations are still necessary. So are the development of new physically based correlations and the collection of new relevant data bases.

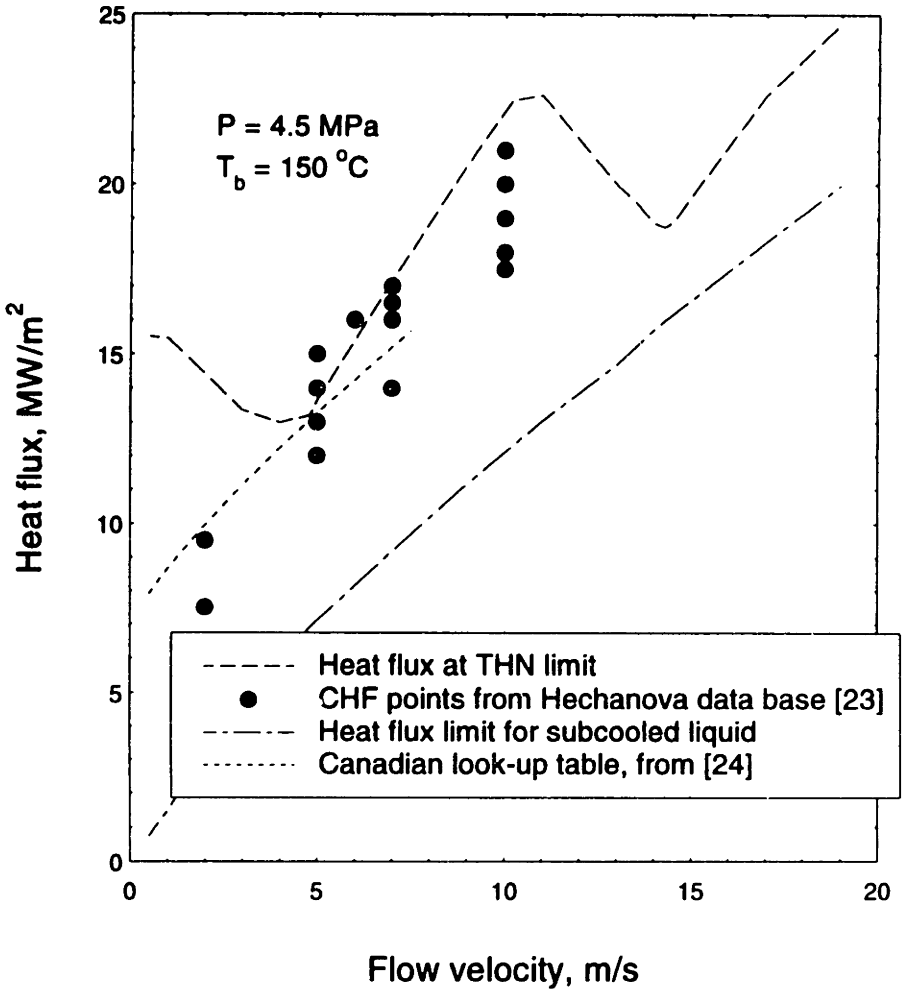

Figure 6-16: CHF as a function of flow velocity

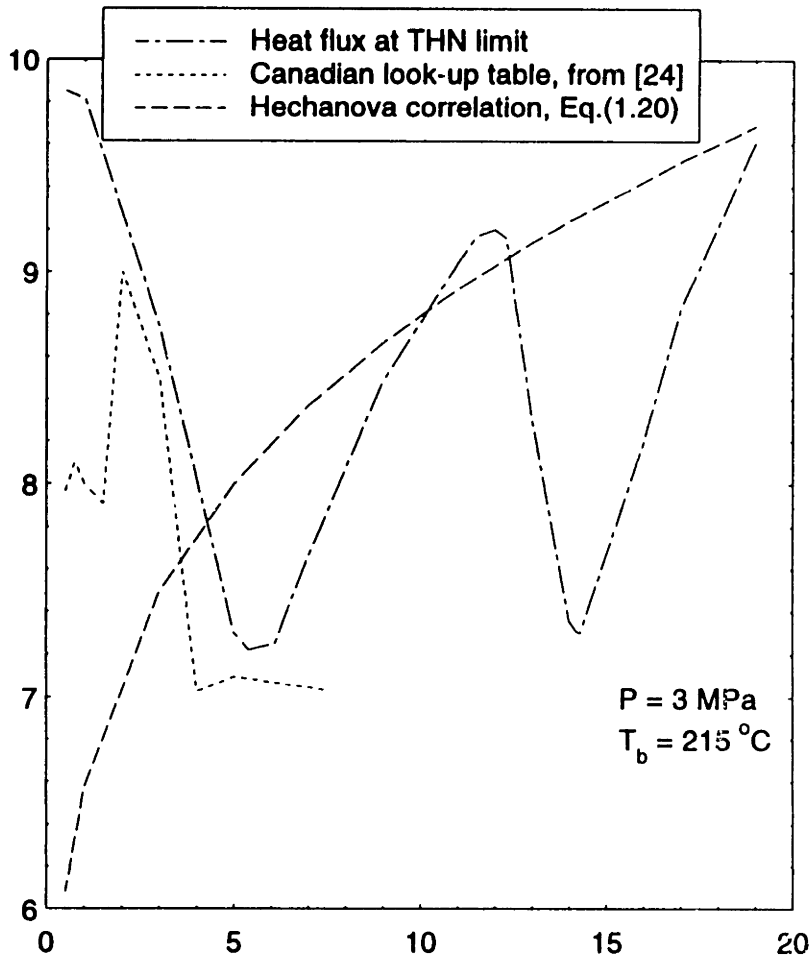

Figure 6-17: CHF as a function of flow velocity

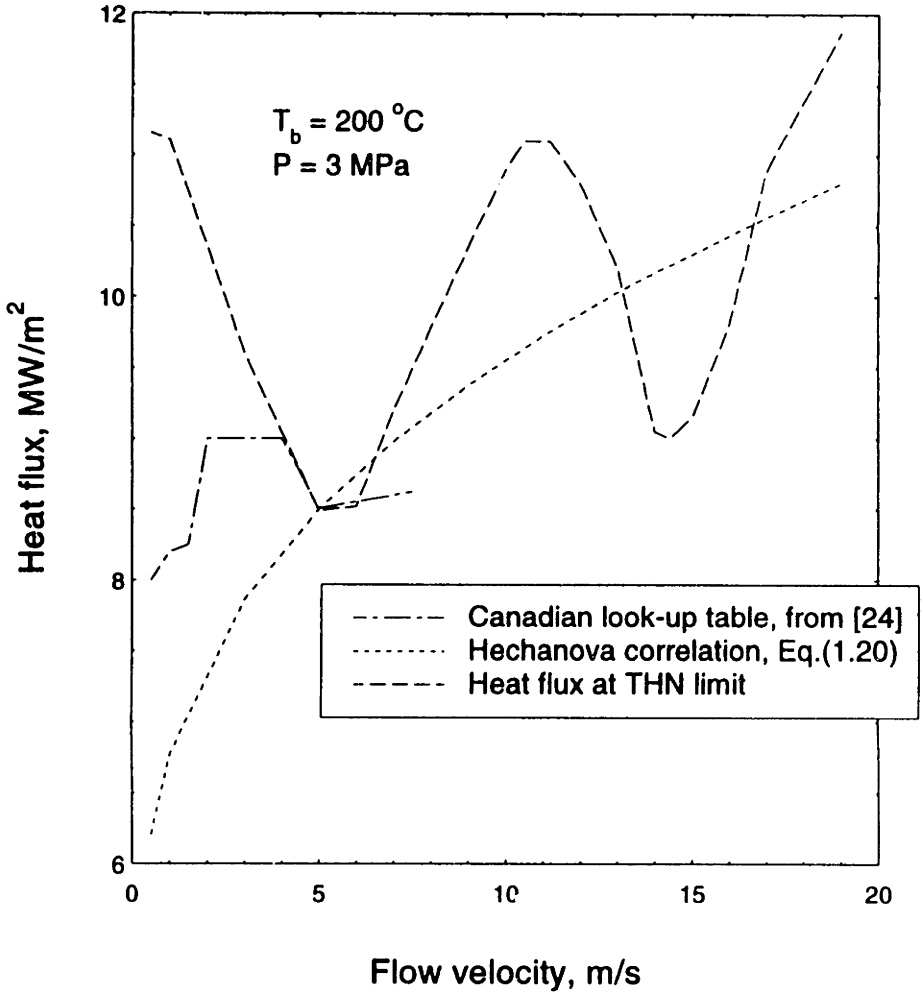

Figure 6-18: CHF as a function of flow velocity

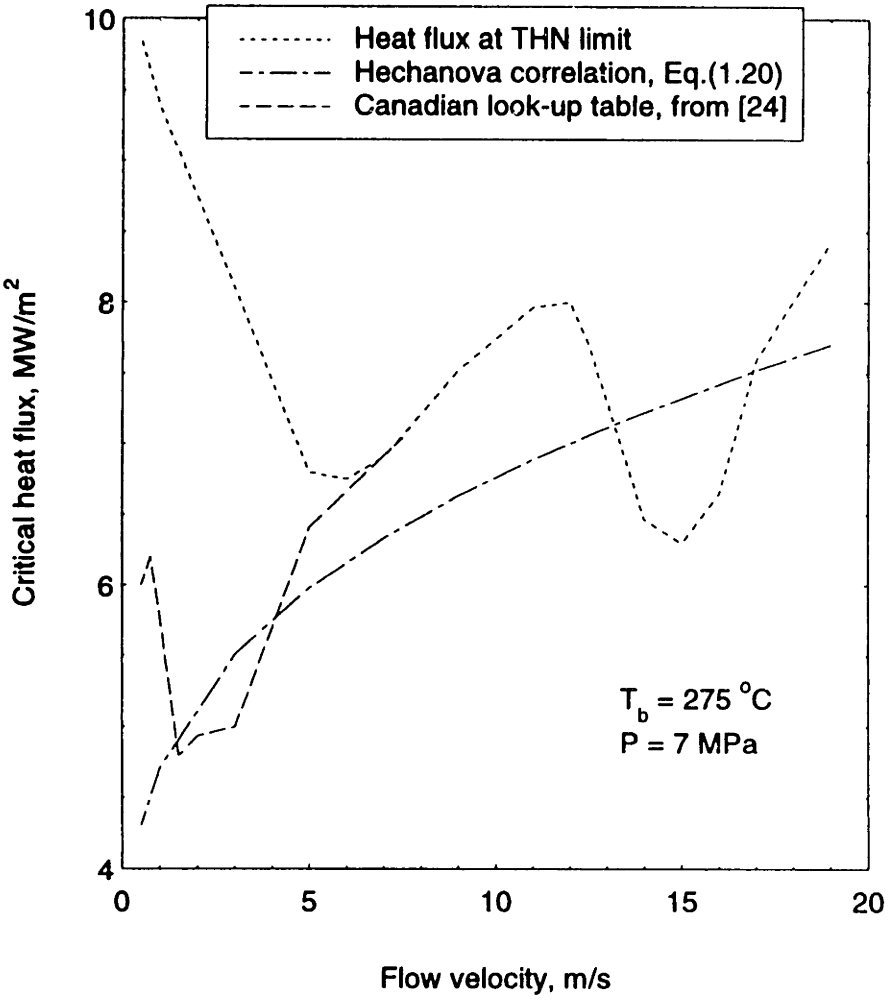

Figure 6-19: CHF as a function of flow velocity

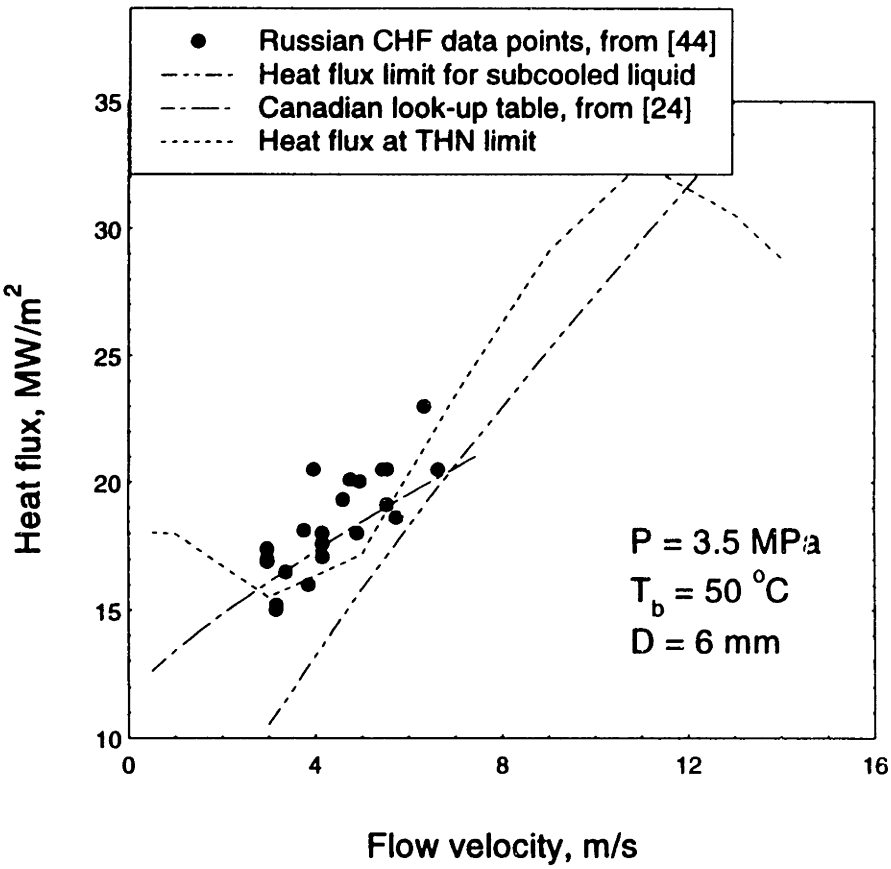

Figure 6-20: CHF as a function of flow velocity

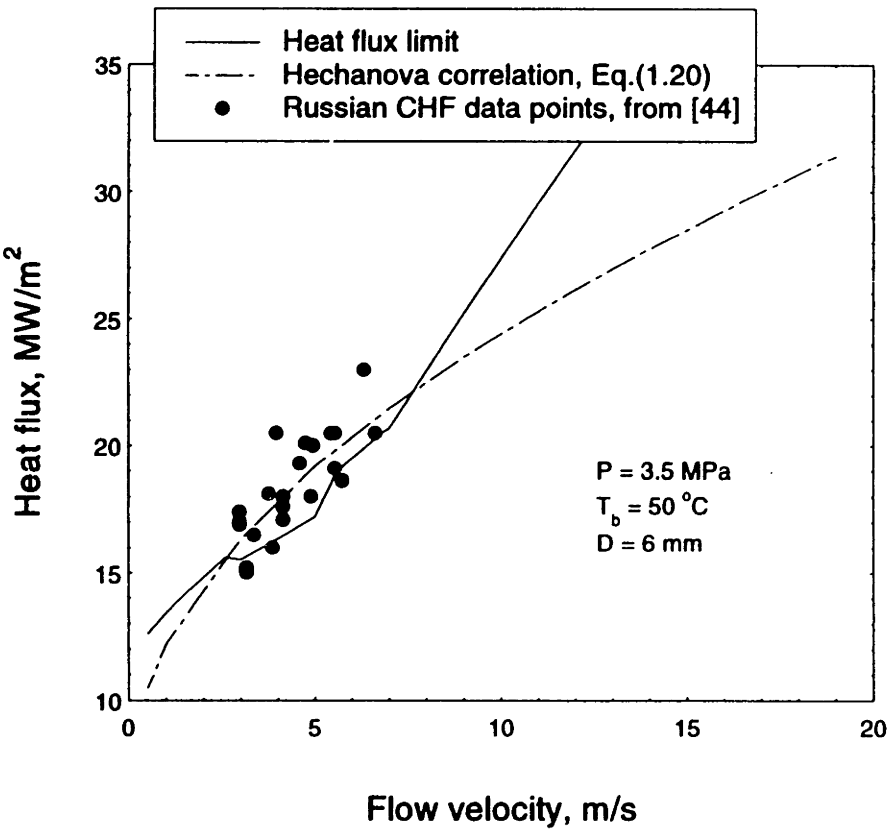

Figure 6-21: Heat flux limit as a function of flow velocity

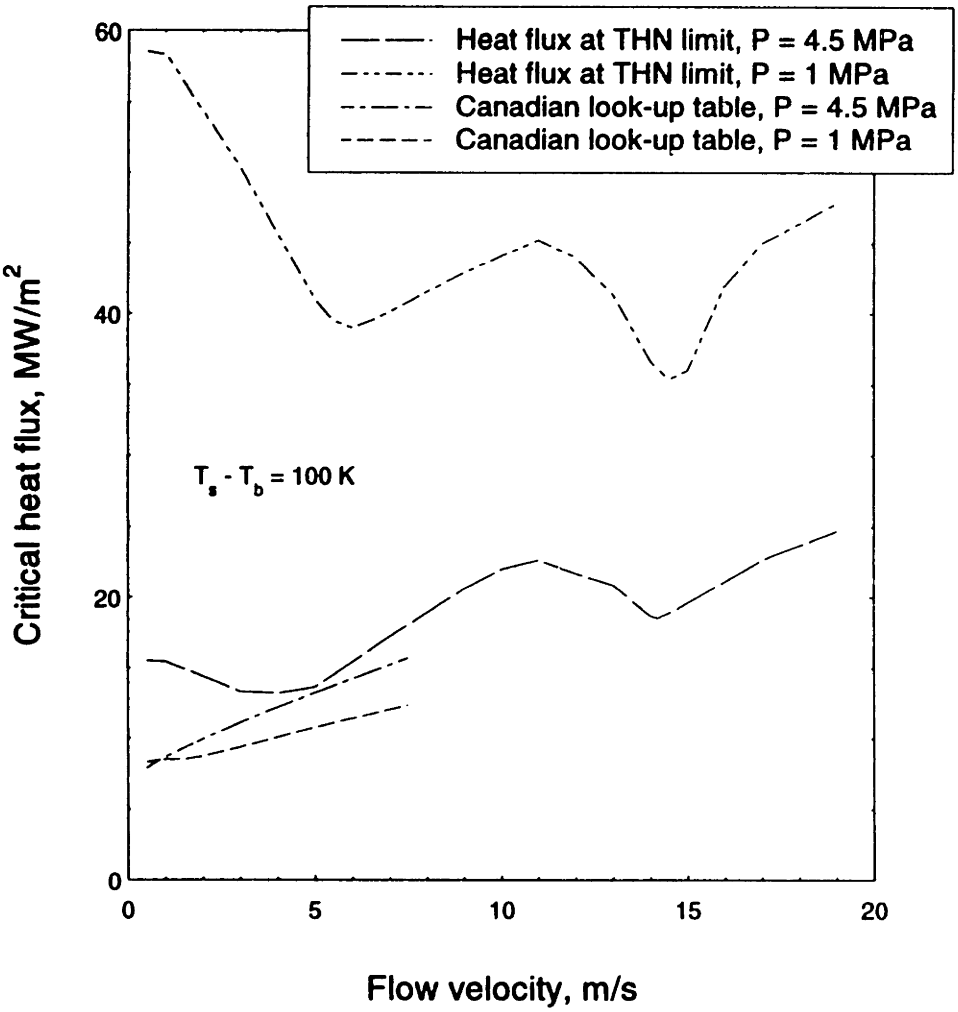

Figure 6-22: CHF as a function of flow velocity and pressure

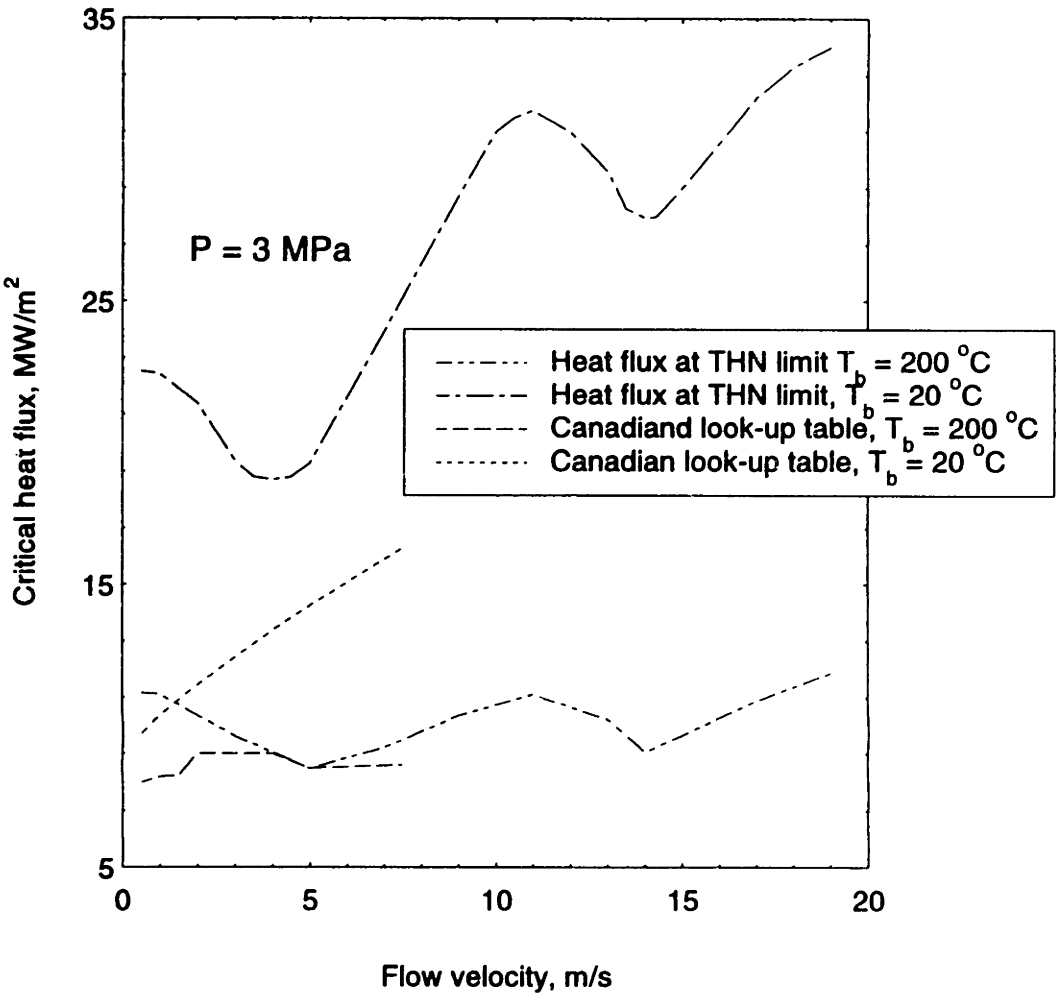

Figure 6-23: CHF as a function of flow velocity and subcooling

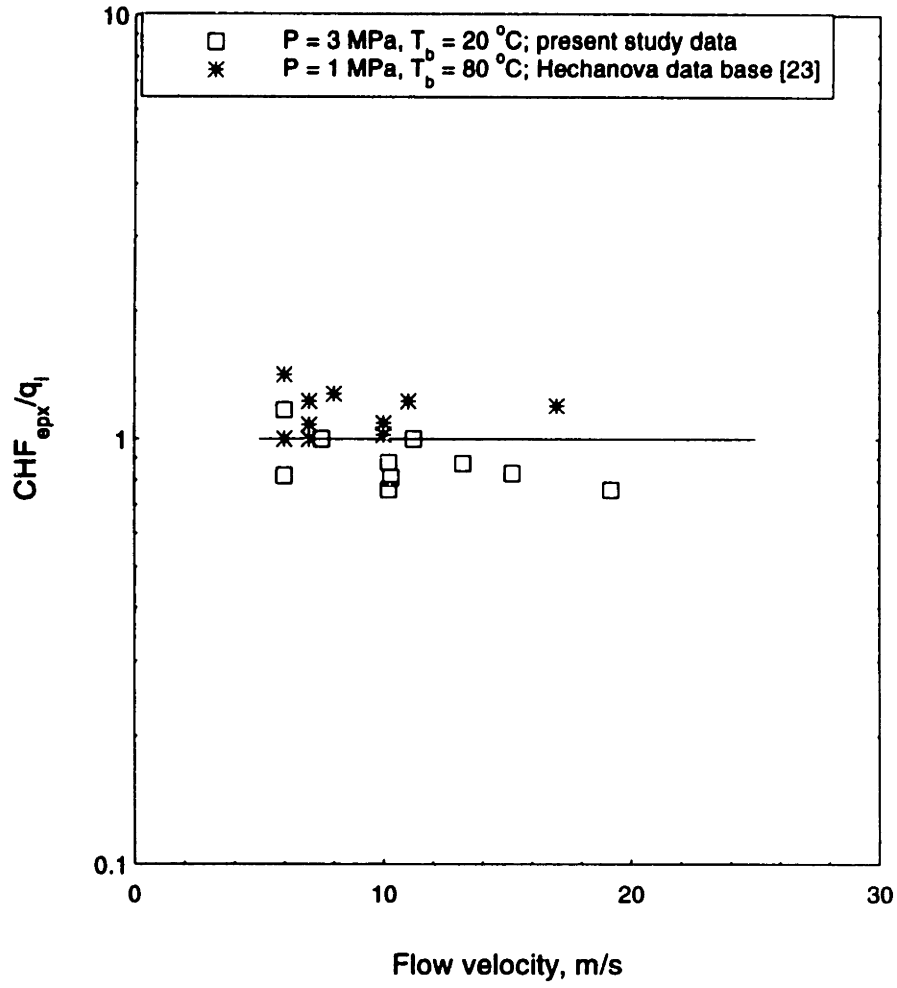

Figure 6-24: Heat flux ratio as a function of flow velocity

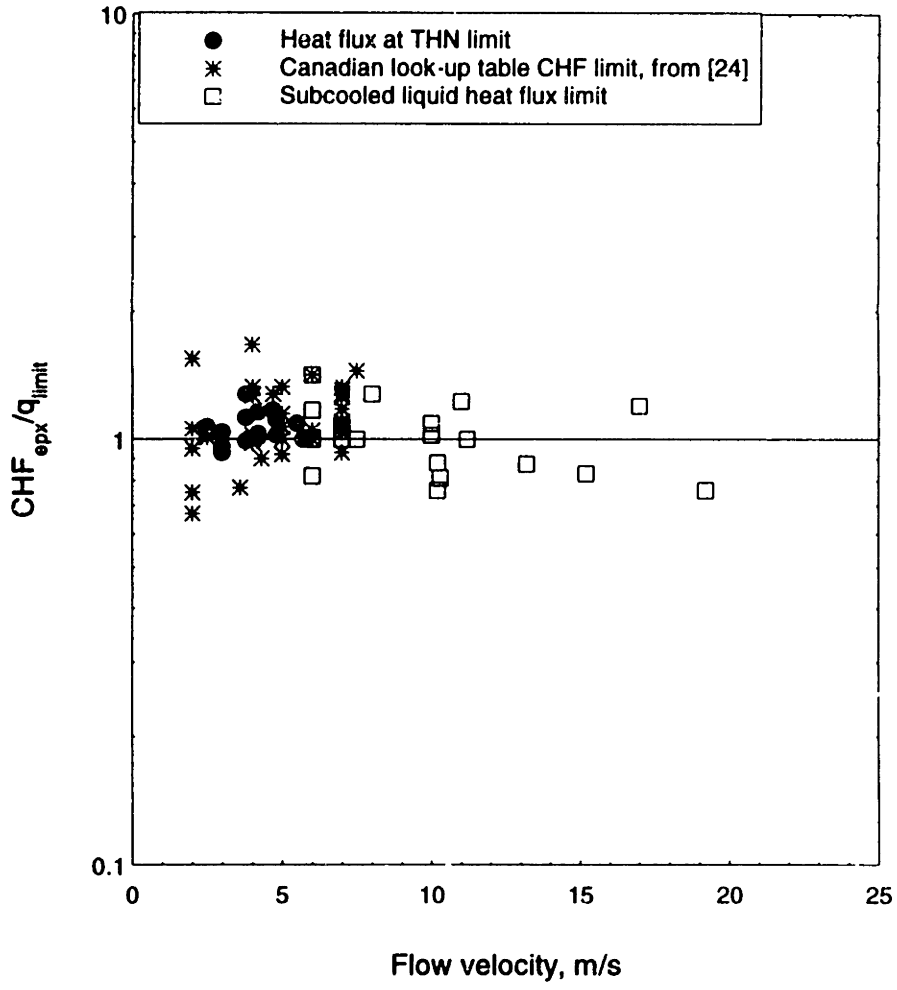

Figure 6-25: Heat flux ratio as a function of flow velocity

Chapter 7

Concluding Remarks

7.1 Summary of Major Accomplishments and Findings

1. Heat conduction methods were developed to obtain the heat flux distribution adjacent to the coolant based on the experimental heat supply and outer wall temperatures. The methods are suitable for both single-phase and nucleate boiling regimes and can be implemented without the use of heat transfer correlations. The uncertainty in the computation of the heat transfer coefficient is 10% (see page 66).

2. For the single-phase region, the Petukhov correlation (Equation (1.2)) is found to be applicable.

3. A subcooled boiling correlation for fusion reactor divertor conditions has been successfully developed.

$$q_w = F(S_v)\left(\frac{T_w}{T_s}\right)^2 h_{sp}(T_w - T_b) + S_p S_v S_q h_{nb}(T_w - T_s) \qquad (5.10)$$

It has been compared with experimental data used in developing the equation, and with other data points none of which were used for equation development. The agreement between calculated and experimental results was found to be in the range of $\pm$ 20% for P=3 MPa, bulk temperatures from 17 to 22 °C and 3-19 m/s velocity range. The new correlation was found to be superior to all of the other correlations tested for nucleate boiling.

4. The proposed correlation predicts physically reasonable results for different velocities, pressures and subcooling out of the experimentally tested range.

5. Since the proposed correlation distinguishes clearly between nucleate boiling and forced convection effects, it can be used as a starting point in understanding the suppression of nucleate boiling which exists at high velocities. It can also be used to calculate the THN limit for high velocity high heat flux flows.

6. Critical Heat Flux can occur if the wall temperature reaches the THN limit. This happens for high velocity flow due to an influence of turbulent vortices on steam bubble growth. Equation (6.11) is proposed to calculate CHF due to the THN limit. There are postulated to be two causes for CHF. One is the heat flux limit and the other is the wall temperature limit (THN limit). The heat flux limit is always much lower than the temperature limit in the ordinary boiling systems (low flow velocity, low pressure (P < 1 MPa) but for high velocity flows (P > 1 MPa) the heat flux limit has a chance to exceed the THN limit. So, special attention has to be paid to THN limit, because an unexpectedly low CHF may occur, especially for low subcooling.

7. When inner wall temperatures are below the THN limit the Critical Heat Flux occurs due to overheating at a nucleation site. The Canadian look-up table [24] is recommended for this particular mechanism.

8. The Critical Heat Flux can occur without accompanying high wall temperatures. Only after exceeding the Heat Flux Limit for Subcooled Liquid in a Post-CHF region are high wall temperatures expected. Equation (6.9) is recommended to evaluate the Heat Flux Limit for Subcooled Liquid in a Post-CHF region. In some cases this heat flux can be a real limit. Burnout can be avoided with very high mass flux and subcooling even at extremely high heat fluxes because of the highly enhanced heat transfer ability of film boiling phenomenon. Thus, a smooth continuous boiling characteristics curve can be achieved by the

combined effects of mass flux and subcooling. Namely, the discontinuity of heat transfer ability between nucleate and film boiling at the transition can be extinguished completely.

9. The following procedure is recommended to assess heat flux limits. First, the likely CHF mechanism should be determined. This can be done with the help of the Canadian look-up table [24] and Equation (6.11) for the THN type of CHF.

$$CHF_{THN} = F(S_v)\left(\frac{THN}{T_s}\right)^2 h_{sp}(THN - T_b) + 0.41 S_v S_p h_{nb}(THN - T_s) \qquad (6.11)$$

The Canadian look-up table [24] provides CHF values due to overheating at a nucleation site - CHF_{OV}. The critical heat flux will be the minimum of these two heat fluxes.

$$CHF = \text{Minimum } \{ CHF_{OV}, CHF_{THN} \} \qquad (6.12)$$

The following equation is proposed in order to evaluate the heat flux limit for a cooling channel.

$$q_{limit} = \text{Maximum } \{ CHF , q_l \} \qquad (6.13)$$

The data points show good agreement with the procedure, since 75% of the data falls within $\pm$ 20% of the predicted value for pressure from 0.2 MPa to 4.5 MPa, steam quality from -0.45 to -0.05 and 3-19 m/s velocity range. However, continuing validation and improvement of CHF correlations are still necessary. So are the development of new physically based correlations and the collection of expanded relevant data bases.

10. At very high heat fluxes, high velocity, low temperature liquid is present at the center of the channel and the wall is covered by a thin film of vapor. The liquid-vapor interface has an irregular and rapidly fluctuating shape. The temperature excursion which would be expected to occur upon transition to film boiling (boiling through a film of vapor) is precluded here since the film is so thin and since the high velocity cold liquid is so effective in condensing actions.

7.2 Recommendations

The present study has addressed an area where few other studies exist, namely, high heat flux thermal hydraulics. Therefore, many areas of expansion and refinement are worthy of pursuit.

First, of the major parameters (flow velocity, pressure, subcooling, diameter and heated length) only flow velocity was sufficiently varied during experiments performed. A similar parametric study of the others would add confidence to interdependent terms in the proposed correlations. Particularly, a study to better describe the heated length effect for short or spike profiles, or to investigate the non-uniform heated diameter effect for non-uniform circumferential heat fluxes.

Second, methods of heat transfer augmentation such as internal twisted tapes or novel channel designs would be a next logical step in increasing heat transfer performance.

Third, refinement of the experimental method would entail more instrumentation such as larger thermocouple arrays to aid in characterizing the actual heat flux profile. In addition, other ways of heating the test section besides the thin film should be explored. Also, computational codes able to solve the inverse heat conduction problem perhaps with the help of finite elements method would have added flexibility to the analysis of the three dimensional heat conduction problem.

Finally, post-CHF heat transfer investigation for fusion reactor conditions should be addressed in the future. The present study only touched upon post-CHF heat transfer mechanisms since the complexity and

sparse data base do not warrant extensive comparison between theoretical and experimental results. Nevertheless, approaches developed in the present study should be helpful during future investigations of post-CHF region.

Bibliography

[1] Draft Report for ITER Concept Definition Phase. Technical Report, IAEA, 1989.

[2] R.D. Watson, editor, ITER Divertor Engineering Design, Summary of Joint Working Session, Garching, Germany, Max Plank Institute for Plasma Physiks. October 1989.

[3] Detail of the ITER Outline Design Report: The ITER Machine Vol. II, San Diego Joint Work Site, January 10-12, 1994.

[4] M.N. Ozisik, "Heat Transfer - a Basic Approach", McGraw-Hill Book Co., 1985.

[5] W.H. Jens, and P.A. Lottes, Analysis of Heat Transfer, Burnout, Pressure Drop for High Pressure Water, ANL-4627, May, 1951.

[6] J.R.S. Thom et.al. Boiling in Subcooled Water During Flow-up in Heated Tubes or Annuli, Symp. Boiling Heat Transfer in Steam Generation Units and Heat Exchangers, Manchester, IMECHE (London), September, 1965.

[7] S.T. Yin et.al., Prediction of Highly Subcooled Flow Boiling For Cooling off High- Flux Components in Fusion Reactors. NURETH-6, October 5-8, 1993, Grenoble.

[8] J.C. Chen, A correlation for Boiling Heat Transfer to Saturated Fluids in Convective Flow, ASME Paper no.63-HT-34, 1963.

[9] J.G. Collier, "Convective Boiling and Condensation", McGraw-Hill Book Co., England, 1972.

[10] H. K. Foster and N. Zuber, Dynamics of Vapor Bubbles and Boiling Heat Transfer, AIChE Journal, 1, 4, 1965, p.531-535.

[11] R.L. Sani, Down Flow Boiling and Non-Boiling Heat Transfer in a Uniformly Heated Tube, UCRL Report, UCRL-9023, 1960.

[12] D. Butterworth, Unresolved Problems in Heat Exchanger Design, Inst. of Chem. Eng. Symp. Ser., 60, 231-48, 1980.

[13] Codes of Thermohydraulic Calculations for Nuclear Power Plants (in Russian) St.Petersburg, NPO TsKTI. 1986.

[14] A.E. Bergles and W.M. Rohsenow, The Determination of Forced-Convection Surface-Boiling Heat Transfer, ASME PAPER no. 63-HT-22, 1963.

[15] F.D. Moles and J.R.G. Shaw, Boiling Heat Transfer to Subcooled Liquids Under Conditions of Forced Convection, Trans. Inst. Chem. Engrs., 50, 76-84,1972.

[16] N.E. Todreas and M.S. Kazimi, "Nuclear Systems 1, Thermal Hydraulic Fundamentals", Hemisphere Publishing Corporation, 1989.

[17] M.M. Shah, A General Correlation for Heat Transfer During subcooled Boiling in Pipes and Annuli, *ASHRAE Transactions*, Part 1, 83, 1987.

[18] W.R. Gambill et.al. Heat Transfer, Burnout and Pressure Drop for Water in Swirl Flow through Tubes with Internal Twisted Tapes, *Chem. Eng. Prog. Symp. Ser.*, 57, 2 , pp.127-137, 1961.

[19] J.A. Blatt and R.R. Adt, The Effects of Twisted Tape Swirl Generation on the Heat Transfer Rate, Pressure Drop of Boiling Freon-11 and Water, ASME Paper no 63-WA-42, 1963.

[20] I.S. Kudryavtsev and B.M. Lekakh, Nucleate Boiling of Water in Twisted-Tape Swirl Flow, Heat Transfer-Soviet Research, 22, 6, pp.705-712, 1990.

[21] A.N. Vasil'yev and P.L. Kirillov, On the Possibility of Break up of Vapor Nuclei by Turbulent Eddies, High Temperature, 13, 5, pp.1118-1120, 1975.

[22] J.A. Koski, R.D. Watson, T.D. Marshall et al., An Experimental Investigation of the Post-CHF Enhancement Factor for a Prototypical ITER Divertor Plate with Water Coolant, *SOFE-95 Abstract Book*, Urbana, 1995.

[23] A.E. Hechanova, Thermal Hydraulics of High Heat Flux Components, Ph.D. Thesis, MIT Nuclear Engineering Department, January 1995.

[24] D.C. Groenveld et al., 1986 AECL-UO Critical Heat Flux Look up Table, Heat Transfer Engineering, 7, 1-2, pp.46-62, 1986.

[25] V.E. Doroshchuk, L.L. Levitan, F.P. Lantzman, Investigations into Burnout in Uniformly Heated Tubes, ASME Paper 75-WA/HT-22, 1975.

[26] L.S. Tong, A Phenomenological Study of Critical Heat Flux, *ASME 75-HT-68,* pages 1-4, 1975.
[27] V.A. Divavin, V.N. Tanchuk, and A.E. Shrubok, Limited Heat Loads and Burnout Heat Transfer in One-Sided Heated Channels, *Heat Transfer Research*, v.24, 5, pp. 612-624, (1992).
[28] A.N. Kolmogorov, Reports of the USSR Academy of Sciences (in Russian) 30, 4, 1941.
[29] V.P. Skripov et al., "Thermophysical Properties of Liquids in the Metastable (Superheated) State", McGraw-Hill, N.Y., 1988.
[30] V.M. Borishanskii, "Convective Boiling and Condensation", (in Russian), Moscow, 1979.
[31] Cole-Parmer Instrument Company, Conductivity Meter Model 1500-10, Instruction Manual.
[32] HEATING Version 7.2b, *Heat Conduction Code: 3D Conduction Profile.* Computing Application Division, Oak Ridge National Laboratory, February 1993.
[33] J.A. Koski, R.D. Watson, P.L. Goranson et al., Thermal-Hydraulic Design Issues and Analysis for the ITER Divertor, *Fusion technology,* 19, May, 1991.
[34] J.A. Koski et al., Experimental Verification of Subcooled Flow boiling for Tokamak Pump Limiter Designs, *ASME 87-HT-45,* 1987.
[35] L.S. Tong, Transient DNB Test on C.V.T.R. Fuel Assembly, *ASME paper 65, WA/NE-3,* 1965.
[36] F. Inasaka and H. Nariai, Critical Heat Flux of Subcooled Flow Boiling with Water for high Heat Flux Application, *High Heat Flux Engineering II (preprint),* July 1989.
[37] L.S. Tong, Boundary Layer Analysis of the Flow Boiling Crisis, *Int. J. of Heat Mass Transfer,* 11:1208-1211, 1968.
[38] S.T. Yin et al., Assessment of a Heat Transfer Correlations Package for Water-Cooled Plasma-Facing Components in Fusion Reactors, Proceedings of Nuclear Thermal Hydraulics - 1991 Winter Meeting of the Am. Nucl. Soc., 1991, San Francisco, pp. 929-938.
[39] G.P. Celata et al., Rationalization of Existing Mechanistic Models for the Prediction of Water Subcooled Flow Boiling Critical Heat Flux, *Int. J. Heat Mass Transfer,* Suppl.1, 37, 1994.
[40] V.H. Valle and D.B. Kenning, Subcooled Flow Boiling at High Heat Flux, *Int. J. Heat Mass Transfer*, v.28, 10, pp. 1907-1920, 1985.
[41] P. Saha and N. Zuber, Point of Net Vapor Operation and Vapor Void Fraction in Subcooled Boiling, *Proceedings 5th International Heat Transfer Conference,* Tokyo, 1974.
[42] W.S. Bradfield et al., Some Effects of Boiling on Hydrodynamic Drug, *Int. J. of Heat Mass Transfer,* 5, 615-622 (1962).
[43] R.S. Dougall and W.M. Rohsenow, Film Boiling on the Inside of Vertical Tubes with Upward Flow of the Fluid at Low Qualities, M.I.T. Report No. 9079-26 (Sept. 1963).
[44] M.A. Gotovskii, Private Communication, 1993.
[45] Y. Fukuyama and M. Hirata, Boiling Heat Transfer Characteristics with High Mass Flux and Disapperance of the CHF Follwing to DNB, Heat Transfer 1982, *Proceedings of 7th Int. Heat Transfer Conference,* Munich, pp. 273-278, 1982.

Nomenclature

	Variables	Units
A	Area	m^2
a	Centrifugal acceleration	m/s^2
CHF	Critical Heat Flux	W/m^2
c_p	Specific Heat at Constant Pressure	J/(kg K)
D	Diameter	m
G	Mass Flux	$kg/(m^2 s)$
E	Enhancement Ratio	
F	Correction Multiplier	
f	Friction Factor, Eqn. 2.6	
H_{fg}	Heat of Vaporization	J/kg
h	Heat Transfer Coefficient	$W/(m^2 K)$
I	Power Supply Current	A
J	Spontaneous Nucleation Rate per Unit Volume	$s^{-1} m^{-3}$
k	Conductivity	W/(m K)
l	Length	m
P	Pressure	Pa
pf	Peaking Factor	
p_r	Reduced Pressure (Absolute/Critical)	
q_o"	Incident Heat Flux	W/m^2
q	Heat Flux	W/m^2
r	Radius	m
S	Suppression factor	
T	Temperature	K
t	Thickness	m
THN	Temperature of Homogeneous Nucleation	K
U	Voltage	V
V	Velocity	m/s
X	Steam Quality	
x	Coordinate	m
y	Coordinate	m

	Greek Symbols	Units
β	Coefficient of Thermal Expansion (fluid volume)	K^{-1}
δ	Thickness	m
ΔT	Temperature Difference	K
ΔP	Pressure Drop	Pa
ε	Energy Dissipation Rate per Unit Mass	W/kg
γ	Subcooled Boiling Location, Eqn. 1.7	
η	Turbulent Vortex Size	m
μ	Kinematic Viscosity	Pa s
ν	Dynamic Viscosity	m^2/s
τ	Kinetic Head	Pa
σ	Surface Tension	N/m
θ	Temperature Difference	K
ρ	Density	kg/m^3
Π	Perimeter	m
ψ	Non-Dimensional Heat Flux Parameter	

	Subscripts
az	Azimuthal
bulk	Bulk
c	Convective Term
CHF	Critical Heat Flux
ex	Exit
exp	Experimental
f	Fluid (or Liquid)
fb	Film Boiling
g	Gas (or Vapor)
HN	Homogeneous Nucleation
h	Heated
in	Inner
inc	Incoming
l	Liquid
limit	Limit
local	Local
m	Middle
nb	Nucleate Boiling Term
o	Incident
onb	Onset of Nucleate Boiling
out	Outer
ov	Overheating
P	Pressure
pet	Petukhov
pb	Pool Boiling
q	Heat Flux
s	Saturation
sp	Single Phase
TC	Thermocouple
THN	Temperature of Homogeneous Nucleation
v	Velocity
w	Wall
x	Axial

	Dimensionless Numbers	
A	Bubble Growth Number (Eqn. 2.2, 2.11, 2.12, 2.15)	$\tau r / (2\sigma)$
Bo	Boiling Number	$q / (G H_{fg})$
Ja	Jacob Number (Eqn. 1.21)	$c_p \Delta T / H_{fg}$
Nu	Nusselt Number	$h D / k$
Pe	Peclet Number (Eqn. 1.20, 6.1)	$G D c_{pf} / k_f$
Pr	Prandtl Number	$\mu c_p / k$
Re	Reynolds Number	$G D / \mu$
Re'_{TP}	Reynolds Two-Phase Number (Eqn. 1.12)	$G(1-x)DF^{1.25}10^{-4} / \mu_f$
St	Stanton Number	$q / (Gc_{pf} (T_s - T_b))$
X^{-1}_{tt}	Lockhart-Martinelli Number (Eqn. 1.9)	$(X/1-X)^{0.9} (\rho_f/\rho_g)^{0.5} (\mu_g/\mu_f)^{0.1}$

	Acronyms
Burnout	Excursion to high wall temperature
CHF	Critical Heat Flux
DNB	Departure from Nucleate Boiling
HEATING7.2	3-D Heat Conduction Code
ITER	International Thermonuclear Experimental Reactor
LOCA	Loss of Coolant Accident
LOFA	Loss of Flow Accident
OSV	Onset of Significant Voids
TC	Thermocouple (K-type)
THN	Temperature of Homogeneous Nucleation

	Constants	
a	$1.52 * 10^{-16}$ Eqn. 5.5	
b	3.37 Eqn. 5.5	
C_oC_l	0.23 Eqn. 1.21	
D_o	0.0127 Eqn. 1.21	m

Appendix

M. A. Gotovskii CHF Data [44]

Flow velocity, m/s	Local CHF, MW/m^2
3.16	15
3.36	16.5
3.86	16
4.9	18
4.95	20
5.44	20.5
6.33	23
6.63	23
6.63	20.5
5.74	18.6
2.97	17.4
3.96	20.5
3.76	18.1
4.75	20.1
2.97	16.9
4.15	17.1
5.54	20.5
2.97	17
4.15	18
5.54	19.1
3.16	15.2
4.15	17.6
4.6	19.3